Guo *et al. Energy Mater.* **2025**, *5*, 500030
DOI: 10.20517/energymater.2024.63

Energy Materials

Review

Open Access

A review of the preparation and characterization techniques for closed pores in hard carbon and their functions in sodium-ion batteries

Yujie Guo[1], Shun Ji[1], Feng Liu[2], Ziyi Zhu[1,*], Jie Xiao[1], Ke Liu[1], Yanjia Zhang[1], Shijun Liao[3,*], Xiaoyuan Zeng[1,*]

[1]National and Local Joint Engineering Research Center for Lithium-ion Batteries and Materials Preparation Technology, Key Laboratory of Advanced Battery Materials of Yunnan Province, Faculty of Metallurgical and Energy Engineering, Kunming University of Science and Technology, Kunming 650093, Yunnan, China.
[2]The State Key Laboratory of Advanced Technologies for Comprehensive Utilization of Platinum Metals, Kunming 650093, Yunnan, China.
[3]The Key Laboratory of Fuel Cell Technology of Guangdong Province, School of Chemistry and Chemical Engineering, South China University of Technology, Guangzhou 510641, Guangdong, China.

***Correspondence to:** Dr. Ziyi Zhu, National and Local Joint Engineering Research Center for Lithium-ion Batteries and Materials Preparation Technology, Key Laboratory of Advanced Battery Materials of Yunnan Province, Faculty of Metallurgical and Energy Engineering, Kunming University of Science and Technology, Kunming 650093, Yunnan, China. E-mail: zyzhu23@kust.edu.cn; Dr. Shijun Liao, The Key Laboratory of Fuel Cell Technology of Guangdong Province, School of Chemistry and Chemical Engineering, South China University of Technology, Guangzhou 510641, Guangdong, China. E-mail: chsjliao@scut.edu.cn; Dr. Xiaoyuan Zeng, National and Local Joint Engineering Research Center for Lithium-ion Batteries and Materials Preparation Technology, Key Laboratory of Advanced Battery Materials of Yunnan Province, Faculty of Metallurgical and Energy Engineering, Kunming University of Science and Technology, Kunming 650093, Yunnan, China. E-mail: zengxiaoyuan@kust.edu.cn

How to cite this article: Guo, Y.; Ji, S.; Liu, F.; Zhu, Z.; Xiao, J.; Liu, K.; Zhang, Y.; Liao, S.; Zeng, X. A review of the preparation and characterization techniques for closed pores in hard carbon and their functions in sodium-ion batteries. *Energy Mater.* **2025**, *5*, 500030. https://dx.doi.org/10.20517/energymater.2024.63

Received: 27 Jun 2024 **First Decision:** 8 Aug 2024 **Revised:** 28 Aug 2024 **Accepted:** 15 Oct 2024 **Published:** 21 Jan 2025

Academic Editor: Jiazhao Wang **Copy Editor:** Fangling Lan **Production Editor:** Fangling Lan

Abstract

With the advantages of simple preparation, cost-effectiveness, abundant raw materials, and environmentally friendly properties, hard carbon is the only commercially available anode material for sodium-ion batteries. However, its unstable capacity is attributed to the complex physicochemical characteristics of the precursors, the intricate and difficult-to-control microstructure, and the debated mechanisms of sodium storage. Although recent reports have revealed a strong correlation between closed pores and the capacity of hard carbon in the low-voltage plateau region, systematic overviews of this relationship remain scarce. This review examines the microstructural properties and precursor selectivity of hard carbon materials and outlines the strategies for the research and

development of closed pores, including design theory and characterization. Finally, it summarizes the technical bottlenecks faced by the closed pore research and looks forward to the future development directions.

Keywords: Hard carbon, sodium-ion batteries, closed pores

INTRODUCTION

Portable devices and electric cars have extensively utilized lithium-ion batteries (LIBs). Nevertheless, their expansion in large-scale energy storage has been hindered by the high manufacturing costs, mainly due to the escalating prices of raw materials such as lithium, cobalt, and nickel. Operating on similar principles as LIBs, sodium-ion batteries (SIBs) offer enhanced cycling stability and safety, utilize a more abundant and cost-effective resource base, and are rapidly emerging as one of the most promising application-specific complements to LIBs[1].

Anode materials are pivotal in the operation of SIBs, serving as both low-potential redox pairs and ion storage sites. There are two main categories of anode materials: carbon-based and non-carbon-based. Non-carbon-based materials primarily include materials based on titanium, organic materials, alloy-based materials, and metal oxides/sulfides. Titanium-based materials exhibit minimal volume changes during cycling but have limited capacity. Despite the low cost of raw materials and environmental friendliness, organic compounds suffer from poor electrical conductivity and a propensity for side reactions with the electrolyte. Alloy materials, while offering low sodium storage potentials, suffer from significant volume expansions after sodium insertion, leading to poor cycling performance. Metal oxides/sulfides possess a large theoretical capacity but exhibit low electrical conductivity, tendency to accumulate, and irreversible conversion reactions[2-4].

Carbon-based materials, known for their low-volume expansion and excellent cycle stability, are highly valued for their use as anode materials in SIBs. Hard carbon (HC) stands out among these materials due to its ease of operation, cost-effectiveness, simple preparation method, and abundance of raw materials, all of which make it highly favorable for commercial manufacturing. HC is considered the most promising anode material currently available for SIBs[5]. The HC anode, while promising, does have certain drawbacks including a low initial Coulombic efficiency (ICE), voltage plateau lag, and an ambiguous sodium storage mechanism. Despite efforts to improve the electrochemical performance of HC anodes through techniques such as heteroatom doping[6-9] and surface modification[10,11], the complex nature of precursors and the difficulty in controlling microstructures have made it challenging to fully understand the relationship between the structure, sodium storage mechanisms, and electrochemical performance. This complexity hinders further exploration and optimization of HC anodes for SIBs.

The primary structure of HC involves randomly dispersed curved graphene sheets. The distance between these graphene sheets (d_{002})[12], the type and concentration of defects[13,14], and the presence of nanopores, particularly closed pores, play crucial roles in influencing the sodium storage performance of HC. Scholars have focused on modifying the size and volume of nanopores by varying precursor types and the pyrolysis process to enhance the electrochemical performance of the HC anode[15-18].

The charging/discharging curves of HC typically exhibit two distinct regions: the high-voltage slope region (voltage above 0.1 V) and the low-voltage plateau region (voltage ranging from 0 to 0.1 V). The specific capacity of HC primarily comes from the plateau capacity. Therefore, it is essential to investigate the sodium storage mechanisms of HC in the plateau region to improve the electrochemical efficiency of HC anodes for SIBs[19].

Scholars have identified the specific mechanism by which sodium is stored in HC at different voltages through various research methods. As early as 2000, Stevens *et al.* proposed the "intercalation-adsorption" sodium storage mechanism when they successfully prepared HC by direct pyrolysis of glucose[20]. They confirmed this mechanism in subsequent studies[21]. However, later research found that this conclusion was insufficient to explain phenomena such as increased carbonization temperature, reduced surface porosity, and increased capacity in the plateau region. In 2012, Cao *et al.* successfully prepared hollow carbon nanowires through the pyrolysis of hollow polyaniline (PANI) nanowires[22]. Electrochemical tests showed that at high voltage regions (0.2~1.0 V), charge was adsorbed on the HC surface, while at low voltage regions (0.0~0.2 V), Na^+ intercalate/extract between graphene layers. Theoretical simulations indicated that Na^+ could intercalate into layered carbon materials with the d_{002} = 0.37 nm, further validating the electrochemical test results. The "adsorption-intercalation" sodium storage mechanism was first proposed. Zhu *et al.* prepared cotton-derived HC microtubes and found through a combination of *in-situ* and *ex-situ* characterization methods that d_{002} did not change before and after charge/discharge, indicating that Na^+ in the plateau region did not undergo intercalation[23]. Thus, they proposed the "adsorption-filling" sodium storage mechanism. Bommier *et al.* proposed that the sodium storage mechanism in HC is "adsorption-intercalation-filling[24]". They characterized the Na^+ diffusion coefficient (D_{Na+}) in sucrose-derived HC anodes using constant current intermittent titration techniques and found that D_{Na+} in the high-voltage slope region was greater than that in the low-voltage plateau region, with a sudden increase in D_{Na+} around 0.050 V. Based on the experimental results and the "adsorption-intercalation" mechanism, they proposed the "adsorption-intercalation-filling" mechanism, where the slope capacity originates from the chemical adsorption of sodium ions at carbon layer defect sites (1.0~0.2 V), the plateau capacity comes from the intercalation of sodium ions between graphene layers (0.2~0.05 V), and the plateau capacity below 0.05 V arises from the adsorption of sodium ions on the pore surface of HC. Subsequently, many researchers studied the sodium storage mechanism in the pores. Li *et al.* carbonized cork at different pyrolysis temperatures to prepare a series of HC anodes[17]. They subsequently characterized the closed pores using techniques such as small angle X-ray scattering (SAXS) and found that the plateau capacity was provided by the filling of sodium in the nanopores, with no intercalation behavior observed. Jian *et al.* prepared HC microspheres using sucrose and investigated their applications in potassium-ion batteries and SIBs[25]. They claimed that two sodium storage behaviors were present in the plateau region: the intercalation/extraction of sodium ions in carbon layers and filling in nanopores. Komaba e*t al.* noted that what appears in the nanopores are sodium nanocrystals (nano-sized quasi-metallic sodium clusters) rather than sodium ions[26].

In addition, theoretical calculation models are also commonly used to describe sodium storage mechanisms. Chen *et al.* further elucidated the sodium storage mechanism in HC through first-principles calculations[27]. They represented the pseudo-graphite domains and nanopore structures of HC with parallel graphite layers and single-walled carbon nanotube structures, respectively, and calculated the binding energies of Na^+ in these two microstructures, evaluating the effect of pore diameter on Na^+ and Li^+ storage. The results indicated that when the pore diameter is less than 1.4 nm, the binding energy of Na^+ is lower than that of Li^+, suggesting that HC with smaller micropore diameters is more favorable for Na^+ storage compared to Li^+ storage. Tang *et al.* prepared a series of spore-derived HCs using concentrated sulfuric acid, sodium hydroxide, and a two-step carbonization method[28]. They then established models with different lattice spacings for graphite layers, different curvatures for graphene models, and other scenarios to simulate the parallel graphite lattices and pore edge structures in HC, further clarifying the specific role of closed pores in electrochemical behavior. The calculations revealed that the binding energy of Na^+ within curved graphene is lower than that on the surface of graphene, indicating that twisted graphene layers with a certain curvature and the closed pore structures they create are more favorable for the storage of Na^+.

It is worth noting that the voltage in the low-voltage plateau region, ranging from 0 to 0.1 V, is very close to the thermodynamic plating voltage of metallic sodium (0 V). Therefore, when the overpotential during the charging/discharging process exceeds the plating voltage of metallic sodium, metallic sodium may deposit on the HC anode and form a coating[29,30]. After conducting ^{23}Na nuclear magnetic resonance (NMR) tests on HC anodes at different voltages, Dai *et al.* found a broad peak around 1,130 ppm[30], which completely disappeared in the range of 800 to 1,200 ppm after complete desodiation from HC. Thus, he concluded that a plating phenomenon occurs on the HC anode during the charging/discharging process. He suggested that this phenomenon might be due to the varied micro-morphology and pore structure of HC; there is competition between the deposition of metallic sodium on the HC surface and the filling of quasi-metallic sodium clusters in closed pores. However, some researchers argue that sodium plating does not occur in the plateau region. Qiu *et al.* obtained cellulose-derived HC (HC-x, where x represents the carbonization temperature) by carbonizing cellulose under an argon atmosphere[31]. To verify whether Na^+ deposition to form a coating occurs on the anode, they over-discharged the HC-1300 anode to below 0 V and performed ^{23}Na NMR tests at different discharge voltages. The results indicated that sodium plating only occurs in the region below 0 V and does not appear in the plateau region. Chen *et al.* prepared two HC materials, mainly pseudo-graphite microcrystals and micropores, using glucose and magnesium gluconate, and further investigated the sodium storage behavior of these two HC materials using ^{23}Na NMR[27]. The results showed that the plateau capacity is contributed by both interlayer insertion and micropore filling, with the contribution ratio varying according to the microstructure. Additionally, Wang also suggested that metallic sodium can only deposit when the nucleation overpotential is overcome, making it nearly impossible to form pure metallic sodium throughout the entire region down to 0 V[32].

Currently, the sodium storage mechanisms in HC remain controversial, and the storage methods in the high-voltage slope region and low-voltage plateau region remain not clearly defined. The microstructure of HC is complex and diverse, and it is easily influenced by other factors, such as the presence of heteroatoms, which makes it difficult to clarify the relationship between electrochemical behavior and sodium storage sites. Furthermore, the closed pores within HC are also challenging to measure accurately, making it impossible to determine the relationship between the pore structure of HC and its electrochemical behavior.

The specific surface area (SSA), d_{002}, and pyrolysis temperature also affect the electrochemical performance of HC. Generally, in electrochemical applications, electrodes with a higher SSA tend to have better charge storage capacity and a larger effective reaction area[33]. However, an excessively high SSA in HC can lead to increased electrolyte decomposition and more side reactions, resulting in a lower ICE[23]. Increasing d_{002} is beneficial for the intercalation/extraction of Na^+, and the d_{002} of HC typically ranges from 0.36 to 0.40 nm[34]. When the temperature exceeds 1,500 °C, the content of disordered structures in HC decreases, indicating an increase in graphitization degree[35]. In summary, the structure of HC has a significant impact on the electrochemical performance of SIBs.

Over time, the application technology of HC has become increasingly mature, and the number of related research reports has grown. Scholars have published numerous reviews on aspects such as the morphology and preparation methods of HC, optimization strategies and effects of heteroatom doping, and electrochemical energy storage mechanisms[36-39], which help us better understand HC and provide a theoretical foundation for future work. However, current reviews have relatively few reports on the formation and role of closed pores. In recent years, our team has conducted systematic research on HCs derived from different precursors, such as cherry petal[40], pine pollen[41], oatmeal[42], laver[43], metal-organic frameworks (MOFs)[44], rhododendron petal[45], litchi pericarp[46], and magnolia grandiflora lima leaf[47]. These materials have been widely applied in alkali metal ion batteries, showing good electrochemical

performance. Based on these theoretical foundations and experimental experiences, this paper starts from the source and structural characteristics of HC to explore the formation mechanism of closed pores, systematically summarizes the methods for preparing and characterizing closed pores and proposes that the specific role of closed pores in electrochemical behavior is to provide storage sites for quasi-metallic sodium clusters. Finally, future research directions for closed pores are discussed to provide some guidance for the design of HC.

PRECURSOR SELECTION

The microscopic structure of HC is affected by the inherent characteristics of the precursor. The choice of precursor material plays a significant role in determining the microscopic structure and properties of HC, which in turn influences its electrochemical performance[48]. Currently, polymers, coal, and biomass are regarded as the most appropriate precursor materials for HC.

The pyrolysis and carbonization process of polymers is relatively mature. HC derived from polymers typically exhibits good conductivity and high mechanical strength. However, the high degree of cross-linking in the polymer reduces the relative displacement and spatial hindrance between polymer chains, leading to the inability of the molecular chains to curl or shrink to effectively create a large number of micropores or mesopores. As a result, the porosity of the prepared HC is relatively low, which is detrimental to enhancing the specific capacity. Coal-derived HC is more cost-effective to produce and is suitable for large-scale manufacturing. However, the chemical composition of coal is complex and varied, with significant differences in the content of carbon, ash, and elements such as O, H, and S among lignite, sub-bituminous coal, bituminous coal, and anthracite. This leads to a complex and variable microstructure of the HC produced, making it difficult to control the electrochemical performance of coal-based HC with a single method. Biomass-derived HC has abundant raw materials and is environmentally friendly, but the natural structure of the biomass or the release of volatile substances during pyrolysis can result in a large number of pore structures, leading to a high SSA. An anode with a large SSA has more contact area with the electrolyte, forming a thicker solid electrolyte interphase (SEI) film, which ultimately leads to a lower ICE for the HC. The removal of ash and impurities in biomass precursors is complex and time-consuming, and some biomass-derived HCs have a narrower d_{002}, which is unfavorable for Na^+ intercalate/extract, leading to poorer cycling stability.

In summary, the choice of precursor material for HC synthesis influences the microscopic structure, porosity, mechanical strength, electrochemical properties, and overall performance of the resulting HC material. Each type of precursor material has its advantages and challenges, and researchers need to continue to explore ways to optimize HC electrochemical performance. The structural composition and precursor sources of HC are shown in Figure 1.

Polymer-derived hard carbon

Polymers can be classified into two main categories: natural and synthetic. These polymers are commonly used as precursors for the synthesis of HC. The presence of aromatic rings in their structures enhances the graphitization of HC. However, the lower porosity of the material results in a decreased SSA, which hampers the enhancement of plateau capacity in the low-voltage region[49]. The main chain structure and spatial arrangements of synthetic polymers can be altered by manipulating monomer species and polymerization processes[50]. The characteristics of polymer-derived carbon materials (PDCMs), including their microstructure, pore structure, and types of defects, are influenced by the choice of precursors. Therefore, it is possible to create PDCMs with controllable microstructure and structure by utilizing appropriate processing techniques[38]. Researchers have employed various polymers, such as

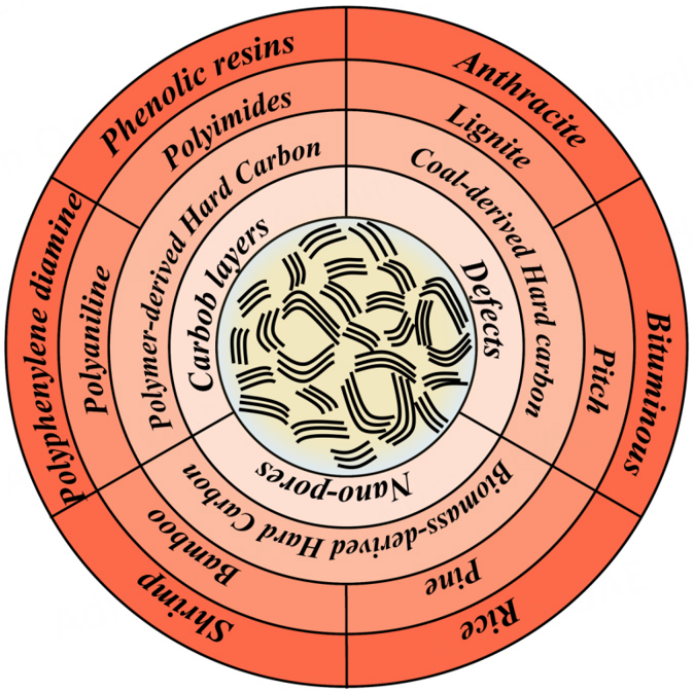

Figure 1. Characterization of different HC precursors and HC structures.

poly(p-phenylenediamine)[38,51], phenolic resins and their derivatives[52-55], and polyimides (PI) and their derivatives[56-58], for the production of PDCMs.

The electrochemical properties of HC materials derived from polymers with different morphologies exhibit variations. Xiao *et al.* synthesized nanometer-sized PANI particles through chemical oxidation using aniline as a precursor and then produced HC nanoparticles (HCNPs) via a one-step pyrolysis process[59]. Their findings indicated that reducing the particle size is an effective approach for enhancing the electrochemical characteristics of bulk HC materials. He *et al.* employed a self-degradation stencil method to fabricate PANI nanotubes incorporated with sulfur[60]. Subsequently, a two-step pyrolysis process converted these PANI nanotubes into HC nanotubes (S/N-CTs) doped with both sulfur and nitrogen. The unique one-dimensional nanotubular structure of S/N-CTs results in an increased SSA, wider spacing between the carbon layers, reduced charge transfer resistance during cycling, and improved reaction kinetics for sodium ions. Consequently, S/N-CTs demonstrate a high specific capacity, excellent cyclic performance, and remarkable long-term stability.

The morphology of HC materials prepared from different polymer precursors varies significantly. Wang *et al.* prepared phenolic resin-derived HC microspheres (PF-HCSs) using hydrothermal and high-temperature carbonization processes[61]. The PF-HCSs possess a perfect spherical structure and an appropriate d_{002}, which facilitates the efficient storage of Na^+. The PF-HCSs carbonized at 1,250 °C achieve a reversible capacity of up to 311 mAh g^{-1} and demonstrate good cycling stability. Han *et al.* synthesized hollow HC nanofibers by pyrolyzing PANI hollow nanofibers (HCNFs)[62]. This material exhibits outstanding electrochemical properties, retaining 70% of its capacity even after 5,000 cycles at 1.6 A g^{-1}. The superior electrochemical performance of HCNFs can be attributed to their distinctive HCNF structure, which forms a three-dimensional interconnected carbon framework. This structure reduces the diffusion path for sodium ions, improves electrode wettability, accommodates volumetric changes during charge-

discharge cycles, provides a continuous pathway for electron transport, and enhances the electronic conductivity of the material. Wang *et al*. synthesized PI using cyclobutane tetracarboxylic dianhydride and diphenylamine via solvothermal methods, and further pyrolyzed it to produce a flower-like porous carbon material[63]. This material features abundant micropores and mesopores, with a large SSA. When assembled into a symmetric cell, it is capable of lighting a light-emitting diode (LED). After one year of storage, its performance slightly declined, indicating potential for practical applications.

Additionally, we summarize some studies on HC derived from waste polymers. Porporato *et al*. successfully prepared HC by directly pyrolyzing two types of discarded masks (after removing the metal parts) under a nitrogen atmosphere[64]. Field emission scanning electron microscopy (FE-SEM) and Raman spectroscopy analyses revealed that the SSA of the produced HC was very low. Electrochemical performance tests showed that HC prepared under such mild conditions (without pre-treatment, low pyrolysis temperature, and short duration) still requires further optimization, but this result validates the potential for high-value applications of disposable masks in SIBs. Chen *et al.* successfully prepared HC materials (named PC-HC and PET-HC) from waste engineering plastics (polycarbonate and polyethylene terephthalate) via high-temperature pyrolysis[65]. The PC-HC and PET-HC prepared at 1,400 °C exhibited the smallest SSAs, with ICE of 84.7% and 86.1%, respectively. They provided reversible capacities of 327 and 342 mAh g^{-1} at 20 mA g^{-1}, with excellent cycling performance. This report offers new insights into the recycling of waste plastics and demonstrates their feasibility as precursors for preparing high-performance HC anodes.

In summary, the morphology of PDCMs is related to the choice of polymer precursors and the synthesis methods used. Generally, PDCMs inherit the intrinsic morphology of the polymer precursors, but the impact of the synthesis strategy cannot be overlooked. Depending on the requirements of different application scenarios, various monomer types and polymerization methods can be selected to prepare polymer materials. Additionally, certain synthesis strategies, such as polymerization techniques, pre-treatment, and electrospinning[66,67], can help us obtain specific morphologies, thereby improving the electrochemical performance of the HC.

Coal-derived hard carbon

The abundant availability of coal resources worldwide, along with substantial reserves, can contribute to reducing the production costs of HC materials, making it feasible for industrial manufacturing applications. However, there is a wide range of coal types, each exhibiting different levels of metamorphism, and most of them contain significant amounts of inorganic impurities. Consequently, the surface chemical composition and morphological structure of HC post-pyrolysis are intricate, making it challenging to optimize its electrochemical properties[68,69].

The complex composition of coal can lead to diverse effects on the properties of coal-derived HC materials, influenced by specific compositions and corresponding contents. Several researchers have delved into this subject.

Zou *et al*. conducted a study where they produced HC materials from lignite through simple pyrolysis at various temperatures[70]. Results showed that the carbonization temperature has a minimal effect on the morphology of HC but significantly influences the microstructure. The authors believe that increasing the carbonization temperature can promote the growth of local microcrystals in HC, leading to a reduction in defect concentration. A decrease in defects results in a lower sodium adsorption capacity, while the intercalation storage capacity of sodium in pseudo-graphitic domains grows, which is beneficial for the intercalation and extraction of sodium ions between graphene layers. Li *et al*. synthesized a variety of HC

materials using coals of different metamorphic levels (anthracite, bituminous, sub-bituminous, and lignite) as precursor materials[50]. The research revealed that the degree of coal metamorphism notably affects the electrochemical properties of HC materials. The lower the degree of coal maturation, the fewer stable aromatic rings in the coal molecule structure, and the more unstable aliphatic side chains. During carbonization, the release of volatiles and the presence of heteroatoms impede the rearrangement of carbon atoms. At a constant carbonization temperature, the capacity slope decreases as the coal's metamorphic level rises. Defects facilitate the adsorption of sodium ions at active sites.

In their reports, Zhao *et al.* effectively synthesized HC materials (PCBCx) from bituminous coal through a pre-oxidation technique[71]. They also investigated how the molecular structure of bituminous coals influences the characteristics of PCBCx. Bituminous coal can be categorized into two distinct molecular structures: vitrinite, containing less stable aromatic rings and more unstable aliphatic side chains, and inertinite, containing more stable aromatic rings. Their research results suggest that the vitrinite group exhibits higher oxidation reactivity than the inertinite group. This leads to the formation of a cross-linked structure during carbonization, resulting in the creation of numerous ultra-micropores, thus enhancing the capacity for electrochemical reactions. On the other hand, the inertinite group significantly influences the graphitization degree of HC. Precursors with a higher inertinite content yield HC materials with increased graphitization and fewer defects.

Biomass-derived hard carbon

Biomass is indeed a plentiful and rapidly renewable resource that is cost-effective. Carbon derived from biomass is known for its high porosity. During the carbonization process, impurity elements such as nitrogen and sulfur that are present in biomass can undergo self-doping, which can be advantageous for improving the reversible capacity of batteries.

However, biomass-derived HC materials often have a significant SSA due to their abundant pore structure. This characteristic can lead to challenges such as low ICE and increased side reactions during the first charging/discharging cycle, resulting in the generation of more irreversible capacity. Moreover, excessively large pore sizes can increase the contact area between the electrode and electrolyte, leading to more side reactions and higher irreversible capacity during the initial charging/discharging cycle. Conversely, pore sizes that are too small can hinder the entry and diffusion of sodium ions[48,49]. The challenges highlighted have hindered the advancement in the commercialization of biomass-derived HC materials. Research has been conducted using diverse biomass feedstocks to develop HC materials for various applications, such as rice husk[72,73], rapeseed[74], pine pollen[41], coconut shells[75], willow branches[76], pine[77], maple[78], lotus stems[79], reed stems[80], mango bark[81], tree bark[82]; shrimp shells[83,84], and waste wool[85].

Plant biomass predominantly contains cellulose, hemicellulose, and lignin. Researchers have extensively studied how various components of biomass play unique roles in the production of solid carbon. Tang *et al.* utilized softwood, yellow sandal, and rosewood as raw materials to produce a range of HC materials with different carbonization temperatures through chemical pre-treatment[86]. During carbonization, cellulose decomposes and forms a graphite-like layer with a specific arrangement, contributing to the creation of closed pores. Hemicellulose and lignin prevent excessive graphitization of graphene sheets at high temperatures by inducing bending and wrinkling, resulting in the formation of additional defects. The resulting material exhibited outstanding electrochemical characteristics, with a reversible capacity of 430 mAh g^{-1} at 20 mA g^{-1} and a plateau capacity of 293 mAh g^{-1} during the second charge-discharge cycle. Wang *et al.* highlighted that removing some lignin from bamboo can increase the number of cellulose free radicals, aiding in the construction of a carbon layer structure with closed pores[87]. However, excessive

removal of lignin can impede the formation of closed pores.

In addition, Gao *et al.* utilized phytic acid and hydrogen peroxide to facilitate the creation of chitin nanosheets and then successfully produced two-dimensional HC nanosheets with a layered porous structure, known as HPCNs, through pyrolysis carbonization[88]. Direct pyrolysis of HPCNs yielded HC materials doped with N and oxygen. N and O atoms were found to enhance active sites in the HC, and improve the wettability of the electrodes, increasing their specific capacity.

Indeed, the selection of precursor materials plays a significant role in determining the microscopic structure of HC materials, which in turn affects their electrochemical characteristics. It is essential to carefully assess and choose precursor materials based on specific criteria to achieve the desired properties in the resulting HC materials.

The synthesis of HC materials involves various techniques beyond the selection of precursors, such as pyrolytic carbonation and hydrothermal carbonization[38]. Pyrolytic carbonation is a common method where the precursor material is heated to a specific temperature in an inert atmosphere such as argon or nitrogen. This process triggers reactions such as dehydrogenation and polycondensation, leading to the formation of HC. It is widely used for producing HC materials due to its effectiveness in controlling the chemical reactions and properties of the final product[89].

On the other hand, hydrothermal carbonization is another technique often utilized for HC material synthesis. This method involves treating precursors at relatively low temperatures, usually below 250 °C, under high-pressure aqueous conditions. It is suitable for producing precursors for HC materials, pre-treating materials, or applying carbon layers on HC surfaces. One distinct advantage of hydrothermal carbonization is its ability to increase the porosity of HC materials, promoting higher carbon generation rates and offering control over the micromorphology of the final product[90].

Both pyrolytic carbonation and hydrothermal carbonization techniques provide researchers with valuable tools for tailoring the properties and characteristics of HC materials to meet specific requirements for various applications. Indeed, the factors mentioned, including synthesis methods, chemical composition, morphology, and thermal stability of precursor materials, all have a significant impact on the final structure of HC materials. Therefore, a thorough evaluation of the structure of HC is essential to optimize the electrochemical characteristics and performance.

MICROSTRUCTURAL PROPERTIES

Carbon atoms can undergo three types of orbital hybridization: sp, sp^2, and sp^3, resulting in the formation of diverse covalent bonds and a wide range of carbon materials. Among these, carbon materials with sp^2 hybridization are generally classified into three main groups: graphite, amorphous carbon, and nanocarbon materials. The variations in crystallization levels and the organization of carbon layers contribute to the distinct physicochemical and electrochemical properties exhibited by these materials. During amorphous carbon, the degree of graphitization is typically low, with a microstructure comprising randomly oriented curved graphite layers that often contain a significant number of flaws. Moreover, amorphous carbon grains are characterized by their small size and the presence of specific heteroatoms. HC materials are a prevalent form of amorphous carbon that cannot undergo graphitization even if the temperatures are beyond 2,800 °C. It is difficult for the structure of HC to transition from short-range order to long-range order[91-96].

Scientists have conducted extensive research on HC materials to unravel their structural characteristics. Figure 2 illustrates various proposed structural models of HC. In 1951, Franklin[97] carried out a report on carbon materials obtained from different sources, which underwent carbonization at temperatures ranging from 1,000 to 3,000 °C. Franklin suggested that carbon can generally be categorized as either graphitized or non-graphitized based on its structural properties. Graphitized carbon originates from precursors rich in hydrogen, where the movement of crystals relative to each other is well preserved during carbonization. The intracrystalline cross-linking is relatively weak, leading to an almost parallel crystal orientation and lower porosity in the material. Non-graphitized carbon is formed from precursors with less hydrogen or more oxygen content. The carbonization process results in strong cross-linking between crystals, creating a highly random crystal orientation and the development of numerous pores. Figure 2A illustrates the structural model of non-graphitized carbon.

With advancements in electron microscopy, the lattice stripe imaging technique has been undergoing continuous refinement. In 1974, Ban[98] proposed that non-graphitized carbon comprises a three-dimensional network structure formed by the bending and intertwining of multiple locally correlated graphite nanoribbons, as illustrated in Figure 2B. However, this model only partially explains the characteristics of non-graphitized carbon, indicating the need for further structural investigations. In 1992, Townsend[99] introduced a computational method for generating graphitic carbon structures on smooth surfaces with a defined number of carbon rings. He termed structures consisting of graphite flakes exhibiting negative Gaussian curvature as "Schwarzite" structures, as depicted in Figure 2C. These graphite sheets can be bent into various shapes such as spheres, cylinders, minimum surfaces, and irregular surfaces. The interlacing bending of these structures contributes to the formation of the final HC material. Additionally, Townsend suggested that amorphous carbon contains a significant amount of sp^2 bonds, and under specific conditions, sp^2 and sp^3 bonds have the ability to interconvert.

In 1997, Harris[100] conducted a study using high-resolution electron microscopy to investigate carbonized carbon materials subjected to temperatures ranging from 2,100 to 2,600 °C. The findings revealed that under high-temperature conditions, the treated materials could form enclosed carbon nanoparticles resembling the structure of fullerenes. Subsequently, Harris proposed a structural model for HC, which comprised distinct fragments resembling the "Schwarzite" structure. HC is believed to contain a significant number of pentagonal carbon rings and a smaller amount of non-hexagonal cyclic carbon. The presence of these pentagonal carbon rings hinders the graphitization process at temperatures as high as 2,800 °C, explaining the resistance of HC to graphitization. This research shed light on the unique structural characteristics of HC, emphasizing the role of pentagonal carbon rings in influencing its properties and behavior at high temperatures.

In 2000, Stevens and Dahn[20] proposed the "House of Cards" structural model, as shown in Figure 2D, while investigating the sodium storage mechanism of HC. They suggested that HC comprises multiple disordered microcrystalline carbon layers that are chaotically arranged and stacked. The material can be divided into two distinct regions: the pseudo-graphitic microcrystalline region, characterized by turbo-stacked layers of graphene, and the amorphous region, consisting of the edges and defects within the graphene layers. This structural model of HC has gained widespread acceptance in the scientific community. In 2016, John[101] conducted an optimization study based on Franklin's non-graphitized carbon model (as shown in Figure 2E). He proposed that under specific carbonation conditions, numerous uniform layers of graphene could be formed in a randomly stacked configuration. These graphene layers, consisting of hexagonal cyclic carbon structures, are typically arranged in a narrow region around 1 to 2 nm in width. The sheets are commonly stacked in groups of three layers to form a fundamental unit. These basic units are further

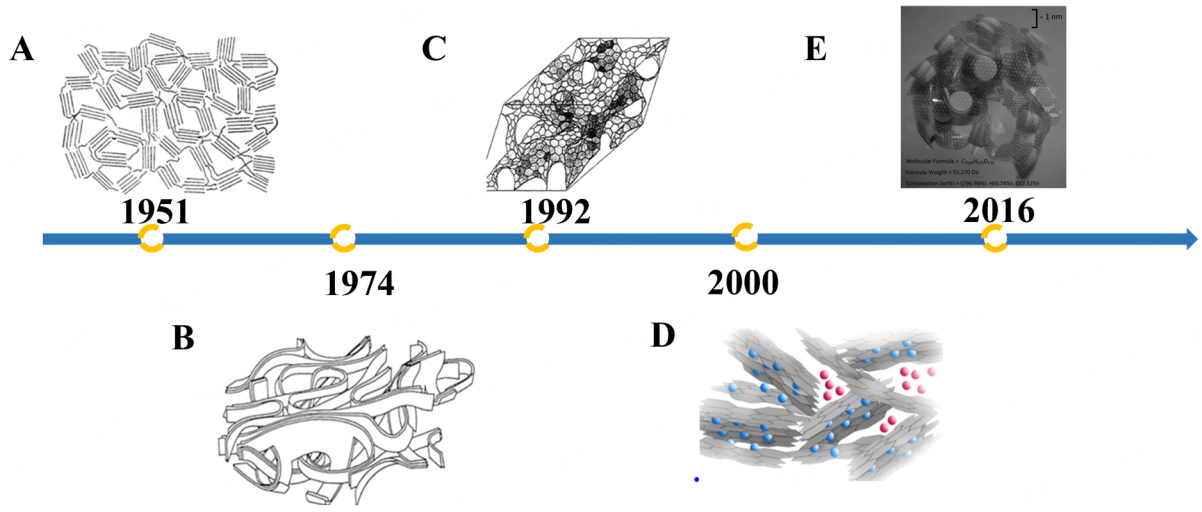

Figure 2. (A) Schematic of the non-graphitized carbon structural model proposed by Franklin in 1951[34] (Copyright 2018, Elsevier Ltd). (B) Schematic of the non-graphitized carbon structural model proposed by Ban in 1974[34] (Copyright 2018, Elsevier Ltd). (C) Schematic of the "Schwarzite" structural model proposed by Townsend in 1992[34] (copyright 2018, Elsevier Ltd). (D) The "House of Cards" model was proposed by Stevens and Dahn in 2000[20] (Copyright 2015, American Chemical Society). (E) The optimization model for Franklin's non-graphitized carbon structure was proposed by John in 2016[101] (Copyright 2016, American Chemical Society).

manipulated, twisted, and interwoven to create the intricate structure of HC. John's work highlighted the potential for generating ordered graphene layers within the chaotic matrix of HC under optimized conditions. By elucidating the structural organization of HC at the nanoscale, researchers can gain insights into its properties and functionalities, paving the way for the development of advanced carbon-based materials for various applications.

To improve the electrochemical performance of HC anodes in rechargeable batteries, researchers have conducted a series of optimization experiments, leading to a more thorough comprehension of the structure of HC.

Pseudo-graphite microcrystals

Sp^2 carbon can be obtained through two methods: directly from natural sources such as coal and natural graphite and through the pyrolytic carbonization of organic precursors in the presence of an inert environment. The process of HC pyrolytic carbonization is a high level of complexity, involving multiple simultaneous reactions such as dehydrogenation, condensation, hydrogen transfer, and isomerization (as depicted in Figure 3A).

During the carbonization process, elements such as hydrogen (H), O, and N are released, leading to the formation of volatile compounds such as water (H_2O), methane (CH_4), carbon dioxide (CO_2), carbon monoxide (CO), and nitrogen gas (N_2). This results in an increase in the carbon content of the remaining material and the creation of numerous pores. When the pyrolytic carbonization process ceases, the solid-phase carbonization process also comes to a halt, marking the completion of HC formation. Throughout the carbonation process, the macromolecular structure of the precursor remains unchanged; therefore, the microscopic structure of HC is primarily influenced by the structure of the precursor[34,102-104].

Carbon materials produced at temperatures near 1,000 °C typically exhibit reduced crystallinity, characterized by broader diffraction peaks and the presence of both organized and turbostratic disordered

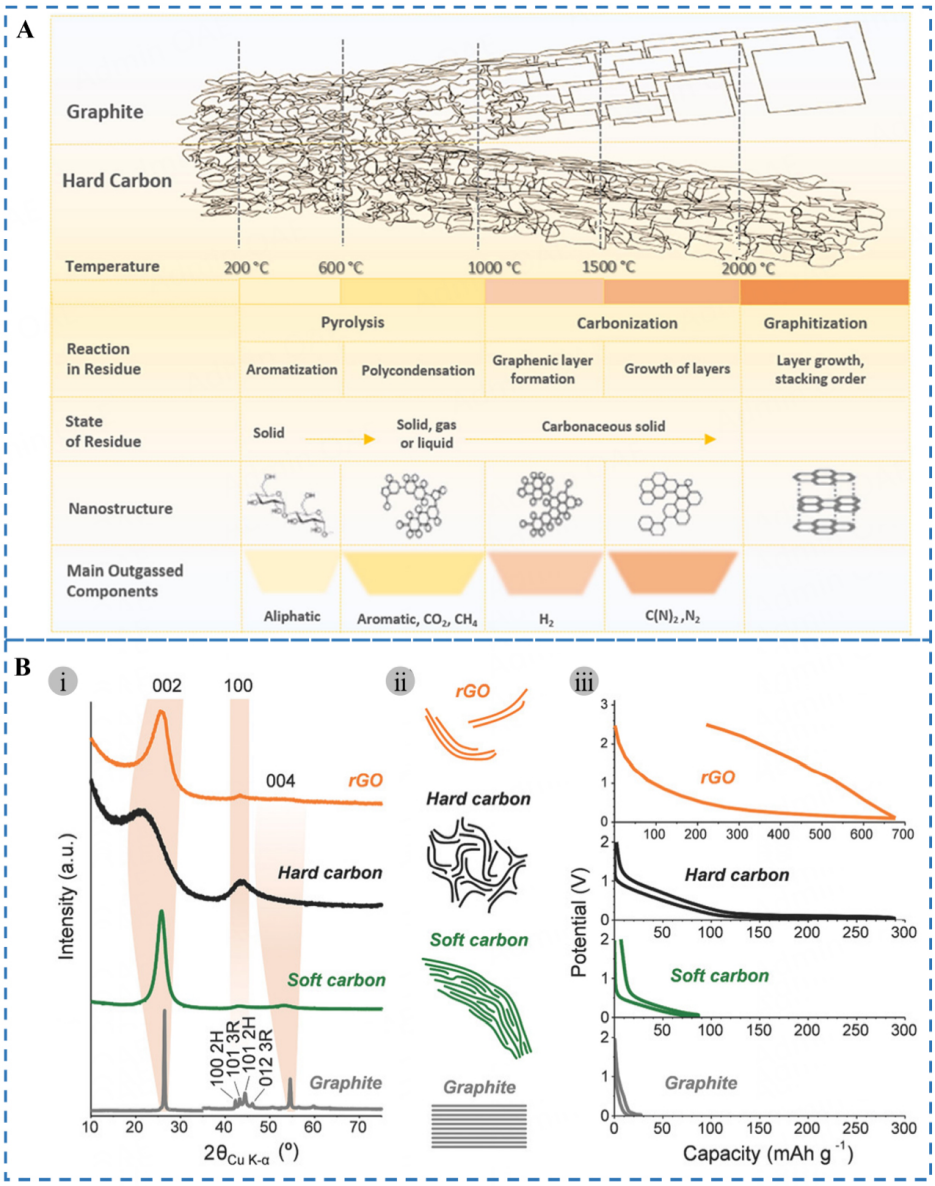

Figure 3. (A) Schematic illustration of the changes in HC precursors with increasing temperature during the pyrolytic carbonization process[34] (Copyright 2018, Elsevier Ltd). (B) (i) Typical XRD patterns (Cu K-alpha source) indexed in 2H graphite referential; (ii) graphical representation of the fine structure; and (iii) typical voltage-charge profiles at the second cycle in sodium half cell of graphite (grey), soft carbon (green), HC (black), and graphene (reduced graphite oxide, orange)[104] (Copyright 2018, WILEY-VCH).

structures resulting from the arrangement of graphene layers. Currently, the graphene layers in soft carbon material are predominantly aligned parallel to one another, with residual crystal defects such as dislocations and tilts, albeit with larger crystal sizes. In contrast, the graphene layers in HC material are arranged in a random fashion, with only a few layers stacked atop each other. This results in a microstructure that is disordered over long distances yet organized over short distances. The X-ray diffraction (XRD) patterns of both soft carbon and HC materials, produced through carbonization at temperatures of 2,500 °C and higher, show significant alterations. As depicted in Figure 3B, the diffraction peaks transition from being broad to becoming sharp and finely defined. This indicates that the internal disorder of the material steadily diminishes and graphitized structure increases over time. As the temperature of carbonization rises, the

degree of crystallinity in HC increases, along with a partial growth in crystal size. However, the overall structure still displays a narrow range of ordered microstructure[104,105].

Experimental evidence has revealed that the arrangement of graphene layers is non-parallel, with defects present in the graphene sheets and a moderate amount of six-membered cyclic carbon contributing to the bending of the sheets. The graphene sheets exhibit an average radius of curvature of approximately 16 Å. The curvature impedes the stacking of sheets in a parallel manner, limiting the level of graphitization and resulting in a highly internally disordered carbon structure. This discrepancy explains why the carbon layer spacing in graphite (0.335 nm) is smaller than that in HC materials (above 0.37 nm)[106].

The diffusion and storage of alkali metal ions during the cycling process are influenced by the interlayer distance of graphene sheets. Olsson *et al.* studied the impact of graphene layer spacing on the diffusion and storage of lithium, sodium, and potassium[107]. Their research revealed that sodium and potassium ions require a larger distance between carbon layers, and the HC anode with wider layer spacing exhibited enhanced effectiveness in storing metal ions. Notably, HC materials with the carbon layer spacing ranging of 3.35 to 6.5 Å are particularly advantageous for metal ion storage. Sun *et al.* have demonstrated that to effectively insert sodium ions into the interlayer and facilitate Na^+ diffusion, it is crucial to regulate the interlayer spacing of the HC carbon layer within the range of 0.37 to 0.40 nm[108].

Reports have demonstrated that incorporating heteroatoms into HC materials can increase the spacing between graphene layers, thereby enhancing the electrochemical performance of the anode. Li *et al.* conducted a study in which they synthesized HC anodes by doping them with phosphorus (P), boron (B), and S atoms using phosphoric acid, boric acid, and sulfuric acid as precursors, with sucrose as the starting material[106]. The electrochemical performance of the batteries significantly improved after testing. Doping P and S in HC materials results in an expansion of the interlayer space of graphene, leading to an enhanced plateau in the low-voltage region and increased capacity in that range. Introducing P and B doping generates more defects, improving the rate capacity in the high-voltage region. Biomass contains a variety of impurity elements that can be utilized to create self-doped HC materials. Wu *et al.* employed a direct pyrolysis method to produce a cost-effective, naturally potassium-doped HC anode[75]. The high potassium content increased the distance between carbon layers, enhancing the diffusion kinetics of sodium ions and boosting the sodium storage capacity of the HC material. This approach demonstrated exceptional electrochemical performance, and it is crucial to guide while preparing self-doped HC made from biomass.

L_a, L_c, and d_{002} are key structural characteristics of HC materials. The degree of graphitization in HC directly influences the dimensions of L_a and L_c. Generally, a higher degree of graphitization results in larger L_a and L_c sizes[75,109]. L_a represents the average width of the graphene layer along the a-axis, L_c indicates the thickness of the stacked graphene layers along the c-axis, and d_{002} is the spacing between adjacent graphene sheets. Elevated temperatures during pyrolysis contribute to the production of more graphitized HC materials as higher graphitization typically requires higher activation energy. Increasing the temperature of pyrolytic carbonization can enhance both L_a and L_c dimensions in HC materials, facilitating the storage of sodium ions and consequently boosting the plateau capacity. Reports have shown that enlarging L_a size improves the reversible capacity of the HC anode; however, it may impede the movement of metal ions between graphene layers[108,110].

Kubota *et al.* conducted an experiment using sucrose as a carbon source to produce a series of HC materials at varying pyrolysis temperatures[111]. They analyzed different characteristics of the graphene sheets, including planar dimensions, number of stacked layers, defects, pores, and layer spacing and findings

revealed that as the pyrolysis temperature increased, the defect concentration in the HC decreased. With higher temperatures, the layer spacing between stacked graphene sheets reduced, the number of stacked layers increased, the planar dimensions expanded, and the pore size enlarged, indicating enhanced graphitization of the HC material.

Alvin *et al.* created HC from lignocellulosic biomass through a two-step carbonization process using fir wood as the initial material[112]. The amorphous carbon was initially produced using low-temperature pyrolysis and subsequently subjected to high-temperature carbonization to provide highly graphitized HC. Currently, the size of the planar crystal in the graphene sheets of HC has increased, whereas the volume of micropores has reduced. The two-step carbonization process effectively suppresses micropore formation, leading to optimal electrochemical performance in the HC anode when there is a balance between graphitization degree and internal defect sites. Gomez-Martin *et al.* synthesized various HC materials using olivine as a carbon source at temperatures ranging from 800 to 2,000 °C[113]. Their research revealed that in the range of 1,200 to 1,600 °C, the internal structure of the HC underwent rearrangement. During this rearrangement, the spacing between graphene sheet layers gradually increased, peaking at 1,400 °C, and then slowly decreased. This trend aligns with the variation in reversible capacity, suggesting that an increase in the size of L_a, representing the graphene sheet layers, leads to a decrease in slope capacity.

Defects

Graphene sheets in HC materials can exhibit two main categories of defects. The first type is inherent defects, which are present in the crystal structure independent of external influences. These defects often involve sp3 hybridized carbon and encompass point defects (such as "Stone-Wales" defects), dislocations, grain boundaries, and the curvature of graphene sheets. The second category is extrinsic defects, which arise from non-carbon atoms, such as impurity atom substitutions or oxygen functional groups, typically found at the edges and vacancies of the material. Defects demonstrate dynamic behavior and can migrate over time. The migration process significantly influences the characteristics of crystal defects, with the migration behavior often dictated by the activation energy barrier of the defects. Moreover, this behavior shows a positive exponential relationship with temperature[114,115].

Multiple methods are utilized for characterizing defects in HC materials. Raman scattering and total neutron scattering, along with their corresponding pair distribution functions, are common techniques for assessing defect quantities. Electron paramagnetic resonance (EPR) is particularly sensitive to vacancies in HC materials and can accurately track changes in vacancy numbers when the materials have consistent volumes. Temperature-programmed desorption combined with mass spectrometry is employed to detect internal defects in HC materials that may be challenging to identify through alternative approaches[110,116,117].

Several reports have highlighted the positive impact of incorporating defects in graphene flakes on the performance of sodium storage. Chen *et al.* synthesized an oxygen-doped HC material using buckwheat hulls[118]. Their first-principles study illustrated that the presence of oxygen atoms enhances the sodium storage capabilities of HC, and the oxygen-containing groups and defect sites promote the adsorption of sodium ions. Sun *et al.* employed *in-situ* engineering techniques to develop a range of HC materials with adjustable levels of oxygen doping and defects[119]. Through theoretical modeling and Raman spectroscopy, they revealed that oxygen-functional groups significantly influence the formation of the SEI film. Guo *et al.* prepared HC materials with varying defect concentrations using a templating method with glucose as the carbon source[120]. Analysis of the material's microstructure and electrochemical properties indicated that inherent defects in HC contribute to enhanced surface adsorption of sodium ions during capacitance, with the quantity of adsorbed sodium ions increasing proportionally with defect concentration. Li *et al.* utilized

microwave technology to generate a high-defect concentration HC material and compared it to HC produced via conventional pyrolysis[13]. Microwave treatment preserved voids in the HC microstructure effectively, leading to energy conservation. High defect concentration in HC materials can enhance the slope capacity, but it is just one of the factors influencing battery capacity. In addition, excellent ionic and electrical conductivity is necessary for increased capacity, which explains why HC materials with large defect concentrations have lower capacity.

In summary, the existence of defects in HC materials, such as vacancies, oxygen-containing functional groups, and impurity atoms, can enhance their electrochemical activity by creating numerous active sites for sodium storage. This enhancement can lead to an overall improvement in their electrochemical performance. However, the presence of flaws can also lead to electrolyte decomposition, secondary reactions, irreversible damage of sodium ions, and other issues, ultimately resulting in reduced ionic conductivity and a decline in cycling capabilities[14,114].

Nanopores

HC materials are characterized by a high density of nanopores, including both open and closed porosity, which generally contributes to their large SSA. Various techniques, such as transmission electron microscopy (TEM), gas isothermal adsorption-desorption measurements, and SAXS, are utilized to characterize the pore structure, distinguishing between open and closed porosity. Typically, increasing the pyrolysis temperature is associated with a decrease in pore volume[113].

The pore structure of HC plays a crucial role in the electrochemical performance of SIBs[121], with closed pores particularly influencing the plateau capacity. It is now understood that the storage of Na^+ in the low-voltage (< 0.1 V) plateau region is predominantly due to the formation of quasi-metallic sodium clusters within the closed pores of HC[19]. The impact of pore structure on the electrochemical properties of HC has been extensively studied. For instance, Xie *et al.* created a hard-soft carbon composite by combining the advantages of a HC precursor with a soft carbon precursor using filter paper and asphalt at a relatively low pyrolysis temperature of 1,000 °C[122]. This approach not only reduces the production cost of the electrode but also results in the formation of closed pores during pyrolysis, which assists in preventing the irreversible loss of sodium ions due to the formation of the SEI film. Furthermore, it provides numerous sites for sodium storage, thereby enhancing the capacity. The report also demonstrated that the size of the closed pores is directly correlated with the plateau capacity, a conclusion that was also reached by Zhang *et al.*[123]. Similarly, Lu *et al.* utilized the sodium chloride stencil method to develop a low-cost bitumen-derived HC with a specific pore structure[124]. They found that the open macroporous structure improves the wettability of the electrode, reduces the distance for sodium-ion migration, increases the number of active sites for sodium storage, and optimizes the reversible capacity and rate performance.

Yang *et al.* pioneered a melt-dispersed carbonization technique to create a HC material with extremely small pores (0.3~0.5 nm) by utilizing activated carbon and perylene-3,4,9,10-tetracarboxylic dianhydride (PTCDA)[125]. Through *in-situ* XRD testing, it was revealed that these ultra-micropores exhibited selective permeability, allowing only bare sodium ions to penetrate while blocking solvated sodium ions. These specialized pores provided abundant active sites for sodium storage, leading to improved battery capacity and enhanced cycling and rate capabilities. Alptekin *et al.* conducted the research where they synthesized various HC materials across a temperature range of 1,000 to 1,900 °C[126]. Their investigations using techniques such as TEM, SAXS, and others unveiled that the sodium-ion capacity within graphene sheets increased as the interlayer spacing expanded. Furthermore, the presence of oxygen-containing functional groups was found to boost the capacity in the slope region. It was also noted that higher pyrolysis

temperatures resulted in an increase in both the number and size of closed pores. The report highlighted that closed pores enhance the proportion of the plateau capacity within the total capacity, reaching levels of up to 75%, and the existence of closed pores was found to restrict electrode volume expansion in the cycling process.

Dahbi *et al.* conducted a comprehensive study to investigate the structural characteristics of HC materials carbonized at varying pyrolysis temperatures[127]. They established a direct relationship between the capacity enhancement and the size of micropores responsible for sodium storage, highlighting the influence of pyrolysis temperature on this correlation. In a separate study, Au *et al.* synthesized a series of HC materials using hydrothermal and high-temperature pyrolysis methods, employing glucose as a carbon source[128]. The study unveiled a clear connection between the presence of quasi-metallic sodium filling within the plateau region's pores and the pore size. It was observed that as the pore size increased, the plateau capacity also showed a corresponding increase. Yamamoto *et al.* proposed that the degree of cross-linking in HC itself played a significant role in determining pore size[129]. Their research found that pre-oxidizing cellulose at temperatures ranging from 275 to 300 °C enhanced the level of dehydration and cross-linking in the precursor, subsequently influencing the microstructure of HC. The dehydration process facilitated the formation of covalent bonds, leading to an expansion in pore size by widening the distance between graphene sheets, ultimately enhancing the material's reversible capacity. However, it was noted that the relationship between pore size and capacity was not linear, with the capacity exhibiting a gradual decrease at pyrolysis temperatures exceeding 1,500 °C.

Researchers and academics have highlighted the crucial role of pores, especially closed pores, in influencing the capacity of the plateau region. Nevertheless, managing the pore structure of HC, which encompasses factors such as size, shape, and pore condition, proves to be difficult due to its inherent complexity. Therefore, there exists a need for a more systematic and comprehensive exploration of closed pores to enhance our understanding of their impact on material performance.

STRATEGIES FOR THE PREPARATION OF CLOSED PORE STRUCTURES

As shown in Figure 4, there are many methods for preparing closed pores, which can be broadly categorized into direct pyrolysis and others. Direct pyrolysis is commonly used to carbonize precursors with inherent porous structures and can be divided into two main types: conventional pyrolysis employing a tube furnace and microwave pyrolysis utilizing a microwave tube furnace.

In addition to direct pyrolysis, alternative techniques include the template-assisted approach, physical treatment methods, and chemical treatment methods, among others. By subjecting the precursor to specific treatments, a significant number of open pores are generated either on the surface or within the precursor material. Subsequently, during the high-temperature pyrolysis step, these open pores transform into closed pores, leading to the formation of HC materials containing a substantial quantity of closed pores.

Direct pyrolysis method

During the carbonization process, precursors typically release volatile chemicals such as H_2O and CO_2, leading to the formation of open pores. As the temperature rises, graphene flakes undergo rearrangement to create closed pores. Additionally, a large portion of the resulting HC material retains the original structure and morphology of the precursors. Effective synthesis of HC with abundant pore structures can be achieved by directly pyrolyzing suitable precursors, with this pyrolysis process typically categorized into conventional and microwave methods based on the equipment utilized.

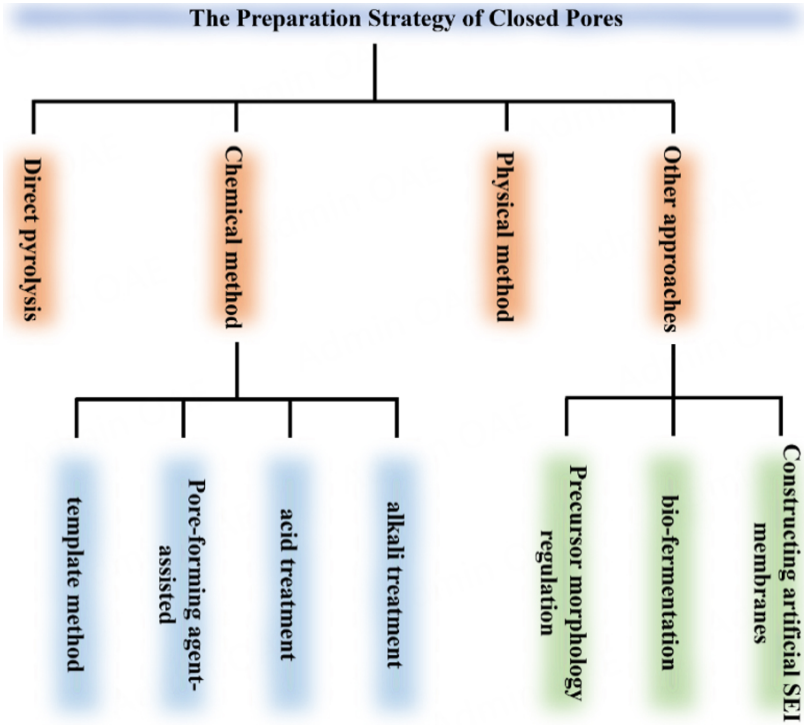

Figure 4. Strategies for the preparation of closed pore structures in HC.

HC possesses the characteristic of preserving the initial shape of its precursor. When precursors featuring a porous structure undergo direct pyrolysis, this commonly results in the generation of HC with a considerable number of closed pores. For instance, Zhang *et al.* conducted the direct pyrolysis of lotus stems, successfully maintaining the inherent macroporous structure of the lotus flower in the resulting HC material[130]. Increasing the carbonization temperature from 1,200 to 1,600 °C led to enhanced graphitization of the HC material, accompanied by a decrease in SSA and pore volume. The predominant pores present were mesopores, with sizes ranging from approximately 2 to 4 nm. Moreover, the proportion of closed pores exhibited an initial rise followed by a decline, with values of 37.7%, 66.4%, and 42.7%, respectively. HC material carbonized at 1,400 °C demonstrated the highest density of closed pores, showcasing superior sodium storage performance. It achieved a plateau capacity of 250 mAh g^{-1} at 100 mA g^{-1} and maintained an impressive capacity retention rate of 94.2% after 450 cycles. This exceptional electrochemical performance can be attributed to the numerous enclosed pores capable of accommodating quasi-metallic sodium clusters.

Liu *et al.* conducted a study where they produced HC anodes (denoted as HC-T, with T representing the carbonization temperature) by directly heating eucalyptus wood blocks at various temperatures (700, 900, 1,100, and 1,400 °C) in an argon atmosphere[131]. The resulting HC materials maintained the original hierarchical and porous structure of the wood blocks. Structural and morphological analysis of the HC revealed that as the carbonization temperature increased from 700 to 1,400 °C, the pore volume expanded from 4.93 to 5.57 nm. Concurrently, the SSA decreased from 352.06 to 6.64 $m^2 g^{-1}$, and the pore volume decreased from 0.17 to 0.011 $cm^3 g^{-1}$. Experimental findings suggest that elevating the carbonization temperature promotes the formation of HC materials with increased graphitization. Moreover, the porous structure inherited from the precursor material facilitates the formation of more closed pores.

Huang *et al.* demonstrated a method to obtain HC materials with closed pores by leveraging the evaporation of certain components of specific precursors during pyrolysis[132]. They successfully synthesized a range of HC materials with different carbonization temperatures (HAHC-T, with T representing the carbonization temperature) using sulfanilamide phenylpropanoid. Through thermogravimetric analysis, it was observed that the precursors melted at around 200 °C, resulting in a gradual reduction in the number of open pores. Between 350 and 450 °C, S, N, and other heteroatoms in the sulfonamide were released as volatile substances, leading to the generation of small pores and defects. Additionally, during the carbonization process at temperatures exceeding 800 °C, the alignment of graphene sheets underwent changes, giving rise to a complex structure with closed pores. As the carbonization temperature increased, the SSA of HAHCs decreased from 163.4 to 17.12 $m^2 g^{-1}$. Meanwhile, the pore diameter expanded from 2.11 to 8.13 nm, accompanied by an increase in the volume of closed pores. This observation corresponds to the previously discussed "house of cards" structural model, illustrating that the plateau's capacity is linked to the storage of sodium ions in enclosed pores. Moreover, a higher volume of closed pores contributes positively to enhancing the plateau capacity.

Given the ability to achieve the necessary closed pore structure by choosing alternative precursors, is it feasible to obtain a preferable HC by subjecting the same precursor to various pyrolysis equipment?

Zhang *et al.* conducted a study on the synthesis of HC materials from poly(terephthalate) (PET) at a reduced temperature of 900 °C using various pyrolysis techniques, including conventional and microwave pyrolysis[133]. The research aimed to explore the feasibility of achieving a preferable HC by subjecting the same precursor to different pyrolysis equipment. The results revealed that the carbonization process of PET involves complex chemical reactions, including the breaking of the benzene ring, hydroxyl group, and methylene group, followed by polycondensation and rearrangement. This series of reactions releases gases such as carbon monoxide and carbon dioxide, leading to the formation of HC with a cross-linked structure. PET, being an efficient wave absorber, exhibits a distinct dielectric reaction that occurs when subjected to microwave pyrolysis, which accelerates the decomposition of molecular chains and creates numerous holes. In contrast, conventional pyrolysis results in HC with a porous structure, known as TF-HC, while microwave pyrolysis produces HC with a significant proportion of closed pores, termed MW-HC. Analysis of the HC materials indicated that the MW-HC samples possessed a notably higher volume of closed pores (0.036, 0.098, 0.139 $cm^3 g^{-1}$) compared to the TF-HC samples (0.027, 0.062, 0.089 $cm^3 g^{-1}$). Moreover, the volume of closed pores increased with pyrolysis temperatures. Microwave pyrolysis was found to accelerate the process and reduce oxygen loss, resulting in a higher oxygen concentration in MW-HC compared to TF-HC. Specifically, MW-HC carbonized at 900 °C exhibited a reversible specific capacity of 344 mAh g^{-1}, attributed to its abundance of closed pores, demonstrating excellent cyclic stability.

Numerous studies have been carried out to produce HC materials with a substantial concentration of closed pores through the direct pyrolysis of diverse precursor materials. Examples include the direct pyrolysis of mixtures containing melamine and terephthalaldehyde[134], pine wood blocks[77], poly (ethylene dibenzoate) (PER), and terephthaloyl chloride (TPC)[135]. It is important to highlight that the HC materials derived from various precursors display notable differences in their pore structures. Precursors that inherently have a porous structure or can generate volatile substances to form pores during subsequent high-temperature pyrolysis are more suitable for using direct pyrolysis to create closed pores. Of course, special synthesis strategies (such as microwave direct pyrolysis of absorbent materials) can also aid in constructing closed pores. Direct pyrolysis is simple and easy to operate and can help reduce the production cost of HC to some extent. However, it has specific considerations and necessitates the screening of precursors.

Physical treatment method

The physical method usually entails carbonizing the precursor in an inert atmosphere to remove impurities, followed by the utilization of a suitable oxidative gasification agent (such as O_2, CO_2, or steam) at temperatures ranging from 600 to 1,200 °C to further carbonize the material. This procedure ultimately results in the generation of numerous closed pores.

Yuan[136] discovered that pitch-derived HC carbonized in oxygen contains a large number of closed pores (as shown in Figure 5A). The plateau capacity is significant, and quasi-metallic sodium clusters are present. Subsequently, some researchers[137] successfully introduced oxygen-containing functional groups into HC by using oxygen as an oxidizing gasifier (as shown in Figure 5B). They then investigated the relationship between oxygen functional groups and the HC structure. The outcomes indicated that the planar cross-linking structure, created by the thermally stable C-O structure, causes a slight movement of the carbon layer in the planar direction, leading to the formation of graphene sheets in short-range order. In contrast, the three-dimensional cross-linking structure, formed by the C(O)-O structure, effectively inhibits the rearrangement of carbon atoms during the initial pyrolysis stage. This structure converts into gas and gives rise to smaller graphite microcrystals during the subsequent carbonization process, thereby facilitating the development of closed pores. The HC-325-9 material exhibits a SSA of 367.94 $m^2 g^{-1}$, a closed pore volume of 0.0618 $cm^3 g^{-1}$, and a reversible capacity of 300.83 mAh g^{-1} at 20 mA g^{-1}. These results corroborate Yuan's findings and provide fresh insights into HC structure adjustment.

As shown in Figure 5C, a starch-derived HC material (HCMP-CO_2) with abundant closed pores was also synthesized using the CO_2 etching method[138]. The experimental results illustrated that CO_2 has the ability to create a substantial number of unobstructed pores within the carbon structure, which were subsequently converted into closed pores during high-temperature carbonization. The utilization of CO_2 etching effectively regulated the size and volume of the closed pores. Specifically, the diameter of the closed pores increased from 3.82 to 4.86 nm, while the corresponding volume expanded from 0.045 to 0.117 $cm^3 g^{-1}$. An impressive SSA value of 562.8 $m^2 g^{-1}$ was achieved, indicating that the open pores generated through etching were largely transitioned into closed pores. The CO_2 etching process is simple and convenient, making it suitable for industrial production and offering a wide array of potential applications.

Chemical treatment method

By incorporating templates or pore-forming agents into the precursor or by chemically treating the precursor in advance, it is frequently observed that the number of closed pores in HC materials increases.

Template method

The template method is a highly efficient technique for synthesizing porous carbon materials. By adjusting the size of the template, it is possible to regulate the internal pore size and distribution of the resulting material. This method is commonly divided into the soft template method, hard template method, and self-template method[139].

Zinc oxide, zinc acetate, zinc gluconate and various other substances can act as templates for controlling the pore size of materials. For example, Qiu *et al.* used zinc gluconate as both a precursor and a template to construct closed pores through a one-step pyrolysis and elucidated the mechanism of closed pore formation[140]. The authors analyzed the pore structure of glucose acid zinc-derived HC anodes (ZGHCx, where x = 1,100, 1,300, 1,500, 1,600 °C) prepared at different carbonization temperatures using N_2 adsorption/desorption isotherms, SAXS, and true density measurements. The SSAs of ZGHC1100, ZGHC1300, ZGHC1500, and ZGHC1600 are 865.7, 583.4, 9.31, and 12.55 $m^2 g^{-1}$, respectively, with corresponding the volumes of open pores of 0.360, 0.249, 0.015, and 0.012 $cm^3 g^{-1}$, and the SSA and volumes

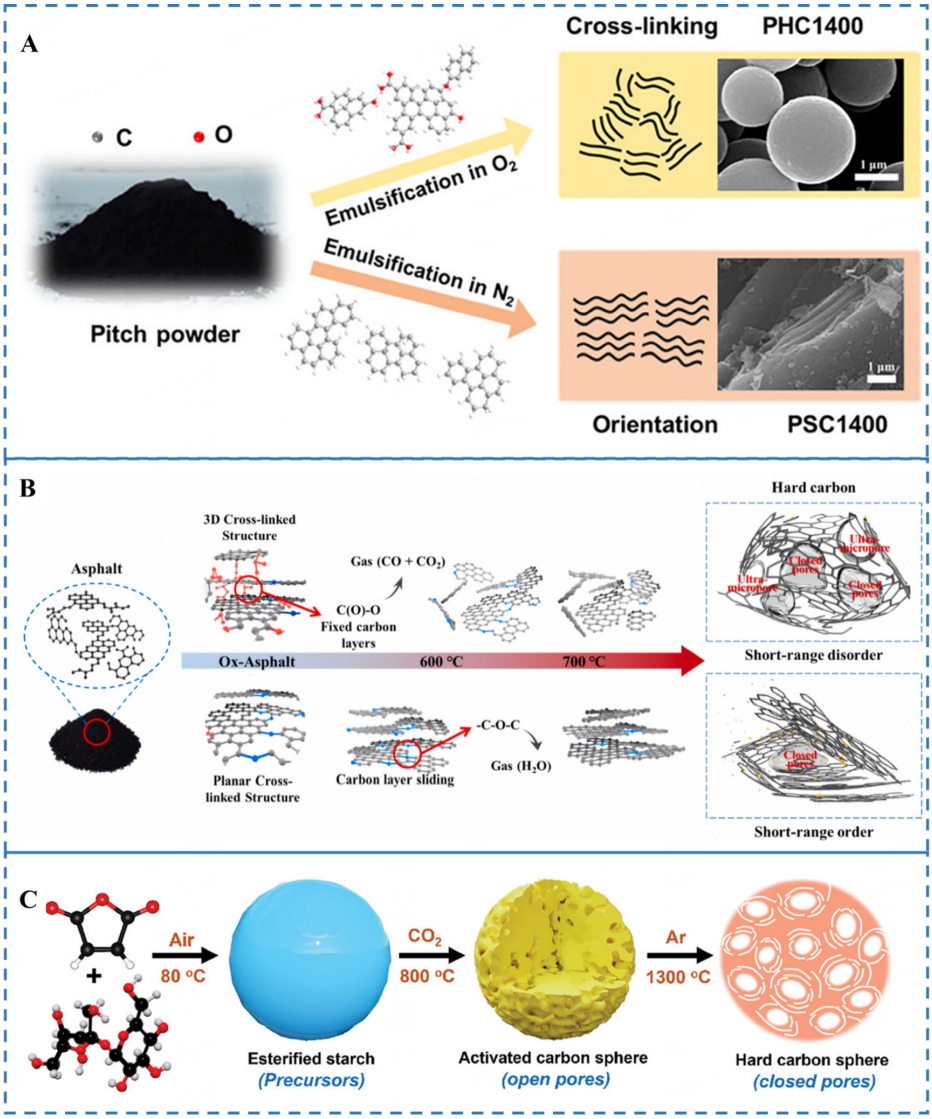

Figure 5. HC with a large number of closed pore structures prepared by physical treatment. (A) Schematic illustration of the structural evolution process of PHC and PSC[136] (Copyright 2022, American Chemical Society). (B) The effects of the oxygen functionalities on the evolution of carbon structure of 325-12 during carbonization[137] (Copyright 2023, Elsevier Ltd). (C) Schematic of the synthesis of HCMP-CO_2[138] (Copyright 2023, Wiley-VCH).

of closed pores are 379.5, 763.1, 1,008.2, and 1,033.0 $m^2 g^{-1}$ and 0.041, 0.054, 0.104, and 0.110 $cm^3 g^{-1}$, respectively. When x < 1,500 °C, the SSA and the volume of open pores of ZGHCx decreased sharply with increasing carbonization temperature. For x > 1,500 °C, the volume of open pores approached 0, while the SSA of closed pores gradually increased with temperature. The process of closed pore formation is illustrated in Figure 6A. ZGHC1500, with its abundant closed pores, has a sodium storage capacity of 481.5 mAh g^{-1}, with a high plateau capacity of up to 389 mAh g^{-1}.

Indeed, certain specific substances can act as templates. As shown in Figure 6B, Glatthaar *et al.* employed the deblock copolymer poly (epoxy resin)-bis-poly (n-hexyl acrylate) (PEO_n-b-PHA_m) as a template for producing lignin-derived HC materials[141]. The PEO_n-b-PHA_m template played a crucial role in creating pores within the HC, ranging in diameter from 20 to 50 nm. The pore structure of the HC materials was

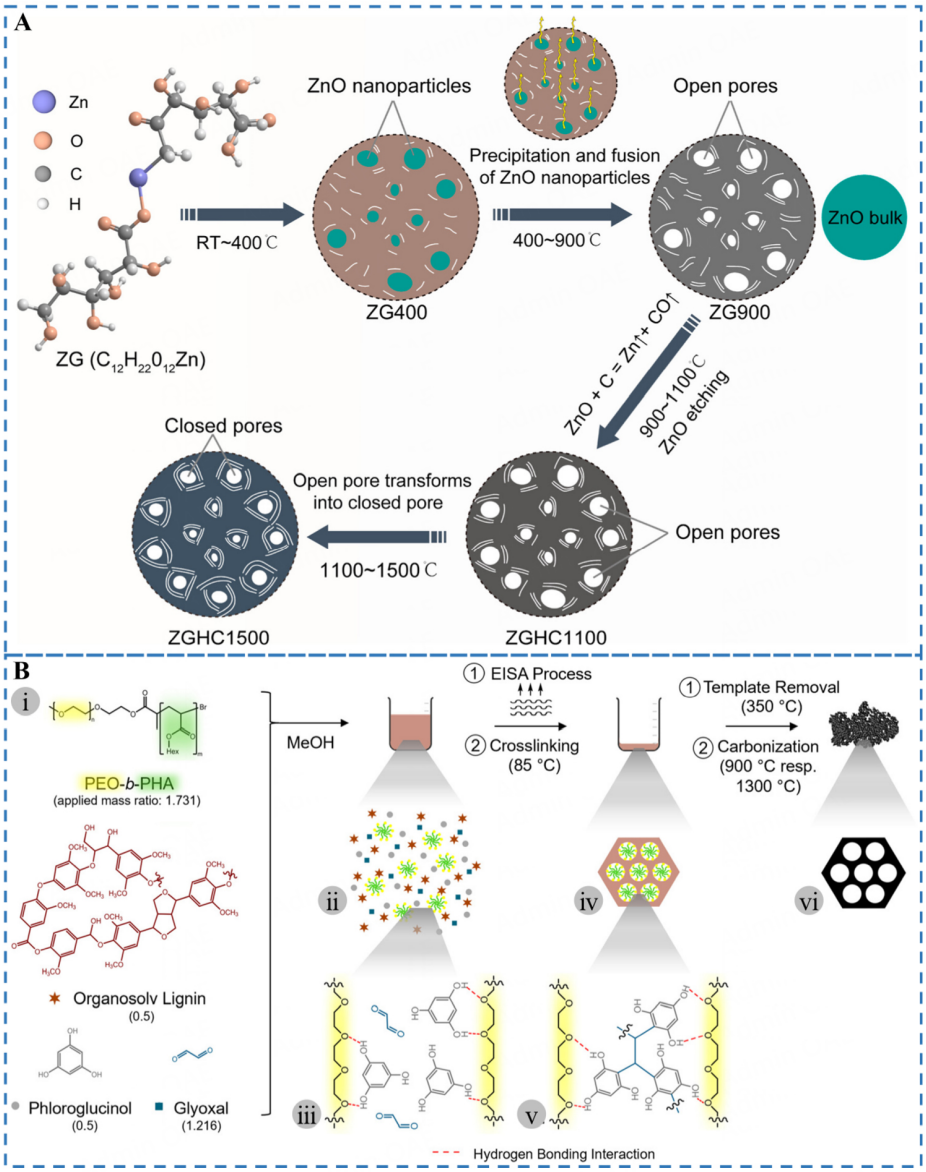

Figure 6. (A) Schematic diagram of the closed-pore formation mechanism in the pyrolysis process of ZG[140] (Copyright 2024, American Chemical Society). (B) Schematic synthetic procedure at macroscopic and molecular level. (i) Molecular structure of PEO_n-b-PHA_m block copolymers. (ii) Schematic representation of initial precursor dispersion with fixed mass ratios of template, carbon precursors, and aqueous glyoxal solution (1.731:1:1.216). and (iii) molecular assembly due to hydrogen bonding interaction. Furthermore, (iv) ordered mesophase after the EISA process and thermopolymerization with (v) the resulting covalent bonding. (vi) Mesoporous carbon after carbonization at 900 °C, respectively 1,300 °C, in a nitrogen atmosphere[141] (Copyright 2023, American Chemical Society).

assessed using SAXS and wide-Angle X-ray Scattering (WAXS). SSA of the HC materials, prepared with various templates, was determined to be 326, 496, 571, and 145 $m^2 g^{-1}$. These values corresponded to the templates used: template-less, F-127, PIB_{50}-b-PEO_{45}, and PEO_{428}-b-PHA_{265}, respectively. Open pores in the electrode can lead to electrolyte decomposition and a reduction in ICE. Maintaining d_{002}, at 3.5~3.6 Å, directly influences the plateau capacity, which is closely related to the size of closed pores. Additionally, the presence of closed pores can effectively inhibit excessive graphitization of HC during the carbonization process.

Moreover, templates such as ZnO[142], K_2CO_3[143], and $MnCl_2$[144] can be utilized to aid in the synthesis of HC materials with a substantial number of closed pores. Although the template method can improve the material's capacity, the removal of templates is complex and time-consuming[137].

Pore-forming agent method

Pore-forming agents are typically defined by their small size, low polymerization level, and ability to penetrate the material's interior. They can generate volatiles that are released or interact with the material's interior during hydrothermal or high-temperature pyrolysis, ultimately resulting in the formation of enclosed pores[145,146].

Ethanol is frequently used as a pore-forming agent. As shown in Figure 7A and B, in a report conducted by Meng *et al.*, ethanol was added as a pore-forming agent to phenol formaldehyde resin[145]. Through solvent heat treatment and high-temperature pyrolytic carbonization, they successfully prepared a high-capacity HC anode material. The different ratios of phenol formaldehyde resin to ethanol used were 1:1, 2:1, 8:1, and 1:0, while the carbonization temperatures were 1,200, 1,400, and 1,550 °C. It was discovered that ethanol can expedite the solidification of phenol formaldehyde resin and promote the formation of small openings in the cross-linked structure of phenol formaldehyde resin. The inclusion of ethanol does not have a notable impact on the degree of graphitization of HC materials, but it can regulate the closure of pores. The random configuration of curved graphene sheets results in the formation of enclosed pores with a dimension of less than 2 nm. The SSA for the resulting HC materials is 0.26 $m^2 g^{-1}$. When the volume ratio of phenol formaldehyde resin to ethanol increases, the SSA of the HC material decreases from 390.84 to 0.39 $m^2 g^{-1}$ at the same carbonization temperature. Similarly, when the carbonization temperature grows, the SSA of the HC material decreases from 33.4 to 1.44 $m^2 g^{-1}$, even with the same amount of ethanol added. The number of closed pores rose in proportion to the ethanol concentration. When the volume ratio of ethanol to phenol-formaldehyde resin is 2:1, the HC-21-1400 anode exhibits the best electrochemical performance, with a specific capacity of 410 mAh g^{-1} (plateau capacity accounts for 70%) and an ICE of 84%.

Additionally, some researchers have utilized the currently popular carbon dots (CDs) as agents that produce pores. As shown in Figure 7C and D, Huang *et al.* synthesized PI through solvent-thermal treatment using benzidine and N,N-dimethylformamide (DMF)[146]. They incorporated varying amounts of CDs as pore-forming agents and successfully produced a range of PI-xCDs composites. These composites were made through high-temperature pyrolytic carbonization resulting in PNDCs-xCDs. Here, x represents the mass of CDs, ranging from 50 to 750 mg. The materials containing CDs exhibit a significant quantity of micropores, each with a diameter smaller than 2 nm. There exists a direct relationship between the pore structure and the quantity of added CDs. When a small amount of CDs is added, ultra-micropores (< 1 nm) are formed; increasing the amount of added CDs leads to a rise in pore size. The SSA of the HC composites, including PNDCs (HC manufactured without CDs), PNDCs-500CDs, and PNDCs-500CDs-1,200 °C, was 195.7, 181.3 and 17.4 $m^2 g^{-1}$, respectively. Additionally, the pore volume fell from 0.1393 to 0.08284 $cm^3 g^{-1}$. PNCDs-500CDs-1,200 °C exhibits the highest ICE (68.4%) and plateau capacity (134 mAh g^{-1}), which is inversely correlated with the SSA and pore volume. The rise in carbonization temperature led to a significant reduction in the open pores of the materials. This phenomenon can be attributed to the formation of graphene sheets and the transition of the open pores into closed pores. Closed pores play a crucial role in preventing direct contact between the electrolyte and the electrode, thereby hindering the formation of SEI film and enhancing the ICE. Additionally, closed pores serve as active sites that are filled with sodium ions, leading to a substantial improvement in the sodium storage performance of HC.

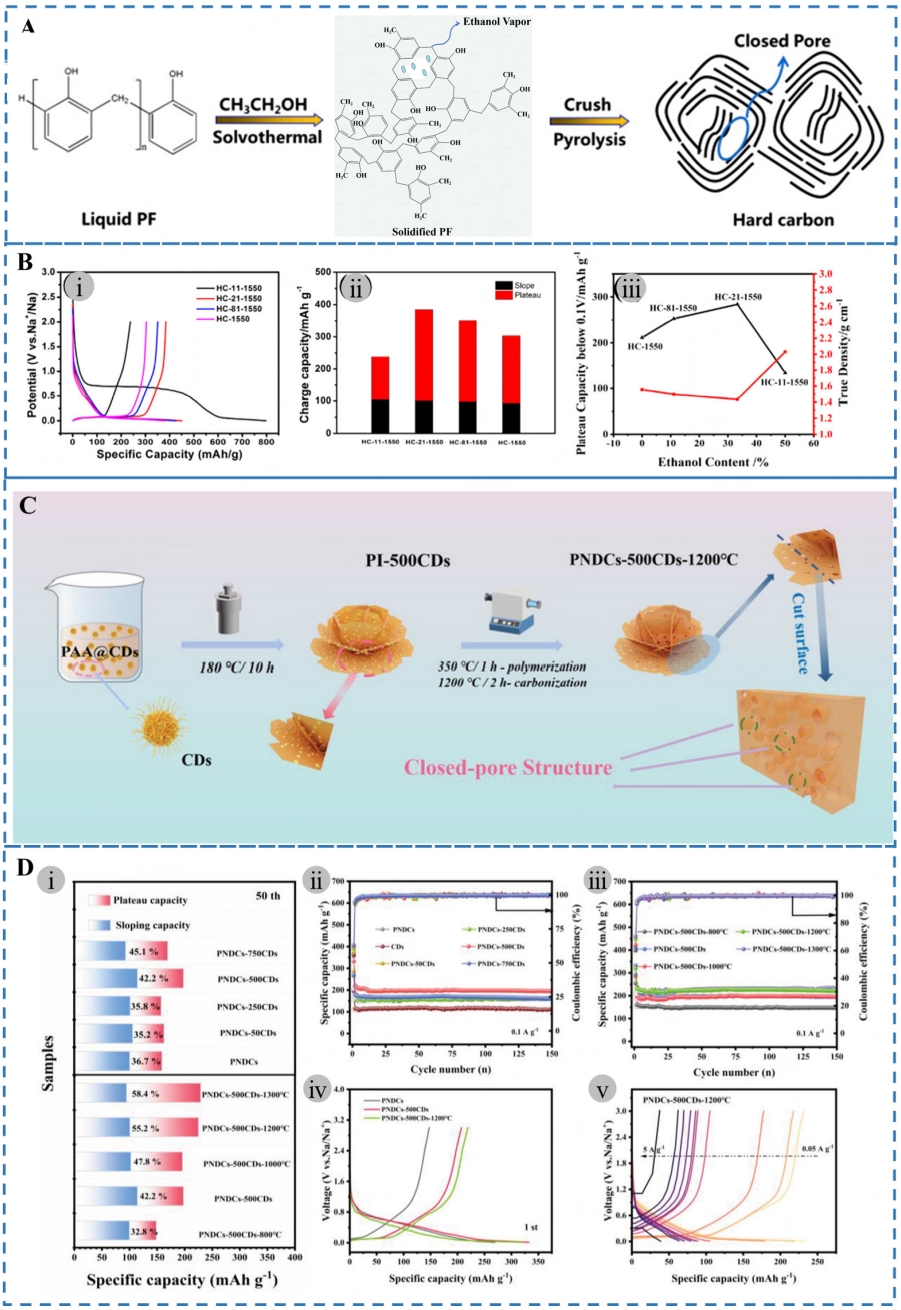

Figure 7. (A) Illustration of the typical synthesis process of HC using liquid phenol-formaldehyde (PF) resin as the precursor and EtOH as the pore-forming agent[145] (Copyright 2019, American Chemical Society). (B) Electrochemical performance: (i) Galvanostatic initial discharge-charge profiles. (ii) Specific capacity of HCs contributed from the slope and plateau region. (iii) Relationship among the plateau capacity (0.1-0 V), true density, and EtOH content[145] (Copyright 2019, American Chemical Society). (C) Schematic of the material synthesis for PNDCs-500CDs-1,200 °C[146] (Copyright 2023, Wiley-VCH). (D) Electrochemical performance: (i) Specific capacity of all samples from the plateau and slope contribution (discharge capacity at the 50th cycle). Cycling curves of samples with (ii) CD content and (iii) annealing temperature as variables. (iv) First galvanostatic discharge/charge curves of PNDCs, PNDCs-500CDs, and PNDCs-500CDs-1,200 °C at 0.1 A g^{-1}; (v) Galvanostatic discharge/charge curves of PNDCs-500CDs-1,200 °C at different current densities from 0.05 to 5 A g^{-1}[146] (Copyright 2023, Wiley-VCH).

Alkali treatment method

Alkaline reagent treatments can introduce micropores and mesopores into the carbon structure of various

carbon substrate materials. Potassium hydroxide stands out as the most frequently employed alkali treatment agent. Throughout the pyrolysis process, KOH engages in a series of intricate reactions with the precursors (as shown in Figure 8A)[147]. These reactions involve the reduction of potassium compounds to generate potassium metal, the oxidative decomposition of carbon resulting in the formation of carbon oxides and other carbonates, and the interaction with other reactive intermediates[148].

Wang *et al.* utilized potassium hydroxide to activate anthracite coal, successfully producing a cost-effective HC material with abundant closed pores through a two-step carbonization technique[149]. They categorized the HC materials into DCx (direct carbonization of anthracite coal), ACx (carbonization after KOH activation), and CACx (further carbonization after KOH activation), where x represents the carbonization temperature. The experimental methods and electrochemical performance are shown in Figure 8B and C. Upon increasing the carbonization temperature from 1,100 to 1,300 °C, the SSA of CACx decreased from 317.3 to 36.7 $m^2 g^{-1}$. Concurrently, the pore volume decreased from 0.19 to 0.05 $cm^3 g^{-1}$, while the size of closed pores increased from 1.74 to 2.37 nm. CAC1300 has the largest SSA of closed pores (341.7 $m^2 g^{-1}$) and the highest volume of closed pores (0.12 $cm^3 g^{-1}$). Electrochemical performance tests indicate that CAC1300 exhibits a significant increase in sodium storage capacity (308 mAh g^{-1}) with ICE at 82.3%. Notably, CAC at 1,300 °C exhibited the highest ratio of closed pores to surface area, featuring a surface area of 341.7 $m^2 g^{-1}$ and a closed pore volume of 0.12 $cm^3 g^{-1}$. The activation of potassium hydroxide generated numerous open nanopore structures. Furthermore, the high-temperature carbonization process involved the random stacking of bent graphene sheets and microcrystals, leading to the reconfiguration of open pores into closed pores. This transformation resulted in an increased number of active sites for sodium-ion storage.

Acid treatment method

The acid treatment of precursors has received considerable attention. Phosphoric acid and sulfuric acid serve as acid treatment agents to promote hydrolysis, condensation, and aromatization reactions during the carbonization of precursors. These agents also facilitate the formation of cross-linked structures and pore structures[150].

Sulfuric acid is commonly used as a convenient acid treatment for precursor materials. Xu *et al.* conducted a study where they produced HC materials with a significant number of closed-pore structures, denoted as HC-T (where T represents the carbonization temperature ranging from 900 to 1,700 °C), by subjecting bamboo powder to pre-treatment with 5 M H_2SO_4 followed by high-temperature pyrolysis[151]. The pore structure of the material could be improved by adjusting the pyrolysis temperature. As the carbonization temperature increased from 900 to 1,700 °C, the SSA of the material decreased from 519.5972 to 3.6883 $m^2 g^{-1}$. Similarly, the pore volume decreased from 0.212 to 0.014 $cm^3 g^{-1}$, while the pore diameter of closed pores increased from 1.495 to 2.206 nm. The material undergoes bending of carbon layers and fusion of nanopores, resulting in the formation of numerous closed pores. Additionally, open pores gradually transition into closed pores during the high-temperature carbonization process. The degree of graphitization of HC, along with the quantity and size of nanopores, increases with pyrolysis temperature. The materials carbonized at 1,300 °C exhibit the best electrochemical performance, with a high specific capacity of up to 420.6 mAh g^{-1} at 30 mA g^{-1}, along with excellent rate performance and cycle stability.

Similarly, Wang *et al.* used acidic solutions prepared with acetic acid and sodium chlorite to partially remove lignin from bamboo, thereby regulating the content of free radicals in the bamboo and successfully fabricating bamboo-derived HC with closed pores (as shown in Figure 9A)[87]. With increasing treatment time (0 to 10 h), the SSA initially increased from 37.7 to 47.5 $m^2 g^{-1}$ (at 6 h) and then gradually decreased to 40.2 $m^2 g^{-1}$. The volume of closed pore followed a similar trend, growing from 0.091 to 0.203 $cm^3 g^{-1}$ (at 6 h)

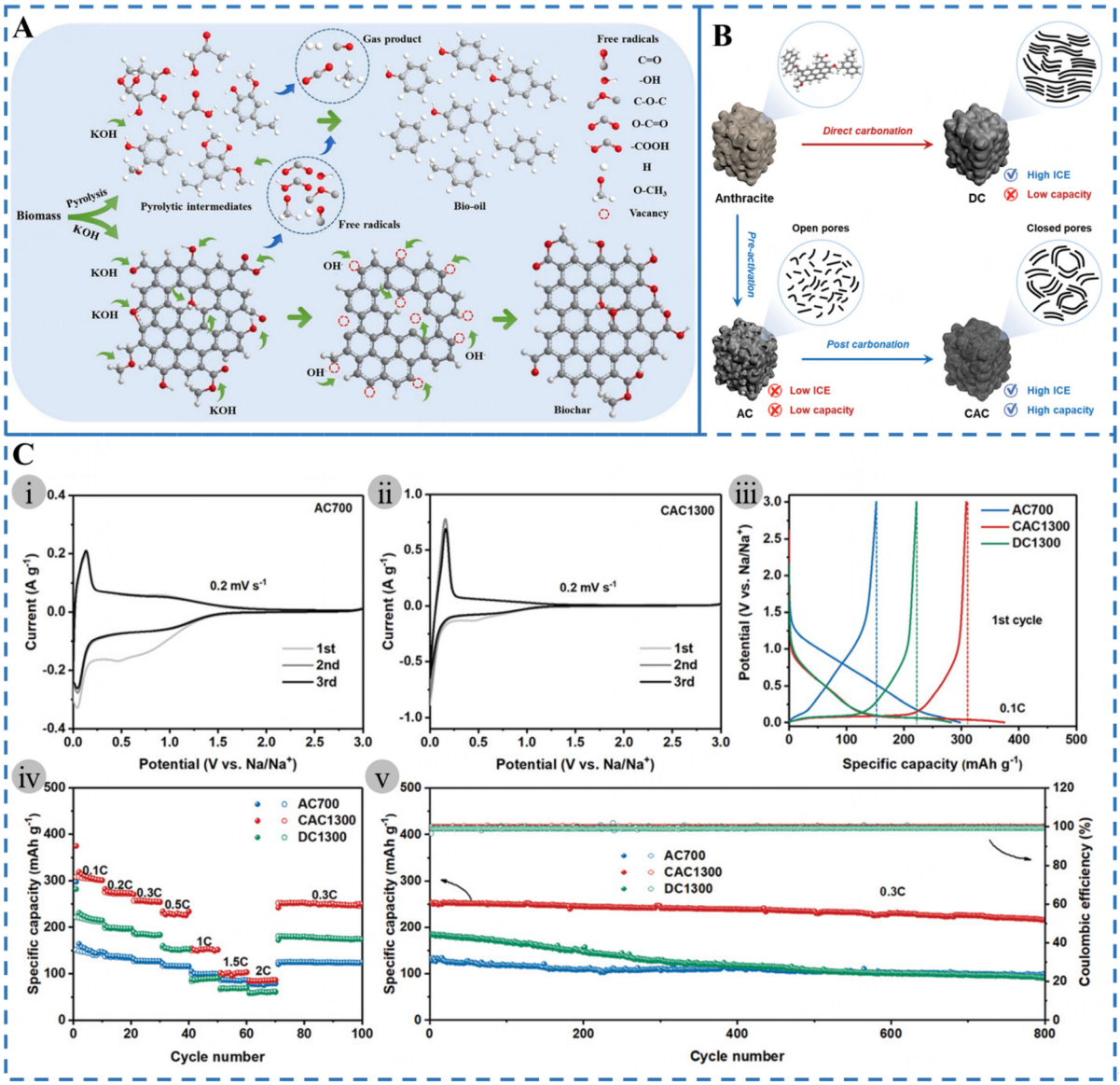

Figure 8. (A) Reaction pathway for KOH activation during biomass pyrolysis[147].(Copyright 2023, Elsevier Ltd). (B)Schematic illustration of the synthesis process of DC and CAC[149] (Copyright 2022, Wiley-VCH). (C) Sodium anodic performance of AC700, CAC1300, and DC1300 with mass loading of ≈ 3 mg cm^{-2}.CV curves of (i) AC700 and (ii) CAC1300 at the scan rate of 0.2 mV s^{-1}.(iii) The first discharge-charge curves of AC700, CAC1300, and DC1300 at the current density of 0.1 C (30 mA g^{-1}). (iv) Rate performance of AC700, CAC1300, and DC1300. (v) Cycling performance of AC700, CAC1300, and DC1300 at the current density of 0.3 C[149] (Copyright 2022, Wiley-VCH).

and then gradually decreasing to 0.041 cm^3 g^{-1}. Experimental results indicate that appropriate removal of lignin from bamboo can expose more free radicals, promoting the growth of graphene layers during pyrolysis and forming a rich number of closed pores. However, excessive removal of lignin can expose too many free radicals, resulting in smaller microcrystalline sizes and a reduction in the number of closed pores in the HC. As shown in Figure 9B, the HC anode with the largest number of closed pores (HC-DB-6) provides a high reversible capacity of up to 350 mAh g^{-1} at 20 mA g^{-1}. Additionally, phytic acid can also be used as an acid treatment agent. The experimental methods and electrochemical performance are shown in Figure 9C and D. The PLHC anode provides a capacity of up to 380.3 mAh g^{-1} at 30 mA g^{-1}, with a plateau capacity ratio of approximately 68%[152].

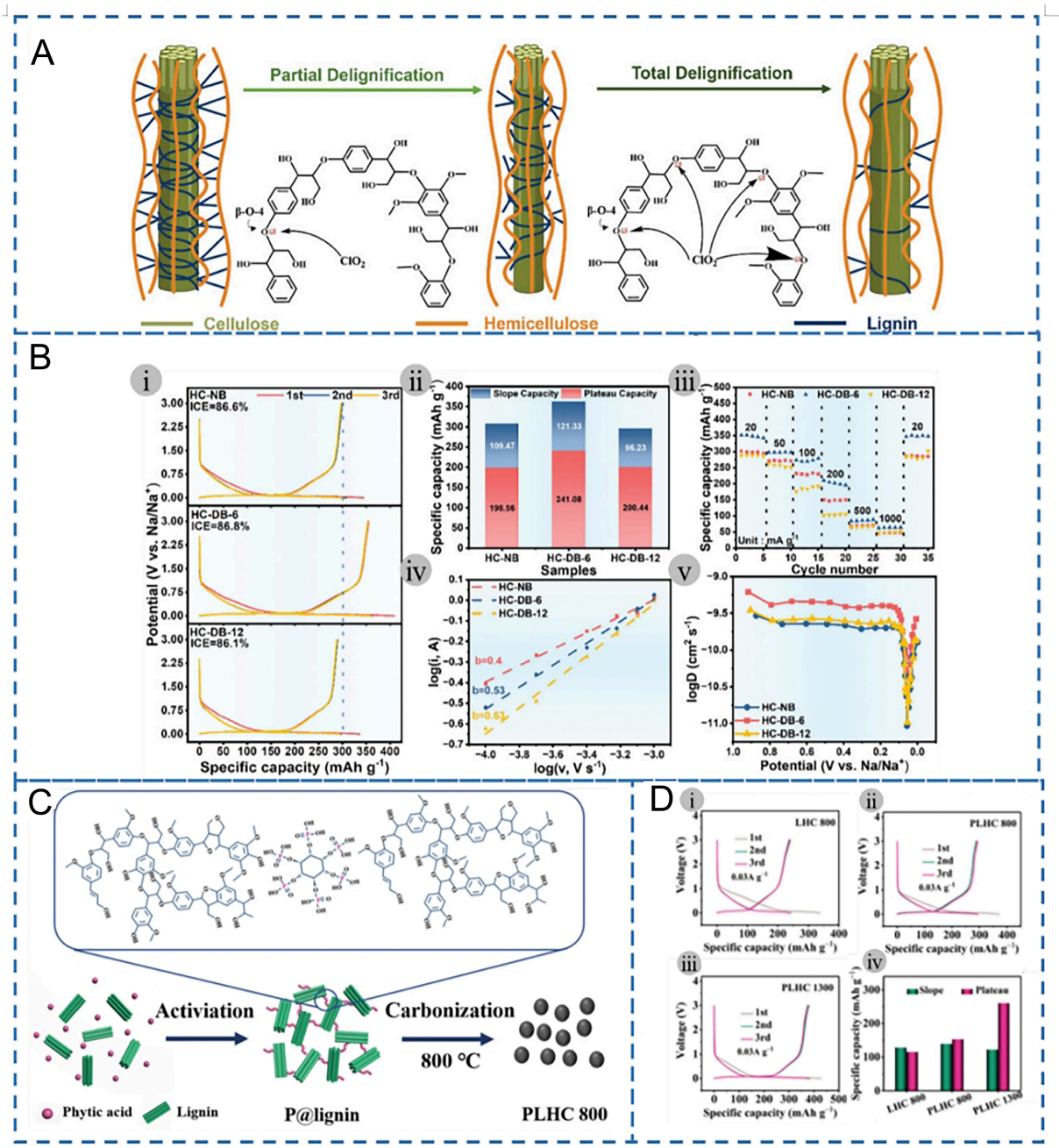

Figure 9. (A) The effect of delignification treatment on precursors. Scheme of delignification[87] (Copyright 2024, Wiley-VCH). (B) Electrochemical properties of HC materials. (i) GCD curves at 20 mA g^{-1}. (ii) Capacity ratios of the slope region and plateau region in the second cycle discharge curve. (iii) Rate performance. (iv) The linear relationship between log *i* and log *v* of cathodic peaks at 0.01 V. (v) GITT curves[87] (Copyright 2024, Wiley-VCH). (C)Schematic preparation process of phytic acid activating lignin-derived HC material[152] (Copyright 2023, Wiley Periodicals LLC). (D) Galvanostatic discharge/charge curves of (i) LHC 800, (ii) PLHC 800, and (iii) PLHC 1300 at 30 mA g^{-1}. (iv) Specific capacities at plateau region[152] (Copyright 2023, Wiley Periodicals LLC).

Other methods

To increase the quantity of closed pores in synthetic precursor materials, one can adjust the proportion of the synthesized raw components. As shown in Figure 10A, Shao *et al.* modified the molecular composition of epoxy resins by altering the distribution of alkyl and aryl groups by varying the ratio of 1,12-

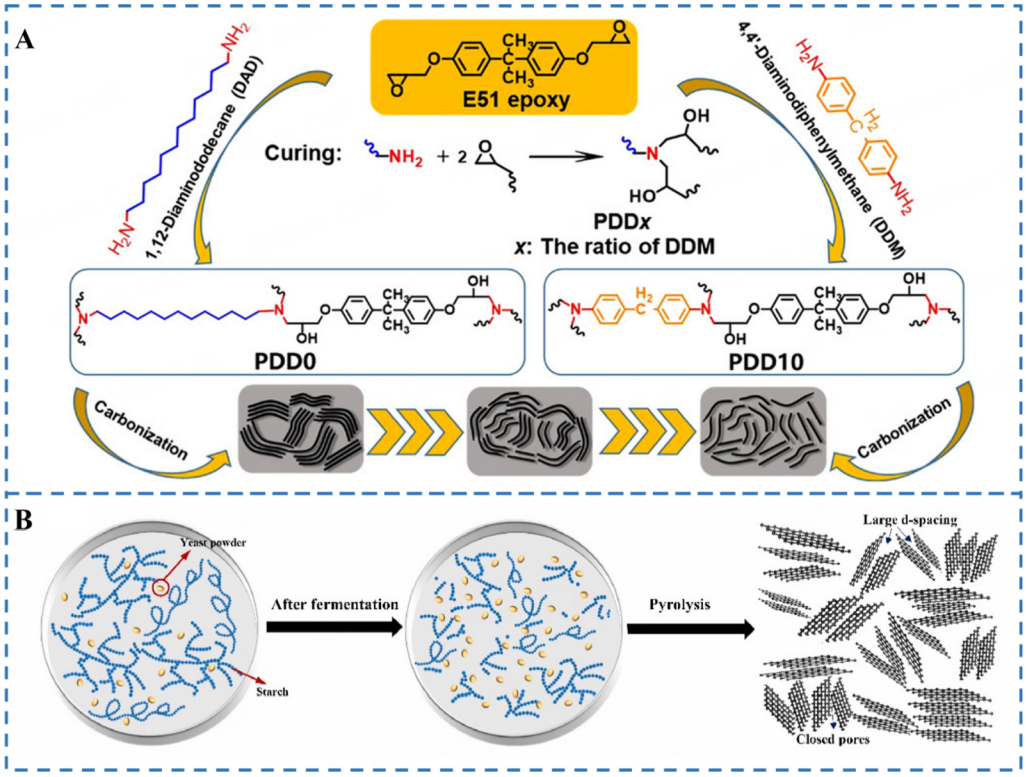

Figure 10. (A) Schematic for the preparation of PDD0 and PDD10[153] (Copyright 2022, Sichuan University and John Wiley & Sons Australia, Ltd). (B) Schematic illustration for the synthesis of starch-based HCs by a fermentation process[154] (Copyright 2022, Elsevier B.V.).

diaminododecane and 4,4'-diaminodiphenylmethane (DDM)[153]. This manipulation resulted in the creation of a series of small, high-density materials with diverse structures. *In-situ* Fourier transform infrared (*in-situ* FTIR) analyses revealed that elevating the DDM content in the mixed curing agent (specifically increasing the aryl content of the epoxy resin) led to enhanced cross-linking within the epoxy resin, impeded the reorganization of carbon atoms during carbonation, and yielded HC materials with reduced graphitization levels. The experimental outcomes illustrate that the presence of intricate aryl structures boosts the thermal stability of the epoxy resin and encourages the graphitization of HC materials. Conversely, a higher concentration of alkyl groups may trigger undesired side reactions in the carbonization process, consequently diminishing the carbon output of the precursor and impacting the degree of graphitization of HC materials. Furthermore, reducing the alkyl content of the precursor leads to a reduction in the size of closed pores in the materials. The HC samples containing varying DDM proportions exhibited SSAs of 75.11, 71.12, 60.83, 61.15, 59.40 and 77.20 $m^2 g^{-1}$ (corresponding to DDM contents of 0% to 100%). Carbon dioxide adsorption-desorption curves indicated a decreased number of micropores in the material, with pore sizes ranging between 0.6 to 0.9 nm and a limited pore volume. The transformation from alkyl groups to aryl groups in the original substance does not affect the open pores in the HC material and has minimal impact on the volume of enclosed pores. However, an augmentation in the aryl group concentration results in a higher residual carbon amount post-pyrolysis of the precursor, leading to the formation of smaller enclosed pores. Additionally, the presence of aryl groups influences the disorder level and d_{002} in the HC.

An abundance of closed pores can also be achieved by employing microbial treatment of precursors. As shown in Figure 10B, Chen *et al.* utilized bio-fermentation technology to effectively generate a variety of

modified HC materials utilizing yeast for starch treatment[154]. The SSA of the resulting HCs (CHC, F-CHC) decreased from 41.91 to 8.13 $m^2 g^{-1}$ after corn starch fermentation. The average pore size reduced to 1.75 nm, and the pore volume declined from 0.037 to 0.007 $cm^3 g^{-1}$. This reduction was attributed to the formation of more closed pores in F-CHC.

In addition, certain academics have underscored the potential of applying a coating to the HC surface to create an artificial SEI membrane, effectively transforming open pores into closed ones. A HC anode featuring a plethora of closed pores, and a robust SEI membrane holds great promise for practical applications. Schutjajew *et al.* selected Kynol Euroba's carbon-based neonatal fiber fabric (5092-CC, -ACC10, -ACC20) as the starting material[155]. A thin, stable artificial SEI coating was uniformly deposited on the HC surface by depositing graphite phase carbon nitride (p-C_3N_4) via chemical vapor deposition (CVD). The precursor exhibits a uniform, rational fiber structure and a modest pore structure, facilitating the uniform growth of p-C_3N_4. Density functional theory (DFT) theoretical calculations reveal that the SSA of the HC derived from 5092-ACC carbon fabric consistently remains below 24 $m^2 g^{-1}$, with a maximum pore volume of 0.043 $cm^3 g^{-1}$. The isothermal adsorption-desorption curves and SAXS experiments indicate that the 5092-ACC10 carbon cloth-derived HC is characterized by narrow pores, with most of its pore volume attributed to pores smaller than 1 nm. After the plasma etching process, the SSA increased from 897 to 1,037 $m^2 g^{-1}$, and the pore volume increased from 0.324 to 0.407 $cm^3 g^{-1}$. The three HCs derived from carbon cloth after depositing p-C_3N_4 exhibit a significant disparity in their SSA [specific surface area obtained from BET test results (SSA_{BET}); specific surface area obtained from SAXS test results (SSA_{SAXS})], suggesting a high concentration of enclosed pores in the materials. As the activation degree and pore size of the HC material approach a certain threshold, the p-C_3N_4 layer on the surface will gradually penetrate into the pores and seal them, leading to the formation of closed pores, particularly noticeable in HC materials with a higher concentration of ultra-micropores. Electrochemical performance tests of the prepared HC materials demonstrated that the artificial SEI membranes formed closed pores capable of storing sodium ions at low voltages. The plateau capacity of 184 mAh g^{-1} (with a reversible capacity of 220 mAh g^{-1}), along with the decrease in the ICE of the electrode, highlighted the protective effect of the p-C_3N_4 layer. The study demonstrated that through CVD, it was feasible to safeguard the electrode by establishing an artificial SEI membrane on the HC surface. Furthermore, this procedure could convert open pores into closed ones, which served as active sites for storing quasi-metallic sodium clusters and enhancing the plateau's capacity.

In summary, alternative strategies for producing closed pores include activating precursors with chemical reagents such as acids, bases, or other inorganic substances. Another approach involves creating abundant open pores in HC through physical methods including using oxidative gasifiers such as O_2, CO_2, or microwave induction. These open pores can then be transformed into closed pores either during carbonization or directly by forming an artificial SEI membrane through surface coating of the HC. By converting open pores into closed ones using an artificial SEI membrane on the HC surface, materials with a considerable number of closed pore structures can be developed.

Currently, various techniques are available for generating closed pores, but the method chosen depends on the morphology of different precursors. It is essential to consider both the surface characteristics of the precursor and the cost-effectiveness of each technique during the preparation phase. By carefully evaluating these factors, one can select the most appropriate preparation method to obtain HC materials as per the desired specifications.

MEANS OF CHARACTERIZATION OF CLOSED PORES

According to the pore structure model proposed by the International Union of Pure and Applied Chemistry (IUPAC) (as illustrated in Figure 11A), pores in HC materials can be classified as open and closed pores. Closed pores specifically refer to pores that are impermeable to helium at a temperature of 303 K[156]. In the HC anodes, closed pores are more desirable than open pores because they provide a larger number of active sites for sodium storage (as shown in Figure 11B and C), thereby enhancing the specific capacity of the battery[19,32]. However, distinguishing between open and closed pores is challenging, highlighting the need for technical methods capable of characterizing closed pores. In addition, we also cite the commonly used characterization methods to explore the mechanism of sodium storage in closed pores.

Methods for the characterization of the closed pores

1. Transmission Electron Microscopy

Electron microscopy technology utilizes electron beams to interact with sample surfaces, offering detailed insights into their microform, structure, and composition. This encompasses techniques such as TEM, scanning electron microscopy (SEM), and electron probe microanalysis (EPMA). The TEM is renowned for its outstanding resolution, enabling the observation of microscopic morphology at a level below ten nanometers. Furthermore, TEM facilitates the examination of material crystal structures through selected electron diffraction and high-resolution imaging. As a result, TEM plays a pivotal role in investigating material morphology and structure on a microscopic scale.

High-resolution transmission electron microscopy (HRTEM) enables the visualization of graphite microcrystal orientations within the HC structure, along with measuring carbon layer distances, size, crystallization level, and other details. HRTEM has been extensively used in diverse studies of HC materials. Li[17] utilized discarded cork as a precursor to generate cork-derived HC materials (CCs). The HC materials produced through a two-step pyrolysis process were labeled as CC-T, with T representing the pyrolysis temperature ranging from 1,200 to 2,000 °C. The samples were analyzed using SEM and TEM to observe pore shapes. Figure 12A illustrates that the surface of sample CC-pre-800 (carbonized material produced at 800 °C) displayed numerous hexagonal pores with widths ranging from 10 to 20 μm, originating from the "honeycomb" pore structure in the cork precursor. Upon subjecting CC-pre-800 to further pyrolysis at higher temperatures, the hexagonal pores transformed into rectangular pores measuring about 30~40 μm in length after carbonization at 1,600 °C. Despite a few irregular pores, the overall pore organization enhanced the wetting ability of the electrodes, facilitating sodium-ion movement between the electrolyte and electrodes. This structure also accommodated electrode expansion during cycling. Two potential reasons for this transformation include the presence of numerous "honeycomb" pore structures in the original precursor and the reorganization of carbon layers due to increased pyrolysis temperatures. Characterization of the internal structural information of the samples using HRTEM revealed that the graphene sheets within the CCs exhibit a vortex-like arrangement, with the overall structure showing short-range order. As the carbonization temperature rises, the arrangement of graphene sheets continuously transitions s from a disordered to an ordered CC structure. Moreover, defects decrease progressively, graphite microcrystal lattice stripes become more defined, and bending and folding of graphene sheets, along with the merging of nanopores, contribute to an increase in closed pore numbers.

Sun *et al.* successfully synthesized HC (Cx, where x represents the pyrolysis temperature) derived from anthracite through pre-carbonization, mechanical treatment, and high-temperature pyrolysis[157]. The influence of pyrolysis temperature and mechanical treatment on the degree of graphitization of the materials was investigated using HRTEM (as shown in Figure 12B). The results indicated that with

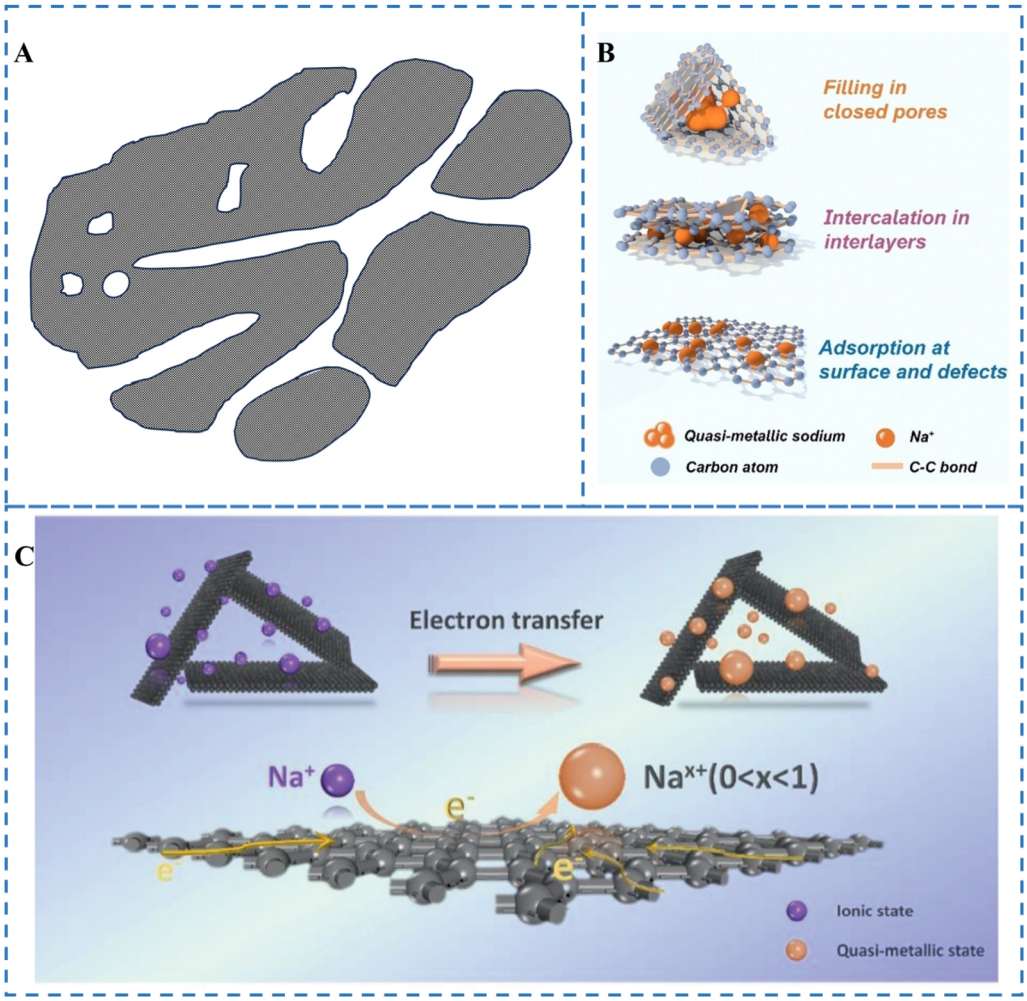

Figure 11. (A) Modeling of pore structure in solids proposed. (B) the sodium storage sites in disordered carbon[19] (Copyright 2022, The Chemical Society of Japan & Wiley-VCH GmbH). (C) Schematic illustration of the steady states of sodium in HC. The insertion of Na^+ ions into the HC electrode is accompanied by partial electron transfer between them with the formation of quasi-metallic sodium[32] (Copyright 2023, American Chemical Society).

increasing pyrolysis temperature, distinct short-range ordered structures appeared within the materials. Moreover, the level of graphitization of Cx was directly proportional to the pyrolysis temperature. Kubota *et al.* produced a variety of HC materials with diverse microstructures by subjecting sucrose, a carbon source, to pyrolysis temperatures ranging from 700 to 2,000 °C[111]. These materials were labeled as HTT-X, where X signifies the specific pyrolysis temperature. The microstructure of the HC materials was examined using TEM, and the results were illustrated in Figure 12C. Selected area electron diffraction patterns (SAED) acquired from HC materials synthesized at different pyrolysis temperatures displayed diffraction rings rather than spots, indicating a composition of polycrystalline nanoparticles.

Notably, the diffraction rings of HTT-700 were the least pronounced, while those of higher HTT values exhibited increasing visibility. Particularly, the diffraction rings of HTT-2000 stood out the most, suggesting a higher level of structural order in the material's planar orientation. The projected images of all samples showcased short-range order and long-range disorder. HC structures carbonized at 700 and 900 °C demonstrated the highest level of disorder, lacking clear graphene sheet stacking. Conversely, HC structures

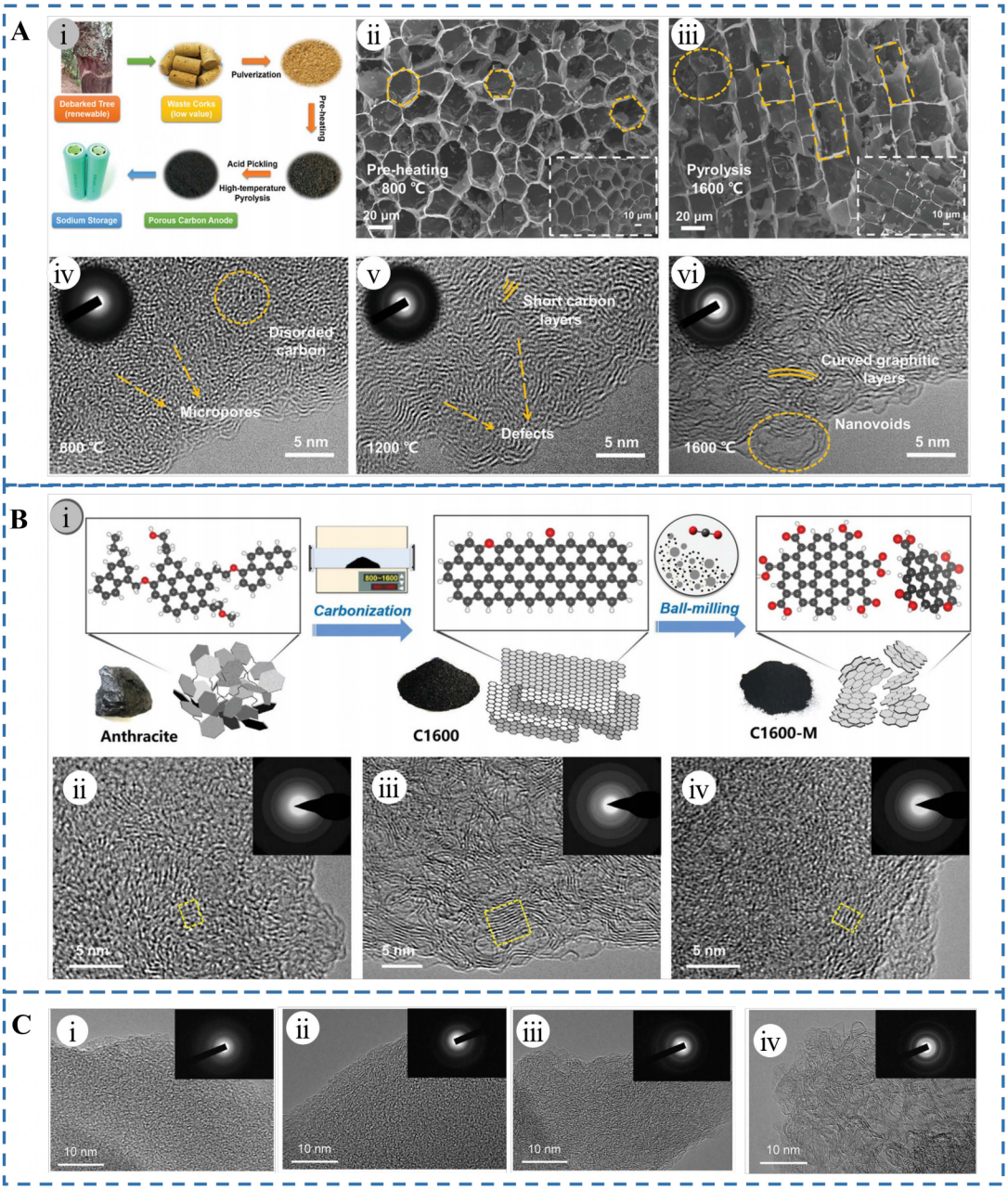

Figure 12. Typical SEM and TEM images of HC: (A) (i) Schematic of the material synthesis for CC (the graph of the debarked tree is reproduced with permission. (ii) CC-Pre-800 and (iii) CC-1600. High-resolution TEM and SAED images of (iv) CC-Pre-800, (v) CC-1200, and (vi) CC-1600[17] (Copyright 2019, WILEY-VCH Verlag GmbH & Co. KGaA, Weinheim). (B) Preparation and structural characterizations. (i) Schematic illustration of C1600-M preparation process. (ii) HRTEM image of C800. (iii) HRTEM image of C1600. (iv) HRTEM image of C1600-M. The inset and bottom show the corresponding SAED and FFT patterns[157] (Copyright 2020, Wiley-VCH). (C) TEM images and SAED patterns of sucrose-derived HC samples prepared at different temperatures: (i) HC700, (ii) HC900, (iii) HC1500, (iv) HC2000[111] (Copyright 2020, American Chemical Society).

carbonized at 1,500~2,000 °C exhibited well-defined lattice stripes resulting from graphene sheet stacking. During carbonization, graphene sheets underwent bending and rearrangement, leading to the formation of enclosed pores, which accords with the model proposed by Ban[98].

TEM offers extremely high resolution, enabling detailed observation of the internal microstructure of HC. However, it requires samples to be very thin (typically less than 100 nm); otherwise, the electron beam cannot penetrate the sample. Additionally, high-energy electron beams may cause radiation damage to the sample, leading to structural changes in the sample. The observation range of TEM is relatively small, and it cannot accurately represent the overall pore structure information of the material. It is also insensitive to distinguishing between closed and open pores. Therefore, TEM is commonly combined with other characterization techniques to obtain accurate data on closed pores, facilitating the formulation of strategies to regulate closed pores[19].

2. Small-angle X-ray Scattering (SAXS)

Researchers commonly utilize the gas isothermal adsorption-desorption method to investigate the pore structure in HC, employing gases such as N_2, CO_2, *etc*. However, not all pores allow the gas to permeate through and reach the sample surface for detection. As a result, this approach can only identify the open pores in HC[19].

SAXS is a testing technique that entails directing X-rays onto the sample surface using a collimator with three apertures. The scattered light and incident light create an angle between 2° and 5°, with the resulting image captured on a flat receiver, as illustrated in Figure 13A. The sample exhibits stronger scattering characteristics when the scattering parameter q has a smaller value. The total porosity of HC samples can be determined through SAXS. By integrating this method with gas adsorption-desorption and analyzing the disparity between the two test results, accurate information on the closed pores can be obtained.

$$q = \frac{4\pi \sin\theta}{\lambda}$$

The SAXS results of HC are depicted in Figure 13B. The curve displays a pronounced decrease at $q < 1$ nm^{-1}, a characteristic feature of distinct interfaces of large particulate objects. A plateau emerges around $q = 1$ nm^{-1}, followed by a continual decline in the curve until approaching $q = 10$ nm^{-1}, indicating the presence of micropores. Furthermore, diffraction peaks corresponding to the (002), (100), and (004) crystallographic planes are observed beyond $q > 10$ nm^{-1}, which are linked to the molecular-scale structure of HC[34].

Numerous researchers have conducted in-depth investigations on the pore structure of HC using SAXS. As shown in Figure 13C, Saurel *et al*. utilized SAXS to analyze a range of carbon materials, including graphite, soft carbon, and HC[158]. They devised a novel geometrical model to accurately interpret the SAXS test results, thereby refining the quality of the experimental data derived from SAXS. The pore structure of the materials was meticulously characterized, and crucial parameters such as surface area, volume percentage, and pore shape were quantified. Through the application of SAXS technology, researchers have effectively managed the microstructure of HC with greater ease. This not only enhances the performance of sodium storage and facilitates the investigation of metal ion storage mechanisms but also boosts the ICE through the regulation of the material's SSA.

Morikawa *et al.* synthesized a series of HC materials derived from sucrose through hydrothermal treatment and high-temperature pyrolysis, with pyrolysis temperatures ranging from 1,000 to 2,000 °C[159]. These materials were labeled as HC-T, with T representing the specific pyrolysis temperature. The researchers utilized SAXS, WAXS, and other testing techniques to examine the relationship between the diverse

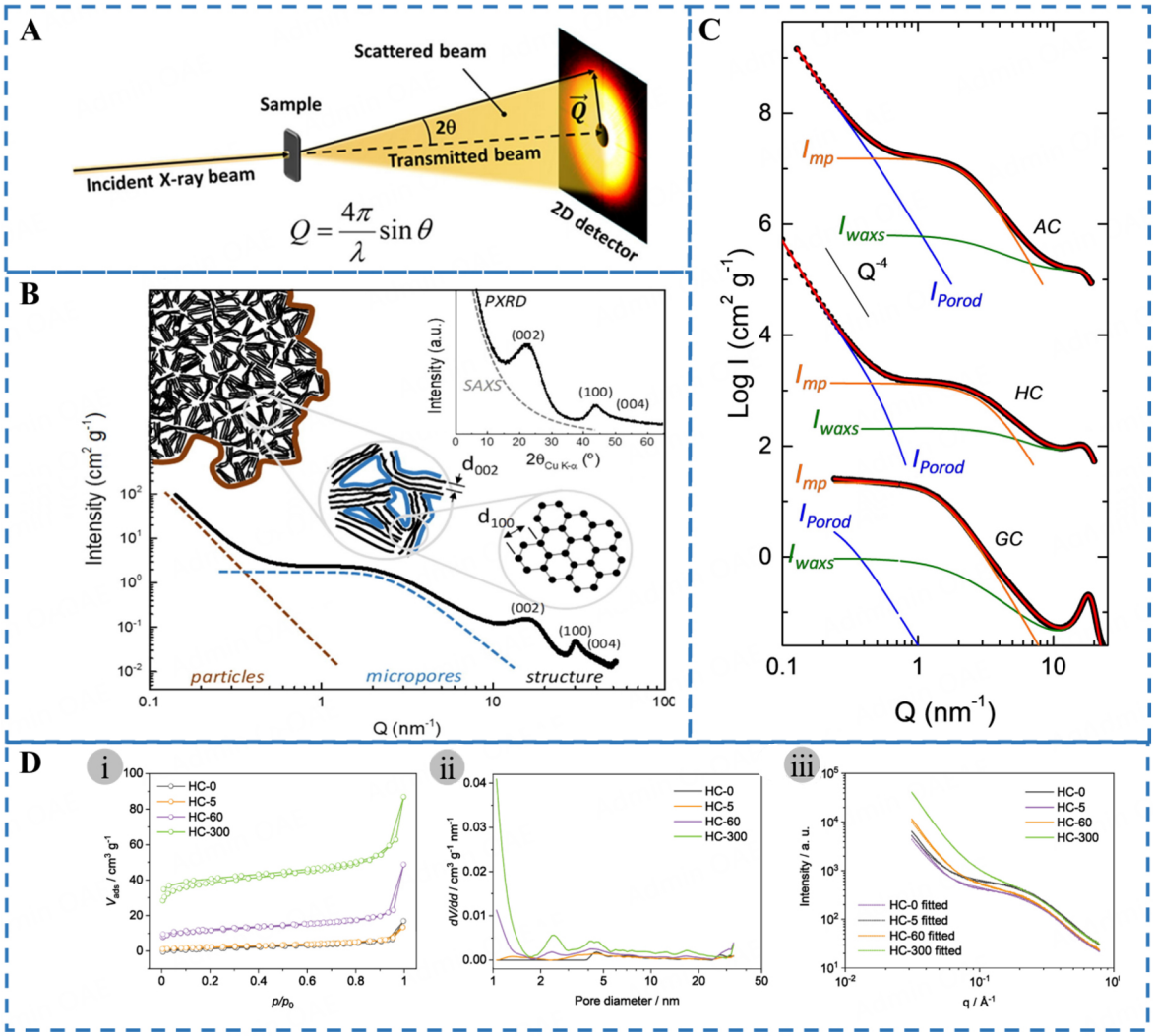

Figure 13. (A) Typical transmission geometry used for SAXS experiments[34] (Copyright 2018, Elsevier Ltd). (B) Main panel: Full-range plot of scattering patterns from SAXS to PXRD, represented as absolute intensity *vs.* the scattering vector Q in log-log scale; the schemes represent the structure and microstructure at various scales, from the macroscopic surface area (left) to micropores (center) to atomic structure (right). Inset: Typical PXRD pattern of a HC with the main reflections indexed according to the 2H graphite structure; the gray discontinuous line indicates the SAXS background signal[34] (Copyright 2018, Elsevier Ltd). (C) Full range fit of microporous carbons AC, HC, and GC. AC and HC intensities were shifted for clarity. Black symbols represent the experimental data; the red curve represents the calculated pattern; the blue curve corresponds to the calculated I_{Porod}; the orange curve to the calculated I_{mp}; and the green curve to the calculated I_{waxs}[158] (Copyright 2019, Elsevier B.V). (D) The porosity of HC without ball-milling (HC-0) and after 5 (HC-5), 60 (HC-60), and 300 min (HC-300) of ball milling as measured by nitrogen physisorption at 77 Kand SAXS. (i) Physisorption isotherms; and (ii) corresponding pore size distributions. (iii) SAXS curves[160] (Copyright 2021, Elsevier Ltd).

microstructures of HC materials and their sodium storage capabilities. The findings suggest that the presence of clusters of quasi-metallic sodium in the HC nanopores significantly enhances the reversible capacity of the electrode. This study provides compelling evidence to elucidate the process through which sodium ions fill the pores and underscores the critical role of SAXS in probing the mechanism of sodium storage.

Ilic *et al.* conducted ball milling on commercial HC using a ball mill to investigate the effects of different ball milling durations on the morphology and structure of the material[160]. The primary objective was to observe the variations in HC porosity pre- and post-ball milling. Analysis of the isothermal adsorption-

desorption defects of nitrogen and carbon dioxide, along with the SAXS results (as shown in Figure 13D), revealed that the pore volume increased with ball milling times, while the volume of closed pores decreased. Additionally, the particle size decreased as the ball milling duration extended, leading to the creation of more pores in smaller particles. The ball milling process resulted in the disruption or opening of the closed pore structure, causing changes in the pore volume. The opening of closed pores was primarily ascribed to the reduction in grain size during ball milling, exposing a considerable number of closed pores on the material's surface. This report illustrates the influence of milling on the morphology and structure of HC materials and establishes the "intercalation-adsorption" mechanism of sodium storage. Nevertheless, future research should concentrate on devising a processing technique capable of reducing the grain size of HC effectively while preserving its electrochemical properties.

As mentioned earlier, researchers commonly rely on gas isothermal adsorption-desorption curves in combination with SAXS to investigate the closed pores of HC. However, due to the limitations of experimental instruments and equipment based on the gas adsorption effect principle, even CO_2 gas, which can detect ultra-micropores, may not be able to identify small-sized pores. Fortunately, helium (He) can infiltrate nearly all non-sealed pores. By employing Archimedes' principle and analyzing the true density using helium, researchers can enhance the results obtained from the initial two methods and obtain more accurate structural information about the closed pores. In a study by Li *et al*., true density analysis and SAXS were utilized to quantify the number and volume of closed pores[17]. The researchers observed that as the temperature increased, the volume of closed pores expanded approximately nine times, from 0.032 to 0.29 $cm^3 g^{-1}$. Subsequently, they determined that the increase in both the number and size of nanopores was the primary factor contributing to the expansion of closed pores.

SAXS is applicable to a variety of samples, including solids, liquids, colloids and thin films. It effectively probes the structural features of materials at the nanometer scale (typically between 1 and 100 nm). However, its spatial resolution is relatively low, only allowing for the detection of overall structural information at the nanometer scale without providing finer details or more complex structural features. The requirements of the sample are harsh. High concentration or non-uniform samples can lead to excessive scattering intensity or interference signals, affecting the accuracy of the data. Accurate description of sample structure depends on the choice and assumptions of theoretical models, and mismatched models can lead to erroneous results. Usually combined gas adsorption/de-adsorption curve, SAXS and true density analysis to verify the existence of closed pores in HC, helping us to optimize the closed pore structure of HC and obtain HC anodes with superior performance.

Methods for characterization of the sodium storage mechanism in closed pores

1. X-ray Photoelectron Spectroscopy

X-ray photoelectron spectroscopy (XPS) is a spectroscopic technique that leverages the photoelectric effect to ascertain the chemical composition, state, and chemical bonding of a sample's surface. Examining the alterations in chemical bonding of the HC anode during charging/discharging serves as a valuable approach to validate the sodium storage mechanism of HC[161].

In 2016, it was reported that sodium ions were found in the plateau region in a quasi-metallic form using XPS (as shown in Figure 14A)[162]. Following charge-discharge cycles, certain researchers[32] investigated the storage behavior of sodium ions in HC anodes using XPS. In Figure 14B, the un-etched HC anode displayed a peak at approximately 1,070.9 eV, corresponding to Na-O-C. This peak was associated with the development of a SEI on the electrode's surface. The binding energy of sodium ions stored in the HC was

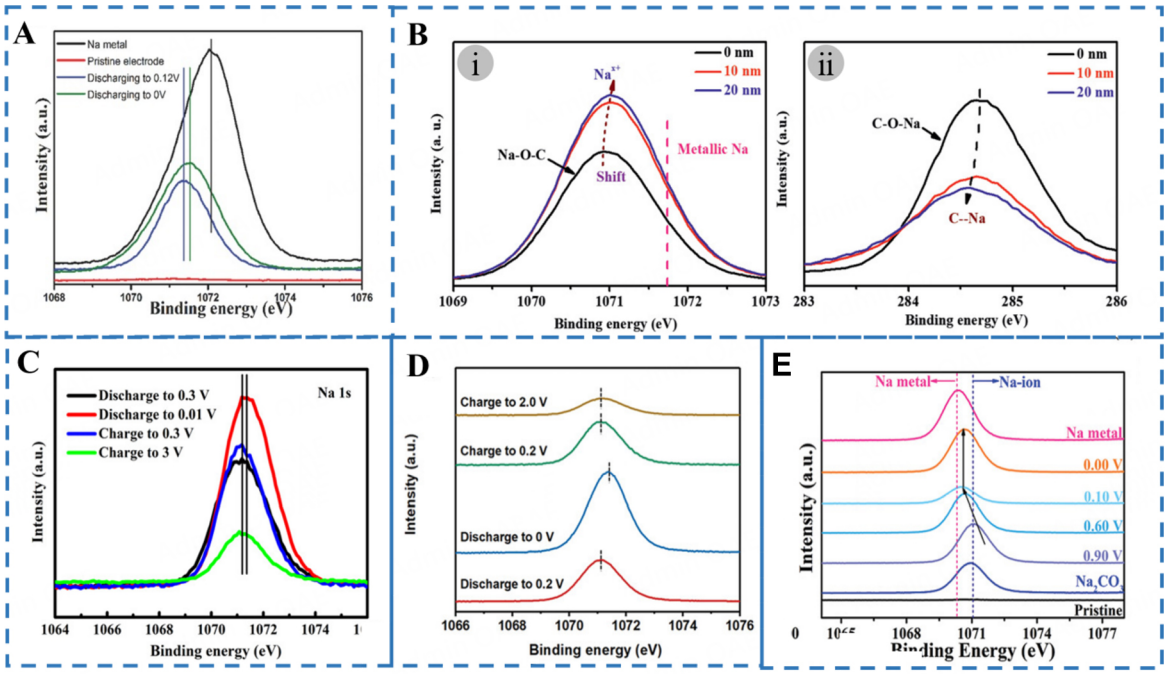

Figure 14. XPS profiles of different HC anodes: (A) *Ex situ* XPS Na 1s spectrum profiles of HCT1300 and Na metal after etching 60 nm[162] (Copyright 2016, WILEY-VCH Verlag GmbH & Co. KGaA, Weinheim). (B) *Ex situ* XPS Na 1s and C 1s spectra depth profiles of HC after full sodiation[32] (Copyright 2021, Wiley-VCH GmbH). (C) Na 1s X ray photoelectron spectroscopy spectra for the CMGL-Na electrodes test at different cut off voltages[47] (Copyright 2021, Wenzhou University and John Wiley & Sons Australia, Ltd). (D) *Ex situ* XPS Na 1s spectra of CAC1300 electrode at various potential states[149] (Copyright 2022, Wiley-VCH GmbH). (E) Na 1s of HCM-1300-ZBEat different voltages[142] (Copyright 2022, Wiley-VC).

identified to be intermediate between metallic sodium and sodium ions in the HC anode, with an etching depth of 10-20 nm. This indicates that the valence state of the sodium ion stored in the HC falls between 0 and 1, suggesting the presence of quasi-metallic sodium in the cycled HC anode.

Zhu *et al.* developed HC materials derived from magnolia leaves (CMGLs) through a simple process involving pyrolysis and acid treatment[47]. They utilized magnolia leaves as a precursor to study the mechanism of sodium storage in these CMGLs. As shown in Figure 14C, XPS testing of the HC anodes at different cutoff voltages revealed that a distinctive peak appeared around 1,071.2 eV when the anode was discharged to 0.3 V, indicating the successful penetration of sodium ions into the HC anode. Subsequent discharge to 0.01 V led to a shift in the valence of the sodium ion, moving the peak to 1,071.4 eV. It was observed that the binding energy of the embedded sodium ion exceeded the adsorption energy of sodium ions on the HC. This difference confirms the insertion behavior of sodium ions in the low plateau region. Upon recharging to 0.3 V, the peak reverted to 1,071.2 eV, demonstrating good reversibility of the overall process. The peak position remained stable even after further charging to 3 V, indicating that the high-voltage slope region did not induce a high valence state, and the active sites on the HC surface predominantly adsorbed sodium ions. Moreover, the presence of the sodium peak persisted even when the battery was charging to 3 V, suggesting that sodium was also adsorbed on the HC surface. This observation provides additional support for the notion that the degradation of the electrolyte resulting in the SEI formation led to a low ICE.

Wang *et al.* also utilized XPS to investigate the valence state of sodium in the HC anode at different voltages[149]. Figure 14D shows that when the CAC1300 anode (anthracite-derived HC carbonized at

1,300 °C) was discharged to 0.2 V, a distinct peak (Na 1s) appeared around 1,071.2 eV, indicating the successful insertion of sodium ions into the anode. Further discharge to 0 V caused the Na 1s peak to shift, indicating a change in the valence state of sodium. The energy required for the formation of chemical bonds in metallic sodium is higher than that for adsorbed sodium on the surface, suggesting that sodium is stored in the HC material in a quasi-metallic state through a closed pore-filling mechanism. Upon recharging to 0.2 V, the Na 1s peak returned to its original position, indicating the reversible nature of sodium filling in enclosed pores. When the voltage was raised to 2.0 V during charging, no significant change was observed in the Na 1s signal. This indicates that the presence of surface-adsorbed sodium on the HC anode does not influence the valence state of stored sodium in the high-voltage region. This finding aligns with a study conducted by Yin *et al.* (as shown in Figure 14E)[142].

XPS can detect the presence of almost all elements (except H and He), even at extremely low concentrations. It provides information about the chemical state and chemical environment of elements, allowing for quantitative analysis. However, XPS mainly analyzes the surface of samples and cannot provide information about internal structure, and it is only suitable for solid samples. Additionally, data analysis is typically performed under ideal conditions, which may deviate from actual situations, and the results are directly related to the choice of fitting models and reference data.

2. Electron Paramagnetic Resonance

Electron paramagnetic resonance (EPR) is a sensitive technology used to analyze the internal structure of materials by studying unpaired electrons. It is commonly utilized to detect electrochemical reaction intermediates and is highly effective in studying the changes in alkali metal ions within HC during charge and discharge processes. EPR is particularly valuable for understanding the sodium storage mechanism in HC batteries[163]. As shown in Figure 15A, Liu *et al.* utilized EPR to investigate the sodium storage mechanism of HC materials under various electrolyte conditions[163]. The EPR report revealed that in ester-based electrolytes, sodium ions were primarily stored through defect adsorption and nanopore filling. Conversely, in the ether-based electrolyte, sodium ions adsorbed in the slope region were capable of being inserted between graphene lamellae during cycling, leading to the development of a more stable SEI film. As a result, the sodium ion storage mechanism of the HC anode in the ether-based electrolyte demonstrated a higher specific capacity. This study provides a thorough and practical guide for the utilization of HC materials in ether-based electrolytes.

Li *et al.* conducted a study on the charge states of three alkali metal ions (lithium, sodium, and potassium) in HC materials derived from glucose during the charging/discharging processes[164]. They employed EPR to analyze the signals, with the results depicted in Figure 15B. The signals revealed the presence of sodium and potassium ions insertion in the HC electrode. Moreover, a narrow peak centered at g = 2.00322 and g = 2.00298 was observed, which is associated with the delocalized electrons of the insertion metals. This indicates the formation of quasi-metallic sodium and potassium clusters. Remarkably, this study marks the first instance where *in-situ* EPR successfully captured quasi-metallic potassium clusters. This finding provides valuable insights for researchers aiming to enhance the energy density of sodium/potassium ion batteries.

Scholars have utilized the hydrothermal approach to produce microsphere materials derived from glucose-based HC sources. Through this method, the process of sodium insertion in HC samples was investigated using EPR and NMR techniques[165]. At elevated temperatures, organic precursors undergo pyrolysis, resulting in the generation of aromatic π radicals. These radicals subsequently react with metallic sodium, a

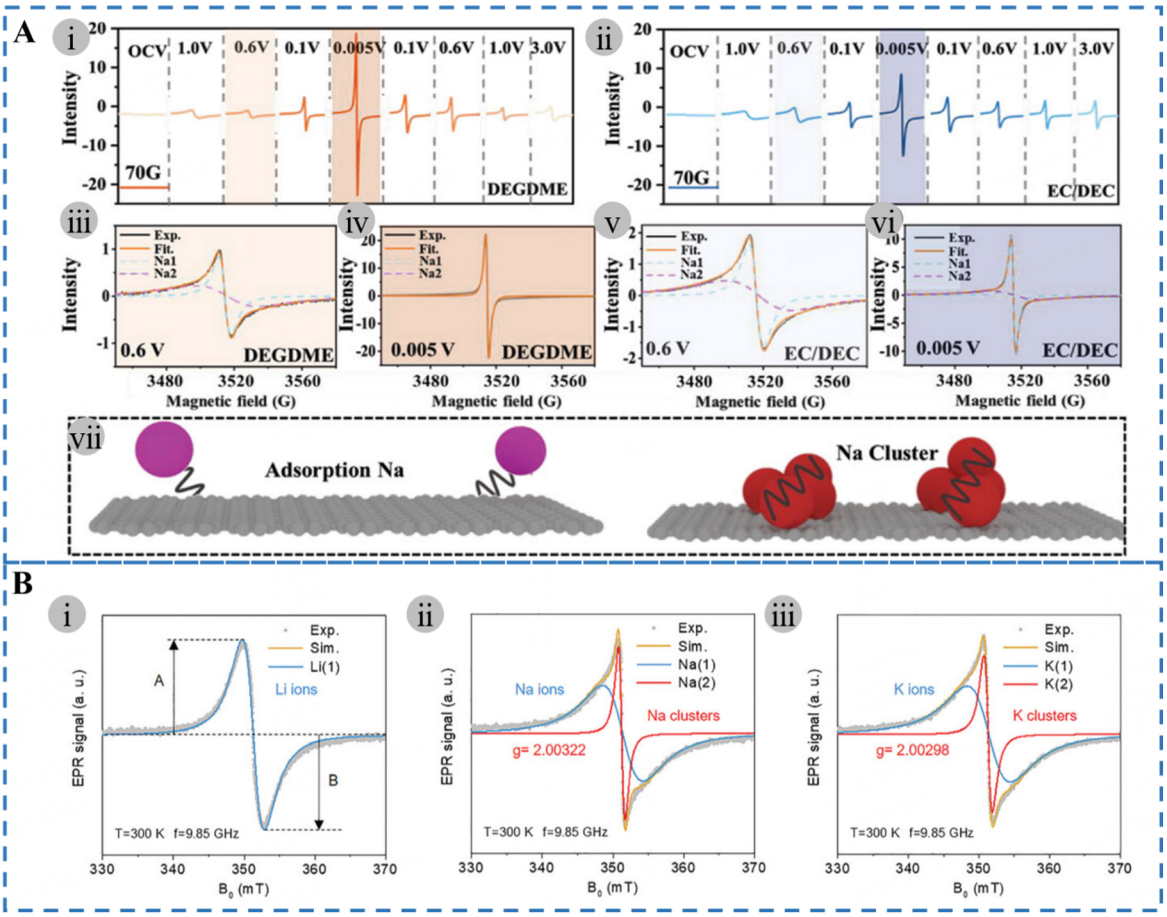

Figure 15. (A) Experimental EPR spectra of HC in (i) DEGDME- and (ii) EC/DEC-based electrolytes. Fitted EPR spectra with Lorentzian line-shape at (iii), (v) slope region and (iv), (vi) plateau region. (vii) Schematic illustration of adsorption-Na and quasi-metallic-Na[163] (Copyright 2023, Wiley-VCH). (B) (i) LIBs, (ii) NIBs, and (iii) KIBs. A and B denote the absolute ratio of the maximum and the minimum signal of the EPR line, respectively[164] (Copyright 2022, Wiley-VCH).

chemical process detectable by EPR. The test outcomes reveal that the EPR spectra of both lithium and sodium display two distinct signal peaks with varying line widths. The first signal peak has a linewidth of approximately 0.9 mT, while the second signal peak has a linewidth of around 3 mT. Furthermore, the g-value of both peaks closely resembles that of oxygen, approximately 2.005. These two signal peaks were identified in the anode material during discharge to 0 V and subsequent recharging to 2.0 V. As the discharge process progressed, the intensities of the peaks increased, indicating the insertion of alkali metal ions into the anode material. The peak intensities at 2.0 V were higher than at 0 V, suggesting that the alkali metal ions clustered within the pore space. Experiments by Nagmani *et al.*[166] and Yu *et al.*[167] further supported the formation of sodium quasi-metal clusters in HC anodes.

EPR provides detailed information on the local environment of unpaired electrons (such as electron density and coordination environment), with high sensitivity and widely applicable. However, it has high requirements for samples. Low-concentration samples may yield insufficient signal strength, and it is not suitable for materials without unpaired electrons. Additionally, interpreting the test results is challenging.

3. Solid-state Nuclear Magnetic Resonance

Nuclei with a non-zero spin have magnetic moments and exhibit Zeeman splitting of their energy levels when exposed to an external magnetic field. NMR is the phenomenon where such nuclei undergo transitions between energy levels in the presence of an external magnetic field. The application of ^{23}Na NMR is well-recognized as a powerful technique for studying the reversible insertion of sodium in HC materials. This method offers valuable insights into the different electronic states of sodium[19].

Alcántara *et al.* successfully synthesized spherical HC material by annealing a mixture of m-diphenol and formaldehyde at 950 °C[168]. Furthermore, the process of sodium-ion insertion in HC was investigated using ^{23}Na NMR with magic angle spinning (^{23}Na NMR MAS) for the first time. The ^{23}Na NMR MAS results of the cell after discharge and recharge, corresponding to voltage levels of 3.0, 0.0, and 2.0 V, were examined. Upon reaching a discharge level of 0.0 V, a distinct peak appeared at around 19 ppm, which disappeared after recharging to 2.0 V. The sodium-ion insertion into the graphene sheets may explain this observation. The authors provided new insights into the mechanism of sodium storage in disordered graphene sheets and enclosed pores.

Qiu *et al.* generated HC (HC-x, with x representing the carbonization temperature) material from cellulose through carbonization in an argon environment[31]. The ^{23}Na NMR spectra of their HC-1300 anodes at various discharge voltages are illustrated in Figure 16A. In the pristine electrode, the absence of sodium ions resulted in the lack of significant peaks. However, following discharge, two distinct signal peaks emerged within the 20 to 20 ppm range. A prominent peak at around 10 ppm can be attributed to electrolyte decomposition on the electrode surface. Additionally, the peak at 7 ppm was generated by the sodium-ion insertion in the dislocated carbon layer and micropores. The signal peak for metallic sodium (≈ 1,130 ppm) only appeared after over-discharge (curve IV in Figure 16A), indicating that sodium plating occurs only in regions below 0 V and does not appear in the plateau region.

Similarly, Chen *et al.* synthesized two HC materials dominated by pseudo-graphite microcrystals and micropores, respectively, using glucose and magnesium gluconate[27]. They further investigated the sodium storage behavior of these two materials (Glu and MgGlu) using ^{23}Na NMR. In Figure 16B and C, the two HC materials mainly exhibit three types of peaks: (i) a signal peak near 0 ppm attributed to antimagnetic substances, such as Na^+ in the SEI, Na^+ adsorbed at defect sites, and residual sodium salts on the anode surface; (ii) a broad peak ranging from 700 to 1,000 ppm, indicating an increase in kinetic diffusion contribution; and (iii) a signal peak at 1,134 ppm. As the discharge process progresses, the signal of Glu shifts gradually from 745 ppm (50 mV) to 937 ppm (10 mV) before stabilizing around the same position at 0 mV. On the other hand, the peak of MgGlu transitions from 680 ppm (50 mV) to 1,018 ppm (0 mV) and then further increases to 1,029 ppm during over-discharge. The signal of the fully discharged sample at 0 V closely resembles that of metallic sodium (1,134 ppm), indicating a higher density of Na 2s states at the Fermi level in MgGlu, resembling metallic sodium. These results suggest that the plateau capacity is influenced by both interlayer insertion and microporous filling behaviors, with the contribution ratio varying slightly based on the microstructure.

The combination of ^{23}Na NMR and SAXS techniques enabled the investigation of the sodium-ion filling process in pores within the low-voltage plateau region. Au *et al.* successfully synthesized a series of HC materials with varying carbonization temperatures using glucose as the carbon source through hydrothermal and high-temperature heat treatments[128]. They characterized the structures of these materials and examined the effects of HC porosity and defect concentration on electrochemical properties using

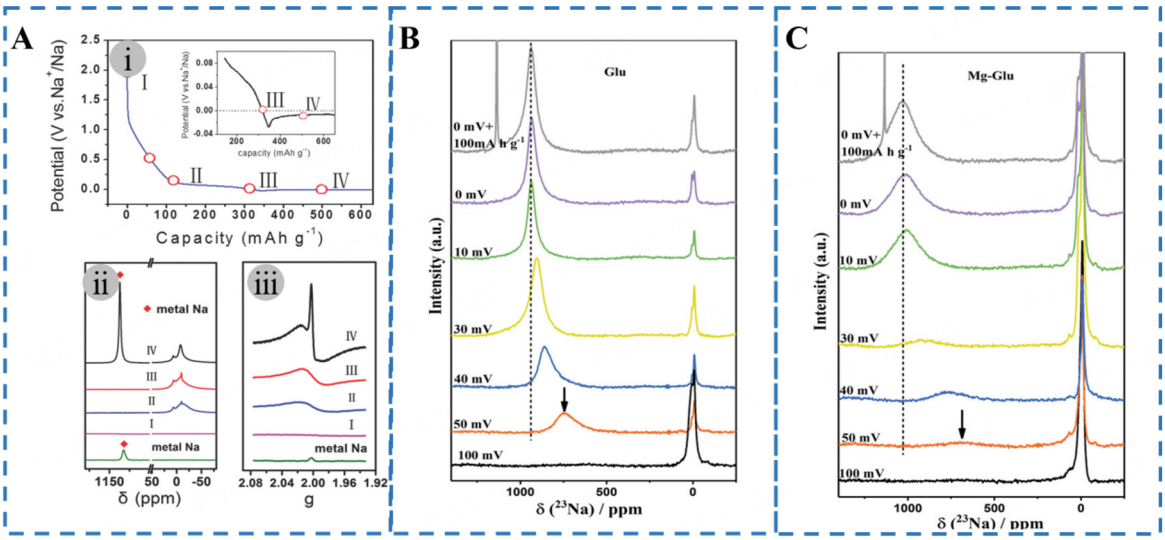

Figure 16. (A) (i) The discharge-charge curve for HC-1300 electrode. (ii) ^{23}Na MAS NMR of HC-1300. (iii) The EPR spectra of the HC-1300 electrode at different discharge states between -0.03 and 2.0 V[31] (Copyright 2017, WILEY-VCH Verlag GmbH & Co. KGaA, Weinheim). *Ex situ* ^{23}Na MAS NMR spectra of (B) Glu and (C) Mg-Glu at different discharge states[27] (Copyright 2022, Wiley-VCH GmbH).

solid-state NMR [Solid-state Nuclear Magnetic Resonance (ssNMR)] and SAXS techniques. By employing SAXS, the layer spacing and in-plane distance of the HC materials were found to approach the values observed in graphite at higher temperatures. NMR results revealed that in the high-voltage slope region, sodium primarily adsorbed as ions on the surface defects of the HC. Conversely, in the low-voltage plateau region, sodium predominantly occupied the pores. As the pore size increased, the sodium located within the pores approached characteristics similar to metallic sodium. This report offers valuable insights and concepts for the design of HC anodes for SIBs, suggesting strategies to optimize layer spacing and enhance porosity for improved performance.

ssNMR offers high-resolution spectra, has a wide range of applicable and with the capability of quantitative analysis, and shows sensitivity to trace components. However, it cannot provide effective information for highly symmetrical crystals or rapidly moving liquids. Furthermore, its data analysis is complex and with lower reproducibility.

4. Chromogenic Reaction

The chemical reaction between sodium and the proton solvent, ethanol, differs based on the form of sodium (metallic or ionic). Following a charge/discharge cycle, the electrode can be immersed in an ethanol solution that includes a phenolphthalein indicator. The presence of sodium in the HC electrode can be ascertained by monitoring the color change.

Thus, Wang *et al.* investigated the storage mechanism of sodium in HC materials derived from sucrose through a color development reaction[32]. The HC electrode pieces were subjected to charging/discharging at different voltages; then, they were immersed in an ethanol solution containing a phenolphthalein indicator. The solution displayed a red color and significant bubble formation in the presence of metallic sodium within the electrode pieces. Figure 17A clearly illustrates the intensification of the ethanol solution color during the discharge process, whereas the color gradually fades during the charging process. To evaluate the

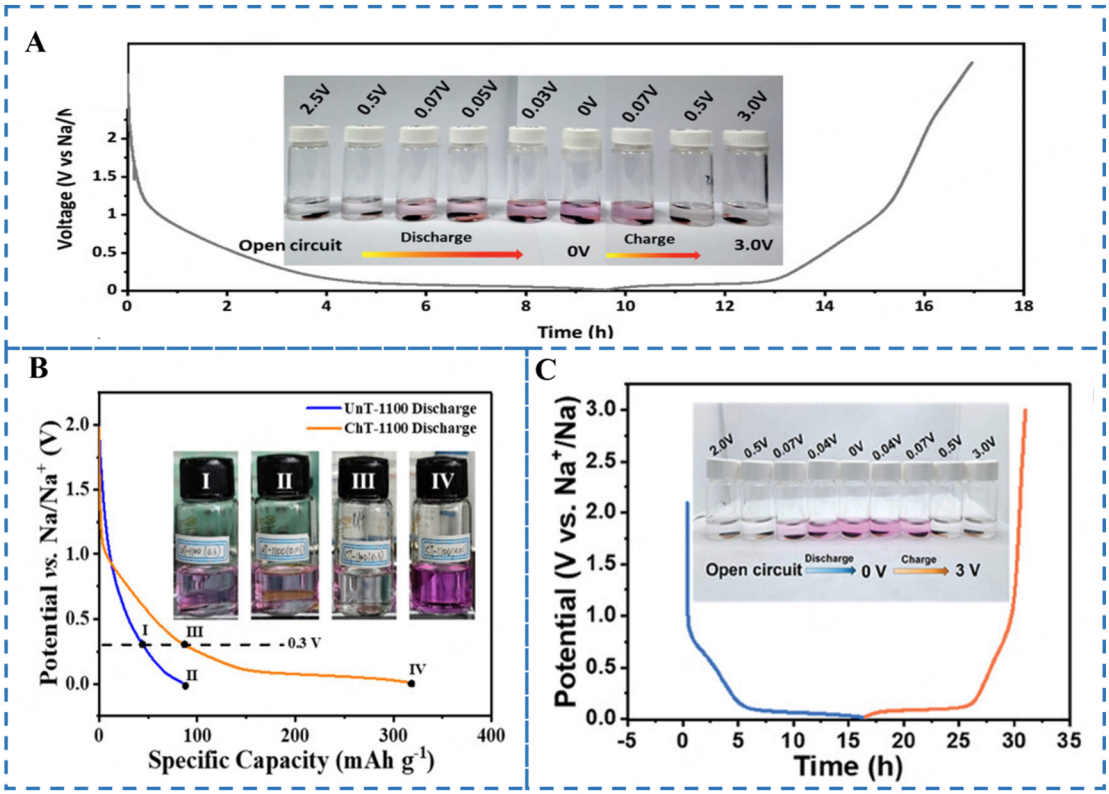

Figure 17. (A) The typical charge/discharge profile of HC electrode and the color changes of ethanol containing 1% phenolphthalein after reaction with HC at different potentials[32] (Copyright 2023, American Chemical Society). (B) Galvanostatic discharge curves of BHCs at 50 mA/g (inset: optical photographs of electrodes at different discharge stages soaked in an ethanol solution containing phenolphthalein, numbered with Roman numerals corresponding to the discharge stage[169]) (Copyright 2022, Sichuan University and John Wiley & Sons Australia, Ltd). (C) Typical charge/discharge curves of HCMP-CO_2 and the corresponding color change of ethanol containing 1% phenolphthalein after reaction with the HCMP-CO_2 electrode at different potentials[138] (Copyright 2023, Wiley-VCH).

state of sodium in the high-voltage slope region, an electrode piece discharged to 0.9 V was placed in an ethanol solution, showing no significant color change, indicating the absence of quasi-metallic sodium clusters in this area. The color change patterns of the pristine electrode piece, electrode piece with deposited sodium (-0.01 V), and metallic sodium immersed in ethanol solution remained consistent with those observed in the control group. It is important to note that the deposition of sodium metal requires surpassing the nucleation overpotential, making it extremely challenging to achieve pure sodium metal across the entire discharge range to 0 V. The authors have successfully validated their proposed theoretical computational model, offering a robust approach to assess the ion state of alkali metals ion in electrode materials.

Similarly, Zhou *et al.* observed that ethanol reacted with quasi-metallic sodium to form sodium ethanol, leading to a red color change in the phenolphthalein indicator[169]. To delve deeper into this phenomenon, they discharged the UnT-1100 and ChT-1100 electrodes to 0.3 and 0.01 V, respectively. The UnT-1100 electrode, derived from mahogany-based HC material, underwent direct carbonization in a tube furnace at 1,100 °C without prior chemical treatment. Conversely, the ChT-1100 electrode, also derived from mahogany-based HC material, underwent chemical pre-treatment before carbonization in a tube furnace at 1,100 °C. Subsequently, any residual electrolyte on the electrodes was removed using 1,2-dimethoxyethane (DME). Finally, both electrodes were individually immersed in a phenolphthalein-ethanol solution for further analysis. As shown in Figure 17B, both UnT-1100 electrodes discharged to 0.3 and 0.01 V exhibited

minimal bubble formation in the ethanol solution, accompanied by a light red color change, indicating that sodium ions in the UnT-1100 electrode were predominantly stored via surface adsorption. The discoloration of the solution suggests weak sodium-ion adsorption, facilitating easy release to form sodium ethanol. In contrast, when the ChT-1100 electrode was discharged to 0.01 V and placed in the ethanol solution, significant bubble formation occurred, turning the solution a deep red hue. These observations confirmed the presence of quasi-metallic sodium in the ChT-1100 electrode and the mechanism by which sodium fills closed pores. Furthermore, Zheng *et al*. corroborated the filling behavior of quasi-metallic sodium clusters in closed pores (as shown in Figure 17C)[138].

Colorimetric reactions are simple to perform, and the results are visually observable, which facilitates rapid assessment and interpretation. However, the color change can be influenced by environmental factors such as light, and strong subjectivity may lead to low accuracy of the results. Moreover, according to the reaction principles, the intercalated compound (NaC_x) formed after Na^+ is intercalated into the graphene sheets will also react with ethanol. This means that colorimetric reactions cannot accurately distinguish whether intercalation or pore filling occurs in the plateau region.

5. Density Functional Theory Calculations

Theoretical calculations play a crucial role in accurately predicting the structural evolution of HC anodes, the sodium storage rate, and various other key factors. These calculations serve as a reliable tool for modeling a wide range of physical and chemical processes in materials. Among the various computational methods available, density functional theory (DFT) calculations are widely utilized[170].

The field of SIB material preparation heavily relies on the application of theoretical calculations. In a report by Tang *et al*., theoretical calculations were used to replicate parallel graphene sheets and pore architectures in HC materials[28]. This involved modeling graphene sheets with varying layer spacings and curvatures to investigate the relationship between the structure of HC materials and their performance in sodium storage. Figure 18A illustrates the storage positions of sodium ions in various microstructures. In parallel graphene sheets, these ions are typically stored in the center of the six-membered carbon ring or adsorbed on the surface of the C-C bond. In curved graphene sheets, sodium ions tend to be embedded within the interior of the C-C bond. DFT calculations were employed to calculate the binding energies of sodium ions in parallel bis-graphite layers with d_{002} values ranging from 3.4 to 5.2 Å. The binding energy of sodium ions gradually decreases as the layer spacing increases, reaching 0 eV at d_{002} = 3.8 Å. The binding energy remains constant as the layer spacing expands to 5.2 Å, indicating that a d_{002} value greater than 0.383 nm is more advantageous for storing Na^+. Comparing the binding energies of sodium ions on the inner and outer surfaces of curved graphene sheets, it was found that the binding energies on the inner surface were lower than those on the outer surface. The study also evaluated the impact of the graphene sheet's curvature on sodium storage. When the curvature exceeded 23.5%, sodium ions began to be absorbed within the graphene sheets, and at a curvature beyond 31.4%, they were absorbed on the outer surface. This suggests that an optimal curvature is beneficial for enhancing the sodium storage capability of HC materials. Additionally, the enclosed pores formed by curved graphene sheets provide advantages for storing sodium ions. This report provides valuable insights into the development of high-performance anodes for sodium storage in SIBs.

Furthermore, Sun *et al*. successfully controlled residual oxygen atoms and defects in HC by manipulating the atmosphere during pyrolytic synthesis using a combination of sucrose and phenolic resin as a precursor[119]. They utilized DFT theoretical calculations to elucidate the relationship between residual

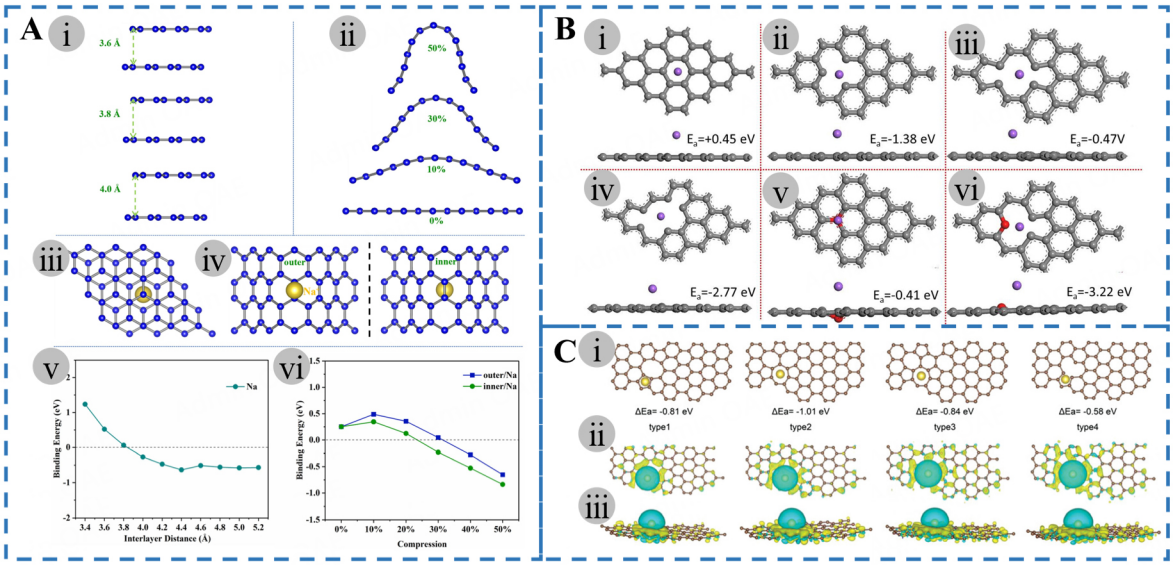

Figure 18. (A) (i) Models of planar graphite layers with various interlayer distances of 3.6, 3.8 and 4.0 Å, (ii) models of single-layer graphene with different compression ratios of 0 %, 10 %, 30 % and 50 %, (iii) the most stable adsorption configuration for Na^+ in planar graphite layers, (iv) the most stable adsorption configuration for Na^+ in the in-plane and out-plane of single-layer curved-graphene, (v) the binding energy of Na^+ in different interlayer distances (3.4 to 5.2 Å) and (vi) Na^+ on graphene with different compression ratios (0 % to 50 %)[28] (Copyright 2023 Elsevier B.V). (B) (i) Atomic structure of Na^+ absorbed on pure graphene. (ii) graphene with mono-defect. (iii) bi-defect, (iv) tri-defect, (v) O doping, (vi) and O/mono-defect doping[119] (Copyright 2019, Elsevier Ltd). (C) Theoretical simulations and related results. Na atom was absorbed on the (i) carbon structures with di-vacancy defects (type1, type2, type3) and single vacancy defects (type4). (ii and iii) Top view and side view of the difference in electron density of Na absorbed by different carbon structures. The yellow and blue regions represent the increased and decreased electron density, respectively. The brown and yellow balls represent the C and Na atoms, respectively[120] (Copyright 2020, WILEY-VCH Verlag GmbH & Co. KGaA, Weinheim).

oxygen atoms and defects and the ICE of HC. As shown in Figure 18B, the calculations reveal that the binding energy of Na^+ in pristine graphene flakes is +0.45 eV, leading to a challenge in Na^+ adsorption. However, in graphene flakes with single, double, and triple defects, as well as in graphene flakes doped with only oxygen atoms or with oxygen atoms in single-deficient substrates, the binding energies are -1.38, -0.47, -0.277, -0.41, and -3.22 eV, respectively. These variations suggest that the presence of oxygen atoms and defects enhances Na^+ adsorption in graphene layers. According to Guo *et al.*, DFT studies unveiled (as shown in Figure 18C) that the intrinsic defects in HC act as active sites for sodium storage, and the concentration of these defects directly correlates with the performance of sodium storage[120]. The Na^+ adsorption energy in ideal graphite structures is +0.22 eV. For graphene sheet substrates with double vacancy defects (types 1, 2, and 3), the adsorption energies are -0.81, -1.01, and -0.84, respectively. In HC with single vacancy defects (type 4), the adsorption energy is -0.58 eV. The Na^+ adsorption capability is more pronounced in carbon structures containing defects, with double vacancy defects exhibiting greater strength than single vacancy defects. Comparing the charge densities of Na^+ in the four models near the Fermi energy level, it is evident that the density of states at the defects is significantly higher than that of ideal graphite. This indicates that the presence of defects benefits the enhancement of electronic conductivity and sodium storage capabilities in HC.

DFT calculations can study various chemical and material systems. They provide information on electronic density, electronic band structure, density of states, and reaction mechanisms, which helps understand the electronic properties and reaction behaviors of samples. However, the accuracy of DFT results depends on the chosen exchange-correlation functional, and different parameters can yield significantly varying results.

Additionally, DFT often needs to be combined with other methods to better study dynamic processes such as chemical reaction pathways and molecular dynamics.

Due to limitations of time and space, existing characterization techniques inevitably have inherent limitations during their application. Single characterization methods often cannot fully reveal the presence of closed pores or accurately validate the storage mechanism of Na^+ within these closed pores. Given the crucial role that closed pores play in enhancing the plateau capacity of HC materials, it is particularly important to use multiple characterization techniques in combination. By integrating the strengths of different techniques, we can obtain more precise and comprehensive information about closed pores. Multi-dimensional characterization methods not only effectively address the shortcomings of individual techniques but also deepen the systematic understanding of closed pore behavior, thereby advancing related scientific research and applications, and providing more reliable data support for exploring sodium storage mechanisms in HC.

SUMMARY AND OUTLOOK

The microstructure of HC materials can be categorized into three components: pseudo-graphite microcrystals, defects, and nanopores. Graphene flakes are curved and stacked (usually in three layers) to create short-range ordered pseudo-graphite domains, within which intrinsic defects such as edges and vacancies, as well as extrinsic defects such as oxygen-containing functional groups, coexist. The presence of nanopores is a result of the random arrangement of carbon layers with specific curvature. The dimensions, configuration, openness, or closure of the nanopores play a crucial role in influencing the electrochemical performance of HC anodes. In regions with low-voltage plateaus, sodium ions are mainly stored in closed pores in the form of quasi-metallic clusters. Therefore, exploring the preparation and characterization techniques of closed pores is essential for producing HC anodes with enhanced reversible capacity.

The process of preparing HC materials typically maintains the inherent morphology of the precursor. The release of gases such as H_2O, CO_2, and CH_4 during pyrolysis promotes the formation of pore structures, and closed pores are ultimately created through the reorganization of carbon atoms and the interconnection of curved carbon layers during subsequent carbonization. By selecting appropriate precursors abundant in pores, HC materials with plentiful closed pores can be directly obtained through pyrolysis. Furthermore, the following techniques can be used to generate HC materials with a substantial number of enclosed pores:

(1) The precursor of HC materials at 600-1,200 °C carbonized by using physical oxidation or gasification agents such as O_2, CO_2, or steam.

(2) Introducing templating or pore-forming agents into the precursors, and subsequently removing them during carbonization or further processing.

(3) Chemically treating the precursors with acids or bases before processing and eliminating residual acids or bases during subsequent treatments.

Introducing numerous pores into materials is achievable; similarly, a high volume of open pores can be transformed into closed pores. Moreover, closed pores can also be generated through the modulation of precursor morphology, bio-fermentation processes, and deposition of an artificial SEI film on the HC surface. Selecting suitable preparation methods is a key strategy for creating abundant closed pores within HC materials.

Numerous advanced techniques have been utilized for characterizing confined pores, with TEM offering insight into the microscopic morphology of pores within HC materials. However, it may not accurately differentiate between open and closed pores. SAXS coupled with gas adsorption-desorption curves and true density measurements can provide more precise information about closed pores. Experimental results from XPS, EPR, ssNMR, and chromogenic reactions can complement each other in exploring the existence state of sodium within closed pores. DFT calculations are instrumental in evaluating kinetic performance parameters of sodium ions in HC anodes. By combining these characterization tools, specific details regarding closed pores and the sodium storage mechanism in HC materials can be obtained.

While numerous researchers have delved into closed pore studies and proposed various preparation methods and characterization tools, there remains a need for more comprehensive investigations to understand the formation mechanisms of closed pores and to enhance the plateau capacity of HC anodes. The following outlook is proposed:

(1) The sodium storage mechanism in HC remains a topic of debate, but closed pores have shown significant potential for increasing plateau capacity. By focusing on the microstructure of HC, especially the closed pore architecture, and by controlling factors such as closed pore size and volume, devising improved closed pore preparation strategies, and advancing high-performance HC anode development, we can pave the way for a promising future in SIB technology.

(2) Further research is required on physical methods, such as CO_2 etching, and the development of artificial SEI films to create closed pores. Effective techniques for preparing enclosed pores are still being explored, with greater focus needed on understanding the formation mechanism of closed pores in biomass-derived HC. Systematic studies on the impact of precursors and constituents with different microstructures on closed pore formation during the carbonization process are essential.

(3) Advanced characterization methods have demonstrated that the size and volume of closed pores play a crucial role in influencing electrochemical properties. Despite numerous characterization techniques available to determine key parameters of closed pores, not all have been fully utilized in research. It is imperative to leverage all available testing methods in future studies to ensure accurate and reliable conclusions are drawn.

DECLARATIONS

Authors' contributions

Investigation, writing - original draft: Guo, Y.
Investigation, formal analysis: Ji, S.
Methodology: Liu, F.
Investigation, writing - review & editing: Zhu, Z.
Methodology, resources: Xiao, J.
Supervision, investigation: Liu, K.
Methodology, resources: Zhang, Y.
Validation, writing - review & editing: Liao, S.
Writing - review & editing, validation, supervision, project administration, investigation, funding acquisition, formal analysis, conceptualization: Zeng, X.

Availability of data and materials
Not applicable.

Financial support and sponsorship
This work is supported by the Natural Science Foundation of Yunnan Province (202401AW070016), the Yunnan Major Scientific and Technological Projects (202202AG050003), the Open Project of Yunnan Precious Metals Laboratory Co., Ltd (YPML2023050255) , the Innovation Capacity Construction and Enhancement Projects of Engineering Research Center of Yunnan Province (2023-XMDJ-00617107) and the Opening Project of Engineering Research Center of Comprehensive Utilization and Clean Processing of Phosphorus Resources, Ministry of Education (2024CUCPPR01) are gratefully acknowledged.

Conflict of interest
All authors declared that there are no conflicts of interest.

Ethical approval and consent to participate
Not applicable.

Consent for publication
Not applicable.

REFERENCES
1. Wang, H. G.; Wu, Q.; Wang, Y.; et al. Molecular engineering of monodisperse SnO_2 nanocrystals anchored on doped graphene with high-performance lithium/sodium-storage properties in half/full cells. *Adv. Energy. Mater.* **2019**, *9*, 1802993. DOI
2. Kim, H.; Kim, H.; Ding, Z.; et al. Recent progress in electrode materials for sodium-ion batteries. *Adv. Energy. Mater.* **2016**, *6*, 1600943. DOI
3. Pan, H.; Hu, Y. S.; Chen, L. Room-temperature stationary sodium-ion batteries for large-scale electric energy storage. *Energy. Environ. Sci.* **2013**, *6*, 2338-60. DOI
4. Wang, Q.; Zhao, C.; Lu, Y.; et al. Advanced nanostructured anode materials for sodium-ion batteries. *Small* **2017**, *13*, 1701835. DOI
5. Huang, G.; Kong, Q.; Yao, W.; Wang, Q. Poly tannic acid carbon rods as anode materials for high performance lithium and sodium ion batteries. *J. Colloid. Interface. Sci.* **2023**, *629*, 832-45. DOI
6. Liu, Y.; Tai, Z.; Zhou, T.; et al. An all-integrated anode via interlinked chemical bonding between double-shelled-yolk-structured silicon and binder for lithium-ion batteries. *Adv. Mater.* **2017**, *29*, 1703028. DOI
7. Goodenough, J. B.; Park, K. S. The Li-ion rechargeable battery: a perspective. *J. Am. Chem. Soc.* **2013**, *135*, 1167-76. DOI PubMed
8. Sekai, K.; Azuma, H.; Omaru, A.; et al. Lithium-ion rechargeable cells with $LiCoO_2$ and carbon electrodes. *J. Power. Sources.* **1993**, *43*, 241-4. DOI
9. Roberts, S.; Kendrick, E. The re-emergence of sodium ion batteries: testing, processing, and manufacturability. *Nanotechnol. Sci. Appl.* **2018**, *11*, 23-33. DOI PubMed PMC
10. Usiskin, R.; Lu, Y.; Popovic, J.; et al. Fundamentals, status and promise of sodium-based batteries. *Nat. Rev. Mater.* **2021**, *6*, 1020-35. DOI
11. Zhang, T.; Li, C.; Wang, F.; et al. Recent advances in carbon anodes for sodium-ion batteries. *Chem. Rec.* **2022**, *22*, e202200083. DOI
12. Katsuyama, Y.; Nakayasu, Y.; Kobayashi, H.; Goto, Y.; Honma, I.; Watanabe, M. Rational route for increasing intercalation capacity of hard carbons as sodium-ion battery anodes. *ChemSusChem* **2020**, *13*, 5762-8. DOI
13. Li, Z.; Chen, Y.; Jian, Z.; et al. Defective hard carbon anode for Na-ion batteries. *Chem. Mater.* **2018**, *30*, 4536-42. DOI
14. Olsson, E.; Cottom, J.; Cai, Q. Defects in hard carbon: where are they located and how does the location affect alkaline metal storage? *Small* **2021**, *17*, e2007652. DOI PubMed
15. Chu, Y.; Zhang, J.; Zhang, Y.; et al. Reconfiguring Hard carbons with emerging sodium-ion batteries: a perspective. *Adv. Mater.* **2023**, *35*, e2212186. DOI
16. Ghimbeu C, Górka J, Simone V, Simonin L, Martinet S, Vix-Guterl C. Insights on the Na^+ ion storage mechanism in hard carbon: discrimination between the porosity, surface functional groups and defects. *Nano. Energy.* **2018**, *44*, 327-35. DOI
17. Li, Y.; Lu, Y.; Meng, Q.; et al. Regulating pore structure of hierarchical porous waste cork-derived hard carbon anode for enhanced

Na storage performance. *Adv. Energy. Mater.* **2019**, *9*, 1902852. DOI

18. Xie, F.; Xu, Z.; Guo, Z.; et al. Disordered carbon anodes for Na-ion batteries - quo vadis? *Sci. China. Chem.* **2021**, *64*, 1679-92. DOI
19. Yue, L.; Lei, Y.; Niu, Y.; Qi, Y.; Xu, M. Recent advances of pore structure in disordered carbons for sodium storage: a mini review. *Chem. Rec.* **2022**, *22*, e202200113. DOI PubMed
20. Stevens, D. A.; Dahn, J. R. High capacity anode materials for rechargeable sodium-ion batteries. *J. Electrochem. Soc.* **2000**, *147*, 1271. DOI
21. Stevens, D. A.; Dahn, J. R. An *in situ* small-angle X-ray scattering study of sodium insertion into a nanoporous carbon anode material within an operating electrochemical cell. *J. Electrochem. Soc.* **2000**, *147*, 4428. DOI
22. Cao, Y.; Xiao, L.; Sushko, M. L.; et al. Sodium ion insertion in hollow carbon nanowires for battery applications. *Nano. Lett.* **2012**, *12*, 3783-7. DOI
23. Zhu, Y. E.; Gu, H.; Chen, Y. N.; Yang, D.; Wei, J.; Zhou, Z. Hard carbon derived from corn straw piths as anode materials for sodium ion batteries. *Ionics* **2018**, *24*, 1075-81. DOI
24. Bommier, C.; Ji, X.; Greaney, P. A. Electrochemical properties and theoretical capacity for sodium storage in hard carbon: insights from first principles calculations. *Chem. Mater.* **2019**, *31*, 658-77. DOI
25. Jian, Z.; Xing, Z.; Bommier, C.; Li, Z.; Ji, X. Hard carbon microspheres: potassium-ion anode versus sodium-ion anode. *Adv. Energy. Mater.* **2016**, *6*, 1501874. DOI
26. Komaba, S.; Murata, W.; Ishikawa, T.; et al. Electrochemical Na insertion and solid electrolyte interphase for hard-carbon electrodes and application to Na-ion batteries. *Adv. Funct. Mater.* **2011**, *21*, 3859-67. DOI
27. Chen, X.; Tian, J.; Li, P.; et al. An overall understanding of sodium storage behaviors in hard carbons by an "adsorption-intercalation/filling" hybrid mechanism. *Adv. Energy. Mater.* **2022**, *12*, 2200886. DOI
28. Tang, T.; Zhu, W.; Lan, P.; et al. Macro-micro structure engineering of bio-spore-derived hard carbon as an efficient anode in sodium ion batteries. *Chem. Eng. J.* **2023**, *475*, 146212. DOI
29. Chen, X.; Liu, C.; Fang, Y.; et al. Understanding of the sodium storage mechanism in hard carbon anodes. *Carbon. Energy.* **2022**, *4*, 1133-50. DOI
30. Dai, S.; Tu, Y.; Yan, L.; et al. Observation and suppression of metallic and metallic-like plating on hard carbon for high-performance sodium-ion batteries. *Mater. Today. Energy.* **2024**, *44*, 101605. DOI
31. Qiu, S.; Xiao, L.; Sushko, M. L.; et al. Manipulating adsorption-insertion mechanisms in nanostructured carbon materials for high-efficiency sodium ion storage. *Adv. Energy. Mater.* **2017**, *7*, 1700403. DOI
32. Wang, Z.; Feng, X.; Bai, Y.; et al. Probing the energy storage mechanism of quasi-metallic Na in hard carbon for sodium-ion batteries. *Adv. Energy. Mater.* **2021**, *11*, 2003854. DOI
33. Paul, R.; Zemlyanov, D.; Roy, A. K.; Voevodin, A. A. Chapter 3 - Characterization techniques and analytical methods of carbon-based materials for energy applications. In: Carbon based nanomaterials for advanced thermal and electrochemical energy storage and conversion. 2019; pp. 63-88. DOI
34. Dou, X.; Hasa, I.; Saurel, D.; et al. Hard carbons for sodium-ion batteries: structure, analysis, sustainability, and electrochemistry. *Mater. Today.* **2019**, *23*, 87-104. DOI
35. Bartoli, M.; Piovano, A.; Elia, G. A.; et al. Pristine and engineered biochar as Na-ion batteries anode material: a comprehensive overview. *Renew. Sustain. Energy. Rev.* **2024**, *194*, 114304. DOI
36. Xie, L. J.; Tang, C.; Song, M. X.; et al. Molecular-scale controllable conversion of biopolymers into hard carbons towards lithium and sodium ion batteries: a review. *J. Energy. Chem.* **2022**, *72*, 554-69. DOI
37. Yang, C.; Zhao, J.; Dong, B.; et al. Advances in the structural engineering and commercialization processes of hard carbon for sodium-ion batteries. *J. Mater. Chem. A.* **2024**, *12*, 1340-58. DOI
38. Zhao, Z.; Sun, L.; Li, Y.; Feng, W. Polymer-derived carbon materials for energy storage devices: a mini review. *Carbon* **2023**, *210*, 118066. DOI
39. Wang, Y.; Li, M.; Zhang, Y.; Zhang, N. Hard carbon for sodium storage: mechanism and performance optimization. *Nano. Res.* **2024**, *17*, 6038-57. DOI
40. Zhu, Z.; Liang, F.; Zhou, Z.; et al. Expanded biomass-derived hard carbon with ultra-stable performance in sodium-ion batteries. *J. Mater. Chem. A.* **2018**, *6*, 1513-22. DOI
41. Zhang, Y.; Li, X.; Dong, P.; et al. Honeycomb-like hard carbon derived from pine pollen as high-performance anode material for sodium-ion batteries. *ACS. Appl. Mater. Interfaces.* **2018**, *10*, 42796-803. DOI
42. Li, X.; Zeng, X.; Ren, T.; et al. The transport properties of sodium-ion in the low potential platform region of oatmeal-derived hard carbon for sodium-ion batteries. *J. Alloys. Compd.* **2019**, *787*, 229-38. DOI
43. Zhang, Y.; Cheng, H.; Liu, J.; Li, X.; Zhu, Z. Laver-derived carbon as an anode for SIBswith excellent electrochemical performance. *Int. J. Electrochem. Sci.* **2020**, *15*, 5144-53. DOI
44. Zhu, Z.; Li, X.; Zhang, Z.; et al. N/S codoping modification based on the metal organic framework-derived carbon to improve the electrochemical performance of different energy storage devices. *J. Energy. Chem.* **2022**, *74*, 394-403. DOI
45. Deng, B.; Huang, Q.; Zhang, W.; et al. Design high performance biomass-derived renewable carbon material for electric energy storage system. *J. Clean. Prod.* **2021**, *309*, 127391. DOI
46. Zhu, Z.; Zeng, X.; Wu, H.; et al. Green energy application technology of litchi pericarp-derived carbon material with high performance. *J. Clean. Prod.* **2021**, *286*, 124960. DOI

47. Zhu, Z.; Zhong, W.; Zhang, Y.; et al. Elucidating electrochemical intercalation mechanisms of biomass-derived hard carbon in sodium-/potassium-ion batteries. *Carbon. Energy.* **2021**, *3*, 541-53. DOI
48. Li, X.; Ding, C.; Liang, Q.; et al. Progress in hard carbons for sodium-ion batteries: microstructure, sodium storage mechanism and initial Coulombic efficiency. *J. Energy. Storage.* **2024**, *98*, 112986. DOI
49. Zeng, Z.; Mao, Y.; Hu, Z.; et al. Research progress and commercialization of biologically derived hard carbon anode materials for sodium-ion batteries. *Ind. Eng. Chem. Res.* **2023**, *62*, 15343-59. DOI
50. Li, Y.; Fu, H.; Feng, W. Recent progress of synthetic polymer-derived hard carbon in sodium-ion batteries. *Sci. Technol.* **2022**, *1*, 11-23. DOI
51. Fox, A. M.; Vrankovic, D.; Buchmeiser, M. R. Influence of the silicon-carbon interface on the structure and electrochemical performance of a phenolic resin-derived Si@C core-shell nanocomposite-based anode. *ACS. Appl. Mater. Interfaces.* **2022**, *14*, 761-70. DOI PubMed
52. Dong, X.; Chen, L.; Liu, J.; Haller, S.; Wang, Y.; Xia, Y. Environmentally-friendly aqueous Li (or Na)-ion battery with fast electrode kinetics and super-long life. *Sci. Adv.* **2016**, *2*, e1501038. DOI PubMed PMC
53. Goujon, N.; Lahnsteiner, M.; Cerrón-Infantes, D. A.; et al. Dual redox-active porous polyimides as high performance and versatile electrode material for next-generation batteries. *Mater. Horiz.* **2023**, *10*, 967-76. DOI PubMed PMC
54. Narzary, B. B.; Baker, B. C.; Yadav, N.; D'elia, V.; Faul, C. F. J. Crosslinked porous polyimides: structure, properties and applications. *Polym. Chem.* **2021**, *12*, 6494-514. DOI
55. Zhao, D.; Wang, H.; Bai, Y.; Yang, H.; Song, H.; Li, B. Preparation of advanced multi-porous carbon nanofibers for high-performance capacitive electrodes in supercapacitors. *Polymers* **2023**, *15*, 213. DOI PubMed PMC
56. Chou, S. C.; Sun, B. Y.; Cheang, W. H.; et al. A flexible bioelectrode based on IrO_2-coated metallized polypropylene micromembrane. *Ceram. Int.* **2021**, *47*, 32554-61. DOI
57. Liu, X.; Ma, C.; Wen, Y.; et al. Highly efficient conversion of waste plastic into thin carbon nanosheets for superior capacitive energy storage. *Carbon* **2021**, *171*, 819-28. DOI
58. Wang, Y.; Luo, Z.; Qian, Y.; Zhang, W.; Chen, L. Monolithic MXene composites with multi-responsive actuating and energy-storage multi-functions. *Chem. Eng. J.* **2023**, *454*, 140513. DOI
59. Xiao, L.; Cao, Y.; Henderson, W. A.; et al. Hard carbon nanoparticles as high-capacity, high-stability anodic materials for Na-ion batteries. *Nano. Energy.* **2016**, *19*, 279-88. DOI
60. He, Y.; Han, X.; Du, Y.; et al. Conjugated polymer-mediated synthesis of sulfur- and nitrogen-doped carbon nanotubes as efficient anode materials for sodium ion batteries. *Nano. Res.* **2018**, *11*, 2573-85. DOI
61. Wang, H. L.; Shi, Z. Q.; Jin, J.; Chong, C. B.; Wang, C. Y. Properties and sodium insertion behavior of Phenolic Resin-based hard carbon microspheres obtained by a hydrothermal method. *J. Electroanal. Chem.* **2015**, *755*, 87-91. DOI
62. Han, H.; Chen, X.; Qian, J.; et al. Hollow carbon nanofibers as high-performance anode materials for sodium-ion batteries. *Nanoscale* **2019**, *11*, 21999-2005. DOI
63. Wang, Y.; Lu, Y.; Liu, X.; et al. Facile synthesis and electrochemical properties of alicyclic polyimides based carbon microflowers for electrode materials of supercapacitors. *J. Energy. Storage.* **2022**, *47*, 103656. DOI
64. Porporato, S.; Bartoli, M.; Piovano, A.; et al. Repurposing face masks after use: from wastes to anode materials for Na-ion batteries. *Batteries* **2022**, *8*, 183. DOI
65. Chen, D.; Luo, K.; Yang, Z.; et al. Direct conversion of ester bond-rich waste plastics into hard carbon for high-performance sodium storage. *Carbon* **2021**, *173*, 253-61. DOI
66. Liu, C.; Xiao, N.; Wang, Y.; et al. Carbon clusters decorated hard carbon nanofibers as high-rate anode material for lithium-ion batteries. *Fuel. Process. Technol.* **2018**, *180*, 173-9. DOI
67. Wu, F.; Dong, R.; Bai, Y.; et al. Phosphorus-doped hard carbon nanofibers prepared by electrospinning as an anode in sodium-ion batteries. *ACS. Appl. Mater. Interfaces.* **2018**, *10*, 21335-42. DOI
68. Dong, D.; Xiao, Y. Recent progress and challenges in coal-derived porous carbon for supercapacitor applications. *Chem. Eng. J.* **2023**, *470*, 144441. DOI
69. Wang, B.; Xia, J.; Dong, X.; Guo, H.; Li, W. Study on sodium storage behavior of hard carbons derived from coal with different grades of metamorphism. *CIESC. J.* **2021**, *72*, 5738-50. DOI
70. Zou, Y.; Li, H.; Qin, K.; et al. Low-cost lignite-derived hard carbon for high-performance sodium-ion storage. *J. Mater. Sci.* **2020**, *55*, 5994-6004. DOI
71. Zhao, G.; Xu, T.; Zhao, Y.; et al. Conversion of aliphatic structure-rich coal maceral into high-capacity hard carbons for sodium-ion batteries. *Energy. Storage. Mater.* **2024**, *67*, 103282. DOI
72. Rybarczyk, M. K.; Li, Y.; Qiao, M.; Hu, Y. S.; Titirici, M. M.; Lieder, M. Hard carbon derived from rice husk as low cost negative electrodes in Na-ion batteries. *J. Energy. Chem.* **2019**, *29*, 17-22. DOI
73. Wang, Q.; Zhu, X.; Liu, Y.; Fang, Y.; Zhou, X.; Bao, J. Rice husk-derived hard carbons as high-performance anode materials for sodium-ion batteries. *Carbon* **2018**, *127*, 658-66. DOI
74. Cao, L.; Hui, W.; Xu, Z.; et al. Rape seed shuck derived-lamellar hard carbon as anodes for sodium-ion batteries. *J. Alloys. Compd.* **2017**, *695*, 632-7. DOI
75. Wu, F.; Liu, L.; Yuan, Y.; et al. Expanding interlayer spacing of hard carbon by natural K^+ doping to boost Na-ion storage. *ACS. Appl. Mater. Interfaces.* **2018**, *10*, 27030-8. DOI

76. Zhang, F.; Yao, Y.; Wan, J.; Henderson, D.; Zhang, X.; Hu, L. High temperature carbonized grass as a high performance sodium ion battery anode. *ACS. Appl. Mater. Interfaces.* **2017**, *9*, 391-7. DOI
77. Deng, W.; Cao, Y.; Yuan, G.; Liu, G.; Zhang, X.; Xia, Y. Realizing improved sodium-ion storage by introducing carbonyl groups and closed micropores into a biomass-derived hard carbon anode. *ACS. Appl. Mater. Interfaces.* **2021**, *13*, 47728-39. DOI
78. Wang, Y.; Feng, Z.; Zhu, W.; et al. High capacity and high efficiency maple tree-biomass-derived hard carbon as an anode material for sodium-ion batteries. *Materials* **2018**, *11*, 1294. DOI PubMed PMC
79. Wang, P.; Qiao, B.; Du, Y.; et al. Fluorine-doped carbon particles derived from lotus petioles as high-performance anode materials for sodium-ion batteries. *J. Phys. Chem. C.* **2015**, *119*, 21336-44. DOI
80. Wang, J.; Yan, L.; Ren, Q.; Fan, L.; Zhang, F.; Shi, Z. Facile hydrothermal treatment route of reed straw-derived hard carbon for high performance sodium ion battery. *Electrochim. Acta.* **2018**, *291*, 188-96. DOI
81. Muruganantham, R.; Wang, F. M.; Yuwono, R. A.; Sabugaa, M.; Liu, W. R. Biomass feedstock of waste mango-peel-derived porous hard carbon for sustainable high-performance lithium-ion energy storage devices. *Energy. Fuels.* **2021**, *35*, 10878-89. DOI
82. Lu, M.; Huang, Y.; Chen, C. Cedarwood bark-derived hard carbon as an anode for high-performance sodium-ion batteries. *Energy. Fuels.* **2020**, *34*, 11489-97. DOI
83. Elizabeth, I.; Singh, B. P.; Trikha, S.; Gopukumar, S. Bio-derived hierarchically macro-meso-micro porous carbon anode for lithium/sodium ion batteries. *J. Power. Sources.* **2016**, *329*, 412-21. DOI
84. Liu, H.; Jia, M.; Yue, S.; et al. Creative utilization of natural nanocomposites: nitrogen-rich mesoporous carbon for a high-performance sodium ion battery. *J. Mater. Chem. A.* **2017**, *5*, 9572-9. DOI
85. Zhu, X.; Li, Q.; Qiu, S.; et al. Hard carbon fibers pyrolyzed from wool as high-performance anode for sodium-ion batteries. *JOM.* **2016**, *68*, 2579-84. DOI
86. Tang, Z.; Zhang, R.; Wang, H.; et al. Revealing the closed pore formation of waste wood-derived hard carbon for advanced sodium-ion battery. *Nat. Commun.* **2023**, *14*, 6024. DOI PubMed PMC
87. Wang, Y.; Yi, Z.; Xie, L.; et al. Releasing free radicals in precursor triggers the formation of closed pores in hard carbon for sodium-ion batteries. *Adv. Mater.* **2024**, *36*, e2401249. DOI
88. Gao, L.; Zhang, G.; Cai, J.; Huang, L.; Zhou, J.; Zhang, L. Rationally exfoliating chitin into 2D hierarchical porous carbon nanosheets for high-rate energy storage. *Nano. Res.* **2020**, *13*, 1604-13. DOI
89. Amiri, A.; Conlee, B.; Tallerine, I.; Kennedy, W. J.; Naraghi, M. A novel path towards synthesis of nitrogen-rich porous carbon nanofibers for high performance supercapacitors. *Chem. Eng. J.* **2020**, *399*, 125788. DOI
90. Guo, Q.; Zhao, X.; Li, Z.; Wang, D.; Nie, G. A novel solid-state electrochromic supercapacitor with high energy storage capacity and cycle stability based on poly(5-formylindole)/WO_3 honeycombed porous nanocomposites. *Chem. Eng. J.* **2020**, *384*, 123370. DOI
91. Bin, D.; Wang, F.; Tamirat, A. G.; et al. Progress in aqueous rechargeable sodium-ion batteries. *Adv. Energy. Mater.* **2018**, *8*, 1703008. DOI
92. Mélinon, P. Vitreous carbon, geometry and topology: a hollistic approach. *Nanomaterials* **2021**, *11*, 1694. DOI PubMed PMC
93. Wahid, M.; Puthusseri, D.; Gawli, Y.; Sharma, N.; Ogale, S. Hard carbons for sodium-ion battery anodes: synthetic strategies, material properties, and storage mechanisms. *ChemSusChem* **2018**, *11*, 506-26. DOI PubMed
94. Wang, G.; Yu, M.; Feng, X. Carbon materials for ion-intercalation involved rechargeable battery technologies. *Chem. Soc. Rev.* **2021**, *50*, 2388-443. DOI
95. Wu, Y. P.; Rahm, E.; Holze, R. Carbon anode materials for lithium ion batteries. *J. Power. Sources.* **2003**, *114*, 228-36. DOI
96. Zhao, C.; Liu, L.; Qi, X.; et al. Solid-state sodium batteries. *Adv. Energy. Mater.* **2018**, *8*, 1703012. DOI
97. Franklin, R. E. Crystallite growth in graphitizing and non-graphitizing carbons. *Proc. R. Soc. Lond. A.* **1951**, *209*, 196-218. DOI
98. Ban, L. L.; Crawford, D.; Marsh, H. Lattice-resolution electron microscopy in structural studies of non-graphitizing carbons from polyvinylidene chloride (PVDC). *J. Appl. Crystallogr.* **1975**, *8*, 415-20. DOI
99. Townsend, S. J.; Lenosky, T. J.; Muller, D. A.; Nichols, C. S.; Elser, V. Negatively curved graphitic sheet model of amorphous carbon. *Phys. Rev. Lett.* **1992**, *69*, 921. DOI
100. Harris, P. J. F.; Tsang, S. C. High-resolution electron microscopy studies of non-graphitizing carbons. *Philos. Mag. A.* **1997**, *76*, 667-77. DOI
101. Mcdonald-Wharry, J. S.; Manley-Harris, M.; Pickering, K. L. Reviewing, combining, and updating the models for the nanostructure of non-graphitizing carbons produced from oxygen-containing precursors. *Energy. Fuels.* **2016**, *30*, 7811-26. DOI
102. Li, Y.; Paranthaman, M. P.; Akato, K.; et al. Tire-derived carbon composite anodes for sodium-ion batteries. *J. Power. Sources.* **2016**, *316*, 232-8. DOI
103. Navarro-Suárez, A. M.; Saurel, D.; Sánchez-Fontecoba, P.; Castillo-Martínez, E.; Carretero-González, J.; Rojo, T. Temperature effect on the synthesis of lignin-derived carbons for electrochemical energy storage applications. *J. Power. Sources.* **2018**, *397*, 296-306. DOI
104. Saurel, D.; Orayech, B.; Xiao, B.; Carriazo, D.; Li, X.; Rojo, T. From charge storage mechanism to performance: a roadmap toward high specific energy sodium-ion batteries through carbon anode optimization. *Adv. Energy. Mater.* **2018**, *8*, 1703268. DOI
105. Cowlard, F. C.; Lewis, J. C. Vitreous carbon - A new form of carbon. *J. Mater. Sci.* **1967**, *2*, 507-12. DOI
106. Li, Z.; Bommier, C.; Chong, Z. S.; et al. Mechanism of Na-ion storage in hard carbon anodes revealed by heteroatom doping. *Adv. Energy. Mater.* **2017**, *7*, 1602894. DOI
107. Olsson, E.; Cottom, J.; Au, H.; et al. Elucidating the effect of planar graphitic layers and cylindrical pores on the storage and diffusion

of Li, Na, and K in carbon materials. *Adv. Funct. Mater.* **2020**, *30*, 1908209. DOI

108. Sun, N.; Guan, Z.; Liu, Y.; et al. Extended "adsorption-insertion" model: a new insight into the sodium storage mechanism of hard carbons. *Adv. Energy. Mater.* **2019**, *9*, 1901351. DOI
109. Emmerich, F. G. Evolution with heat treatment of crystallinity in carbons. *Carbon* **1995**, *33*, 1709-15. DOI
110. Bommier, C.; Surta, T. W.; Dolgos, M.; Ji, X. New mechanistic insights on Na-ion storage in nongraphitizable carbon. *Nano. Lett.* **2015**, *15*, 5888-92. DOI PubMed
111. Kubota, K.; Shimadzu, S.; Yabuuchi, N.; et al. Structural analysis of sucrose-derived hard carbon and correlation with the electrochemical properties for lithium, sodium, and potassium insertion. *Chem. Mater.* **2020**, *32*, 2961-77. DOI
112. Alvin, S.; Yoon, D.; Chandra, C.; et al. Extended flat voltage profile of hard carbon synthesized using a two-step carbonization approach as an anode in sodium ion batteries. *J. Power. Sources.* **2019**, *430*, 157-68. DOI
113. Gomez-Martin, A.; Martinez-Fernandez, J.; Ruttert, M.; Winter, M.; Placke, T.; Ramirez-Rico, J. Correlation of structure and performance of hard carbons as anodes for sodium ion batteries. *Chem. Mater.* **2019**, *31*, 7288-99. DOI
114. Banhart, F.; Kotakoski, J.; Krasheninnikov, A. V. Structural defects in graphene. *ACS. Nano.* **2011**, *5*, 26-41. DOI PubMed
115. Yazyev, O. V.; Louie, S. G. Topological defects in graphene: dislocations and grain boundaries. *Phys. Rev. B.* **2010**, *81*, 195420. DOI
116. Bommier, C.; Mitlin, D.; Ji, X. Internal structure - Na storage mechanisms - electrochemical performance relations in carbons. *Prog. Mater. Sci.* **2018**, *97*, 170-203. DOI
117. Zhang, B.; Ghimbeu, C. M.; Laberty, C.; Vix-Guterl, C.; Tarascon, J. M. Correlation between microstructure and Na storage behavior in hard carbon. *Adv. Energy. Mater.* **2016**, *6*, 1501588. DOI
118. Chen, C.; Huang, Y.; Zhu, Y.; et al. Nonignorable influence of oxygen in hard carbon for sodium ion storage. *ACS. Sustain. Chem. Eng.* **2020**, *8*, 1497-506. DOI
119. Sun, D.; Luo, B.; Wang, H.; Tang, Y.; Ji, X.; Wang, L. Engineering the trap effect of residual oxygen atoms and defects in hard carbon anode towards high initial Coulombic efficiency. *Nano. Energy.* **2019**, *64*, 103937. DOI
120. Guo, R.; Lv, C.; Xu, W.; et al. Effect of intrinsic defects of carbon materials on the sodium storage performance. *Adv. Energy. Mater.* **2020**, *10*, 1903652. DOI
121. Shen, F.; Luo, W.; Dai, J.; et al. Ultra-thick, low-tortuosity, and mesoporous wood carbon anode for high-performance sodium-ion batteries. *Adv. Energy. Mater.* **2016**, *6*, 1600377. DOI
122. Xie, F.; Xu, Z.; Jensen, A. C. S.; et al. Hard-soft carbon composite anodes with synergistic sodium storage performance. *Adv. Funct. Mater.* **2019**, *29*, 1901072. DOI
123. Zhang, X.; Dong, X.; Qiu, X.; et al. Extended low-voltage plateau capacity of hard carbon spheres anode for sodium ion batteries. *J. Power. Sources.* **2020**, *476*, 228550. DOI
124. Lu, P.; Sun, Y.; Xiang, H.; Liang, X.; Yu, Y. 3D amorphous carbon with controlled porous and disordered structures as a high-rate anode material for sodium-ion batteries. *Adv. Energy. Mater.* **2018**, *8*, 1702434. DOI
125. Yang, J.; Wang, X.; Dai, W.; et al. From micropores to ultra-micropores inside hard carbon: toward enhanced capacity in room-/low-temperature sodium-ion storage. *Nanomicro. Lett.* **2021**, *13*, 98. DOI PubMed PMC
126. Alptekin, H.; Au, H.; Jensen, A. C.; et al. Sodium storage mechanism investigations through structural changes in hard carbons. *ACS. Appl. Energy. Mater.* **2020**, *3*, 9918-27. DOI
127. Dahbi, M.; Kiso, M.; Kubota, K.; et al. Synthesis of hard carbon from argan shells for Na-ion batteries. *J. Mater. Chem. A.* **2017**, *5*, 9917-28. DOI
128. Au, H.; Alptekin, H.; Jensen, A. C. S.; et al. A revised mechanistic model for sodium insertion in hard carbons. *Energy. Environ. Sci.* **2020**, *13*, 3469-79. DOI
129. Yamamoto, H.; Muratsubaki, S.; Kubota, K.; et al. Synthesizing higher-capacity hard-carbons from cellulose for Na- and K-ion batteries. *J. Mater. Chem. A.* **2018**, *6*, 16844-8. DOI
130. Zhang, N.; Liu, Q.; Chen, W.; et al. High capacity hard carbon derived from lotus stem as anode for sodium ion batteries. *J. Power. Sources.* **2018**, *378*, 331-7. DOI
131. Liu, J.; Wang, L.; Huang, Z.; Fan, F.; Jiao, L.; Li, F. Facile synthesis of high quality hard carbon anode from Eucalyptus wood for sodium-ion batteries. *Chem. Pap.* **2022**, *76*, 7465-73. DOI
132. Huang, Z.; Qiu, X.; Wang, C.; et al. Revealing the effect of hard carbon structure on the sodium storage behavior by using a model hard carbon precursor. *J. Energy. Storage.* **2023**, *72*, 108406. DOI
133. Zhang, P.; Shu, Y.; Wang, Y.; Ye, J.; Yang, L. Simple and efficient synthesis methods for fabricating anode materials of sodium-ion batteries and their sodium-ion storage mechanism study. *J. Mater. Chem. A.* **2023**, *11*, 2920-32. DOI
134. Ilic, I. K.; Schutjajew, K.; Zhang, W.; Oschatz, M. Sodium storage with high plateau capacity in nitrogen doped carbon derived from melamine-terephthalaldehyde polymers. *J. Mater. Chem. A.* **2021**, *9*, 8711-20. DOI
135. Cheng, D.; Zhou, X.; Hu, H.; et al. Electrochemical storage mechanism of sodium in carbon materials: a study from soft carbon to hard carbon. *Carbon* **2021**, *182*, 758-69. DOI
136. Yuan, M.; Cao, B.; Liu, H.; et al. Sodium storage mechanism of nongraphitic carbons: a general model and the function of accessible closed pores. *Chem. Mater.* **2022**, *34*, 3489-500. DOI
137. Xu, R.; Yi, Z.; Song, M.; et al. Boosting sodium storage performance of hard carbons by regulating oxygen functionalities of the cross-linked asphalt precursor. *Carbon* **2023**, *206*, 94-104. DOI

138. Zheng, Z.; Hu, S.; Yin, W.; et al. CO_2-etching creates abundant closed pores in hard carbon for high-plateau-capacity sodium storage. *Adv. Energy. Mater.* **2024**, *14*, 2303064. DOI
139. Morishita, T.; Tsumura, T.; Toyoda, M.; et al. A review of the control of pore structure in MgO-templated nanoporous carbons. *Carbon* **2010**, *48*, 2690-707. DOI
140. Qiu, C.; Li, A.; Qiu, D.; et al. One-step construction of closed pores enabling high plateau capacity hard carbon anodes for sodium-ion batteries: closed-pore formation and energy storage mechanisms. *ACS. Nano.* **2024**, *18*, 11941-54. DOI
141. Glatthaar, C.; Wang, M.; Wagner, L. Q.; et al. Lignin-derived mesoporous carbon for sodium-ion batteries: block copolymer soft templating and carbon microstructure analysis. *Chem. Mater.* **2023**, *35*, 10416-33. DOI
142. Yin, X.; Lu, Z.; Wang, J.; et al. Enabling fast Na^+ transfer kinetics in the whole-voltage-region of hard-carbon anodes for ultrahigh-rate sodium storage. *Adv. Mater.* **2022**, *34*, e2109282. DOI
143. Xi, Y.; Wang, Y.; Yang, D.; et al. K_2CO_3 activation enhancing the graphitization of porous lignin carbon derived from enzymatic hydrolysis lignin for high performance lithium-ion storage. *J. Alloys. Compd.* **2019**, *785*, 706-14. DOI
144. Zhao, J.; He, X. X.; Lai, W. H.; et al. Catalytic defect-repairing using manganese ions for hard carbon anode with high-capacity and high-initial-coulombic-efficiency in sodium-ion batteries. *Adv. Energy. Mater.* **2023**, *13*, 2300444. DOI
145. Meng, Q.; Lu, Y.; Ding, F.; Zhang, Q.; Chen, L.; Hu, Y. S. Tuning the closed pore structure of hard carbons with the highest Na storage capacity. *ACS. Energy. Lett.* **2019**, *4*, 2608-12. DOI
146. Huang, Y.; Zhong, X.; Hu, X.; et al. Rationally designing closed pore structure by carbon dots to evoke sodium storage sites of hard carbon in low-potential region. *Adv. Funct. Mater.* **2024**, *34*, 2308392. DOI
147. Rawat, S.; Wang, C. T.; Lay, C. H.; Hotha, S.; Bhaskar, T. Sustainable biochar for advanced electrochemical/energy storage applications. *J. Energy. Storage.* **2023**, *63*, 107115. DOI
148. Wang, J.; Kaskel, S. KOH activation of carbon-based materials for energy storage. *J. Mater. Chem.* **2012**, *22*, 23710-25. DOI
149. Wang, K.; Sun, F.; Wang, H.; et al. Altering thermal transformation pathway to create closed pores in coal-derived hard carbon and boosting of Na^+ plateau storage for high-performance sodium-ion battery and sodium-ion capacitor. *Adv. Funct. Mater.* **2022**, *32*, 2203725. DOI
150. Jagtoyen, M.; Derbyshire, F. Activated carbons from yellow poplar and white oak by H_3PO_4 activation. *Carbon* **1998**, *36*, 1085-97. DOI
151. Xu, T.; Qiu, X.; Zhang, X.; Xia, Y. Regulation of surface oxygen functional groups and pore structure of bamboo-derived hard carbon for enhanced sodium storage performance. *Chem. Eng. J.* **2023**, *452*, 139514. DOI
152. He, J.; Lan, N.; Yu, H.; Du, D.; He, H.; Zhang, C. Chemical crosslinking regulating microstructure of lignin-derived hard carbon for high-performance sodium storage. *J. Polymer. Sci.* **2024**, *62*, 3216-24. DOI
153. Shao, W.; Cao, Q.; Liu, S.; et al. Replacing "Alkyl" with "Aryl" for inducing accessible channels to closed pores as plateau-dominated sodium-ion battery anode. *SusMat* **2022**, *2*, 319-34. DOI
154. Chen, Y.; Li, F.; Guo, Z.; et al. Sustainable and scalable fabrication of high-performance hard carbon anode for Na-ion battery. *J. Power. Sources.* **2023**, *557*, 232534. DOI
155. Schutjajew, K.; Giusto, P.; Härk, E.; Oschatz, M. Preparation of hard carbon/carbon nitride nanocomposites by chemical vapor deposition to reveal the impact of open and closed porosity on sodium storage. *Carbon* **2021**, *185*, 697-708. DOI
156. Zhu, Z.; Men, Y.; Zhang, W.; et al. Versatile carbon-based materials from biomass for advanced electrochemical energy storage systems. *eScience* **2024**, *4*, 100249. DOI
157. Sun, F.; Wang, H.; Qu, Z.; et al. Carboxyl-dominant oxygen rich carbon for improved sodium ion storage: synergistic enhancement of adsorption and intercalation mechanisms. *Adv. Energy. Mater.* **2021**, *11*, 2002981. DOI
158. Saurel, D.; Segalini, J.; Jauregui, M.; et al. A SAXS outlook on disordered carbonaceous materials for electrochemical energy storage. *Energy. Storage. Mater.* **2019**, *21*, 162-73. DOI
159. Morikawa, Y.; Nishimura, S.; Hashimoto, R.; Ohnuma, M.; Yamada, A. Mechanism of sodium storage in hard carbon: an X-ray scattering analysis. *Adv. Energy. Mater.* **2020**, *10*, 1903176. DOI
160. Ilic, I. K.; Schutjajew, K.; Zhang, W.; Oschatz, M. Changes of porosity of hard carbons during mechanical treatment and the relevance for sodium-ion anodes. *Carbon* **2022**, *186*, 55-63. DOI
161. Song, X.; Xu, L.; Sun, X.; Han, B. In situ/operando characterization techniques for electrochemical CO_2 reduction. *Sci. China. Chem.* **2023**, *66*, 315-23. DOI
162. Li, Y.; Hu, Y. S.; Titirici, M. M.; Chen, L.; Huang, X. Hard carbon microtubes made from renewable cotton as high-performance anode material for sodium-ion batteries. *Adv. Energy. Mater.* **2016**, *6*, 1600659. DOI
163. Liu, G.; Wang, Z.; Yuan, H.; et al. Deciphering electrolyte dominated Na^+ storage mechanisms in hard carbon anodes for sodium-ion batteries. *Adv. Sci.* **2023**, *10*, e2305414. DOI PubMed PMC
164. Li, Q.; Zhang, J.; Zhong, L.; et al. Unraveling the key atomic interactions in determining the varying Li/Na/K storage mechanism of hard carbon anodes. *Adv. Energy. Mater.* **2022**, *12*, 2201734. DOI
165. Alcántara, R.; Ortiz, G. F.; Lavela, P.; Tirado, J. L.; Stoyanova, R.; Zhecheva, E. EPR, NMR, and electrochemical studies of surface-modified carbon microbeads. *Chem. Mater.* **2006**, *18*, 2293-301. DOI
166. Nagmani, Manna S, Puravankara S. Hierarchically porous closed-pore hard carbon as a plateau-dominated high-performance anode for sodium-ion batteries. *Chem. Commun.* **2024**, *60*, 3071-4. DOI PubMed
167. Yu, Z. E.; Lyu, Y.; Wang, Y.; et al. Hard carbon micro-nano tubes derived from kapok fiber as anode materials for sodium-ion

batteries and the sodium-ion storage mechanism. *Chem. Commun.* **2020**, *56*, 778-81. DOI

168. Alcántara, R.; Lavela, P.; Ortiz, G. F.; Tirado, J. L. Carbon microspheres obtained from resorcinol-formaldehyde as high-capacity electrodes for sodium-ion batteries. *Electrochem. Solid. State. Lett.* **2005**, *8*, A222. DOI
169. Zhou, S.; Tang, Z.; Pan, Z.; et al. Regulating closed pore structure enables significantly improved sodium storage for hard carbon pyrolyzing at relatively low temperature. *SusMat* **2022**, *2*, 357-67. DOI
170. Qiu, D.; Hou, Y. Carbon materials toward efficient potassium storage: rational design, performance evaluation and potassium storage mechanism. *Green. Energy. Environ.* **2023**, *8*, 115-40. DOI